SCC FORMWORK PRESSURE

TASK 1: CAPTURING EXISTING KNOWLEDGE ON

FORMWORK PRESSURE EXERTED BY SCC

Kamal Henri Khayat (PI), Université de Sherbrooke
David Bonen (co-PI), Purdue University
Surendra Shah, Northwestern University
Peter Taylor, CTLGroup

February 13, 2007

PHASE I - EXECUTIVE SUMMARY

INTRODUCTION

Self-consolidating concrete (SCC) is based on an emerging technology of a relatively new type of high performance concrete that is able to flow and consolidate under its own weight. Materials wise, SCC differs from conventional concrete by the increased amount of fine hydraulic / pozzolanic materials, such as portland cement, fly ash, or slag, or non-reactive fillers, such as ground limestone. In addition, SCC is characterized by high content of high-range water reducers (i.e., superplasticizer) typically based on polycarboxylate ethers or polynaphthalene sulfonate. In turn, the high amount of superplasticizer markedly reduces both the yield stress of the concrete and its plastic viscosity. The low yield stress and plastic viscosity impart the characteristic of high fluidity and passing ability that enable the concrete to perform its intended use; flow laterally or vertically into the forms and through congested reinforcement and self-consolidate without the need of any mechanical vibration.

As detailed in the proposal and the literature review document attached, SCC has numerous benefits vis-à-vis better properties, labor reduction, shortening the placing and finishing time, eliminating hazardous noise and vibration and increasing the overall profitability. However, in cast-in-place applications, the inherent low yield stress and plastic viscosity of SCC increase the lateral pressure that the SCC can exert on the forms to a degree in which the lateral pressure may be as high as the hydrostatic pressure. This adverse effect compromises the profitability and increases the liability because of the need to build expensive and robust formwork. The goal of Task I of this research project is to capture the existing knowledge related to the effect of SCC on formwork pressure and incorporate this knowledge into our research investigation.

The State-of-the Art report attached (hereafter the report) is a comprehensive review on the subject matter providing detailed information on the effects of key parameters affecting formwork pressure and its decay over time. The parameters reviewed include: raw materials, concrete mix design, placement conditions, and formwork characteristics. In addition, the

report reviews existing code regulations and recently proposed models that can be used to predict formwork pressure exerted by conventional concrete, flowable concrete, and SCC. A detailed account on the relationships between the rheological properties of the concrete and formwork pressure is given. More specifically, the report highlights the role of thixotropy and makes connection between the rate of structural build-up of the mixture and the pressure decay. Review of measurement systems used to monitor form pressure is also given. Finally, the report reviews some case studies aimed at determining the formwork lateral pressure exerted by different SCC mixtures.

This executive summary points at the main variables that are critical for understanding the phenomenon of formwork pressure. It is clear that these key issues are essential for modeling the lateral pressure, its rate of decay, and devising strategies to controlling and reducing it. Therefore, all these key variables are taken into account in our investigative work.

FACTORS AFFECTING FORMWORK PRESSURE

Materials

Formwork pressure exists as long as the concrete is in a plastic state, and its rate of decay is related to the rate of the stiffening of the concrete mixture. It follows that the lower the yield stress and plastic viscosity of the concrete are (i.e. high flowability), the greater the initial lateral pressure. Conversely, a faster rate of stiffening brings about a faster rate of decay of the lateral pressure.

As is evident, SCC can be formulated in various ways and consequently does not have any specific composition. The report cites numerous papers on the effect of SCC composition on the formwork pressure. It is shown that any of following parameters aggregate content and size, *w/cm*, cement type and content, silica fume, fly ash, slag, ground limestone filler, superplasticizer type and content, and VMA type and content can affect the lateral pressure characteristics. Generally speaking, it is shown that increasing aggregate content and size gives rise to a lower initial lateral pressure. In contrast, rich concrete mixtures develop greater pressure than normal and lean mixtures. This is attributed to internal friction of coarse aggregate carrying some of the hydrostatic load. However, if the content of the fines (the

paste component of the concrete) is increased, the ability of the coarse aggregate to carry loads decreases, and the lateral pressure is increased.

Increasing the *w/cm* or/and superplasticizer content increases the lateral pressure and vice versa. However, different superplasticizers have been found to affect differently both the initial lateral pressure and its rate of drop after casting. It is also shown that addition of supplementary cementitious materials (SCM), such as fly ash, silica fume, or granulated blast-furnace slag, affect the lateral pressure and more specifically its rate of decay. This is attributed to the thixotropic nature of the concrete that changes with the inclusion of these materials. However, the literature mainly provides qualitative information on the effects of the various ingredients listed above and occasionally, disagreements on the effects of some ingredients are encountered.

Placement Conditions

The placement rate is a critical parameter for formwork pressure of SCC. The higher the rate of placing, the higher the lateral pressure is, and to reiterate, this pressure may be as high as full hydrostatic pressure. Conversely, if placement rates are reduced, the concrete mixture, especially that possessing thixotropic properties, undergoes structural build-up, and the pressure is reduced. Similarly, the placement method has a significant effect on formwork pressure. Concrete pumped into the fromwork from the bottom of the form exhibits higher pressures than that placed from above. These effects are to a great extent related to the shearing forces to which the plastic concrete is subjected to during placement, being greater once the concrete is pumped into the forms from the bottom up.

Since the mechanical properties of concrete are temperature dependant, the higher the initial temperature of the concrete and/or the ambient temperature, the lower the lateral pressure is. Subsequently, a higher rate of pressure decay is recorded. This is attributed to a faster rate of structure build-up and hydration takes place at higher temperatures. The set time of concrete has similar effects. After placement, mixtures with longer setting times display longer lateral pressure cancellation time.

Formwork Characteristics

There is little data pertaining to the effects of formwork dimensions and formwork pressure. One study showed that smaller cross-sections exhibit lower maximum pressure. It was explained that this relationship was due to an arching effect that limits lateral pressure. The presence of reinforcement theoretically helps to decrease the formwork pressure because it can hold part of the concrete load, although this may be a negligible effect in SCC. Research also has shown that the type of formwork used has an effect on formwork pressure. Specifically, rigid and smooth formwork materials result in higher lateral pressure and lower rate of pressure drop after placement.

The roughness of the forms also plays a role due to the dynamic friction that develops upon concrete placement. It was shown that the application of demolding agents, such as oil, to the formwork can decrease friction and lead to an increase in lateral pressure.

FORM PRESSURE MODELS

Numerous models and code regulations aiming at predicting form pressure are reported in the literature. However, in most cases the models do not pertain to SCC. The models available include the following input parameters: pore water pressure, rate of casting, vibration, setting time, consistency, form permeability and surface texture, form dimensions, coarse aggregate, temperature, and concrete unit weight.

Of the few models pertaining to SCC, thixotropy has been identified as a main factor that affects the lateral pressure and its rate of decay. Accordingly, both the Sherbrooke and Northwestern research groups have shown that thixotropy can be monitored and quantified by measuring the area confined in the hysteresis loop (of shear rate vs. shear stress plot) obtained by studying the rheological characteristics of the mixture or by evaluating the drop in shear stress between initial and equilibrium states determined at different shear rates. The resulting area in the hysteresis loop or in the drop in shear stress vs. shear rate is used to quantify the energy required for structural breakdown during mixing and the ensuing structure build-up once the mixture is at rest. Indeed, Khayat and his coworkers successfully

implemented this concept and made a connection between the rate of pressure decay and the degree of thixotropy.

CONCLUDING REMARKS

Although the main factors related to formwork pressure are well documented, occasionally, disagreements about the role of specific ingredients/variables are encountered. Of perhaps greater importance, the relative weights of the ingredients/variables are not established. Therefore, the literature reports that the actual pressure of SCC can vary in a relatively wide range from full hydrostatic pressure down to about 60% relative hydrostatic pressure at rates of casting that make SCC economically attractive. Nonetheless, there is no single model that correlates the properties of the mixture and form with the initial lateral pressure. Similarly, there is no consensus on the rate of decay of lateral pressure.

In light of the literature review, it is suggested that our investigative work be based on the following systematic and methodological main principles:
1. Evaluating the effect of SCC mixtures on the formwork pressure by quantifying the effects of the individual ingredients of the paste (i.e., cement, fly ash, silica fume, superplasticizer, VMA), *w/cm*, and aggregate characteristics.
2. Utilizing factorial design methods thus determining the relative weight of each variable so the results will be applicable to a wide range of compositions.
3. Quantifying the effects of methods of placement, casting rate, and formwork dimension.
4. Quantifying the thixotropy of the various mixtures and correlating it with the casting rate and method of placement.
5. Modeling the effects of the above variables and testing the validity of the model in a full field test.

SCC FORMWORK PRESSURE

PHASE II - STATE-OF-THE ART REVIEW OF FORMWORK PRESSURE EXERTED BY SELF-CONSOLIDATING CONCRETE

Submitted to

THE NATIONAL READY-MIX CONCRETE RESEARCH FOUNDATION

and

THE STRATEGIC DEVELOPMENT COUNCIL, AMERICAN CONCRETE INSTITUTE

K. H. Khayat, Professor
A. Omran, Ph.D. Candidate

UNIVERSITÉ DE
SHERBROOKE

Table of Contents

List of Figures

1. INTRODUCTION

Over the years, concrete technology has advanced at a relatively slow pace that has been associated with a labor-intensive industry and tedious placing in the formwork. The two milestones that have probably had the greatest impact on propelling this low-skill industry to a technology-driven one are the introduction of superplasticizer and the development of self-consolidating concrete (SCC).

SCC is a new class of high-performance concrete that flows readily under its own weight and consolidates without the use of mechanical vibrations and with minimum risk of segregation. SCC is a complex system that is usually proportioned with a number of chemical admixtures and supplementary cementitious materials. Such concrete exhibits low resistance to flow and moderate plastic viscosity necessary to maintain homogeneous deformation during placement and thereafter until the onset of hardening.

The first SCC prototype was successfully completed by Ozawa et al. [1989] in the late 1980s. Since then, the market share of SCC has rapidly increased in precast applications or for ready-mix concrete applications, due to a number of economic opportunities and the improvement in the work environment associated with its use. SCC has been successfully used in North America in the precast industry. A recent overview on SCC types, test methods, and properties are given by Khayat [1999], Khayat et al., [1999], and Bonen and Shah [2004, 2005].

The benefits obtained from using SCC can be summarized as follows:
- Decrease in construction cost due to labor reduction.
- Reduction in construction time.
- Simplification of the casting process as no vibration is needed.
- Improvement of working conditions through less noise hazards.
- Ability to cast congested and complex structural elements in various shapes and dimensions that are not attainable by any other conventional techniques.
- Ability to cast hard-to-reach areas that represent difficulties to placement, and consolidation.

- Improving appearance and quality of the finished surfaces and reduction in the occurrence of bugholes, honeycombing, and other surface imperfections.
- Producing a better and premium concrete product.
- Larger variety of architectural shapes by using any form shape. This is one of the major advantage of SCC where it is possible to cast heavily reinforced elements and structures with a complicated geometry that otherwise are not attainable by any other conventional techniques [Khayat et al., 2001, Walraven, 2002, Okamura and Ouchi, 2003, Mullarky and Vaniker, 2002].
- Higher durability of concrete structures.
- Lowering pumping pressures, and as a consequence, reducing wear and tear on pumps, i.e. extends their service life.
- Lowering the need for cranes to deliver concrete in buckets at the job site by facilitating concrete delivery through pumping.

Despite the various benefits that can be gained by using SCC, there are some limitations that should be taken into consideration when using such new material, including:

- Raw materials cost of SCC can be 13% to 30% higher than the cost of conventional mixtures with similar mechanical properties [Schlagbaum, 2002, Martin, 2002]. Nonetheless, cost analysis shows that even if the selling cost of SCC is reduced by only a few percent because of the decrease in labor and construction time, the profitability is increased by about 10% [Szecsy et al., 2002].
- SCC requires greater quality control and quality assurance measures to ensure proper workability, including high resistance to segregation and stability of entrained air voids.
- SCC has greater potential for shrinkage and creep and care should be taken in designing the concrete elements. Greater risk of shrinkage and creep arise from the large volume of fine materials in use, particularly in the case of SCC without any VMA, and the lower content of coarse aggregate.
- Lack of knowledge on the relative lateral pressure that SCC could exert on formwork systems. This adverse effect may compromise profitability, due to the need to design for robust formwork construction and detailed joint sealing.

Of the benefits listed above, the greatest incentives for the industry to adopt this technology are related to the potential profitability brought about by shortening of the casting time, reduced labor, minimized logistics due to elimination of the need for vibrations, and production of esthetic surfaces with high quality. In turn, a rapid rate of casting of concrete in a formwork system leads to an increase in lateral pressure exerted by the concrete, which could reach full hydrostatic pressure. Such high pressure is attributed to two factors:

(i) The initial low shear stress of the plastic SCC, and

(ii) The rate of vertical placing in the formwork that exceeds the rate of stiffening of the concrete in the formwork.

Formwork systems for wall and column elements can contribute up to 40% of the overall cost of construction projects [Rodin, 1952]. This was recently reported to be up to 60% of the total cost of completed concrete structure in place in the USA [ACI Guide to Formwork for Concrete, 2004]. Any savings in the cost of formwork, for example by reducing the design loads affecting lateral pressure exerted by plastic concrete, would be of great interest. The relatively high lateral pressure exerted by SCC is considered the main technical hindrance that slows down the widespread use of SCC in cast-in-place applications. Lateral pressure exerted by concrete is of concern to construction engineers because its overestimation results in expensive formwork, while its underestimation can lead to bulging of the formwork or, in extreme cases, failure of the formwork system.

Additionally, high formwork pressure presents a major safety issue. As the lateral pressure of the concrete increases, so does the potential risk for liability in the event of a failure. According to the current provisions, responsibility for the safe construction of formwork rests on the contractor or the engineer hired by the contractor to design the formwork. Provisions in ACI 347R-7 document stipulate that when working with mixtures with high slump characteristics, such as SCC, the presumed lateral pressure should be equal to the hydrostatic pressure of the fresh concrete "until the effect on formwork pressure is understood." Similarly, the European Federation of Producers and Contractors of Specialist Products for Structures (EFNARC) recommends that forms higher than 3 m are designed for full hydrostatic head [EFNARC, 2002]. If the formwork system is prudently designed

for full hydrostatic pressure, either the total cost of the formwork has to be increased or the rate of placing should be decreased.

To date, limited information exists regarding the magnitude of the lateral pressure that can be developed by SCC on vertical wall or column elements. Contractors and engineers recognize design recommendations elaborated with the use of normal-consistency concrete, which cannot be fully applied to SCC due to the higher fluidity level of the SCC that could result in the lateral pressure reaching full fluid pressure. Therefore, existing equations for estimating lateral pressure that are necessary for the design of formwork need to be modified to account for the high flowability of SCC. So far, formwork is designed prudently by assuming that the SCC exerts full hydrostatic pressure until setting time. Such pressure is expressed as: $P_{max} = \rho \times g \times H$ where: ρ, g, and H correspond to the concrete unit weight, gravity, and head of concrete, respectively. This approach can result in increased construction costs and can limit the rate of rise of the concrete in the formwork. Designing for high values of hydrostatic pressure requires a robust formwork construction and detailed joint sealing, which could adversely affect profitability.

The objective of the state-of-the art review that is reported herein is to capture existing knowledge regarding formwork issues related to SCC. The report reviews existing code regulations and recently proposed models that can be used to predict formwork pressure exerted by conventional concrete, flowable concrete, and SCC. The report reviews key parameters affecting formwork pressure, including raw material properties, concrete mix design, placement conditions, and formwork characteristics that have major influence on the maximum formwork pressure and its decay in time. The report also reviews recent research relating formwork properties exerted by SCC and the rheological properties of the concrete, including the rate of structural build-up of concrete at rest and thixotropy. Review of measurement systems used to monitor form pressure is also given in the report. Finally, the report reviews some case studies regarding field monitoring of formwork lateral pressure exerted by SCC.

This report will be updated by the end of the project to include other investigations reported in the literature as well as the results that will be generated by the research team at the Université de Sherbrooke, Northwestern and Purdue Universities, and the CTLGroup.

2. REVIEW OF VARIOUS RECOMMENDATIONS FOR FORMWORK DESIGN

In conventional construction practice, concrete is cast into wall or column forms in lifts, which are vibrated to consolidate the concrete. The concrete is usually consolidated using poker-type vibrators, which are immersed into the concrete at the top layer (about 1 m). The vibration causes the development of full fluid pressure at the top layer.

In considering formwork pressure, two main items should be considered to ensure safely designed and cost-effective formwork systems. The first item is the initial maximum lateral pressure developed by the plastic concrete immediately after casting. This relative lateral pressure (K_o) is defined as the maximum lateral pressure divided by the hydrostatic liquid head at the same level ($K_o = P_{max} / P_{hydrostatic}$). Such value is the most critical because it directly affects the design of formwork systems. The rate of pressure drop with time [$\Delta K_0(t)$] is also of special interest in designing formwork systems. In most lateral pressure investigations carried out using normal-consistency concrete, the pressure can be found to decrease slowly before dropping to zero approximately 3 h after casting. However, this is not always applicable for cast-in place SCC where the set can be delayed. Better knowledge of the rate of pressure drop enables better scheduling of the placement of subsequent concrete lifts. This is particularly true in case of casting into deep and large elements requiring considerable volume of concrete. The elapsed time before pressure cancellation is also important for better scheduling of the re-use of formwork.

2.1 Models proposed to evaluate formwork pressure

Several equations were proposed in the literature to evaluate the magnitude and shape of the lateral pressure envelope. Some of these models elaborated to estimate formwork pressure for conventional concrete and few recent studies targeting formwork pressure of SCC are summarizes below.

2.1.1   Rodin's models [1952]

Rodin [1952] reviewed published experimental data on lateral pressure of fresh concrete against formwork. He concluded that the major factors influencing lateral pressure were rate of pouring, vibration, mixture consistency and mixture proportion, concrete temperature, concrete setting time, and size and shape of the form. Rodin [1952] reported that the formwork should be designed according to two cases: externally vibrated and non-externally vibrated concrete. The latter case was consequently divided into two categories: internally vibrated concrete and hand-placed concrete. The concrete pressure distribution on the formwork as proposed by Rodin [1952] is shown in Fig. 1. The details of the two cases can be expressed as follows:

For externally vibrated concrete

 The formwork should be designed for full hydrostatic pressure of a liquid having the same density as concrete.

For non-externally vibrated concrete

 For internally vibrated concrete $\boxed{P_{max} = 23.4\ H_{max}}$ ……………………………….. (1)

 For hand-placed concrete $\boxed{P_{max} = 17.2\ H_{max}}$ ………..……………………….. (2)

 where, H_{max} : head at which the maximum pressure occurs, m

  $\boxed{H_{max} = 1.63\ R^{1/3}}$ ……………………….. (3)

  P_{max} : maximum lateral pressure, kPa

  R : rate of placing, m/h

Note: These equations are for concrete having 1:2:4 cement:sand:coarse aggregate mass fractions, a unit weight of 2,400 kg/m^3, a slump consistency of 150 mm, and a temperature of 21 °C.
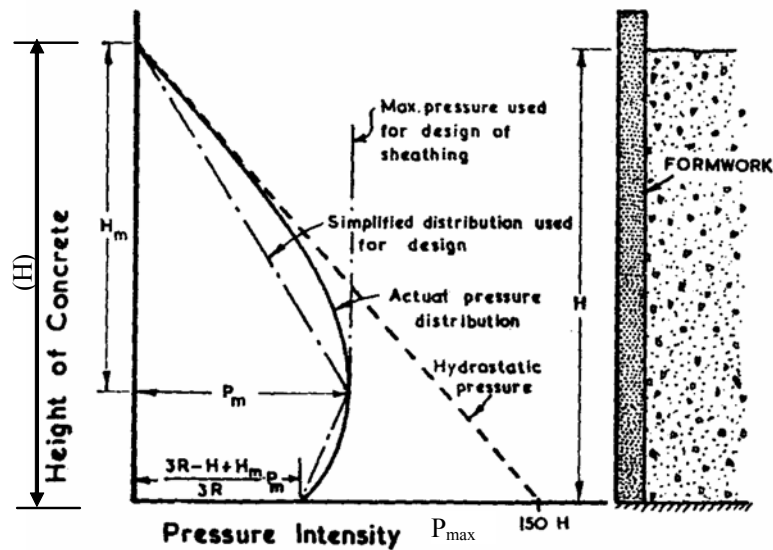
Fig. 1 - Concrete pressure distribution on formwork [Rodin, 1952]

2.1.2 Schojdt's models [1955]

Schojdt [1955] developed a theoretical model for determining the pressure envelope using soil mechanics concepts, including pore-water pressure and lateral pressure coefficient. The factors considered in Schojdt's derivation were the rate of casting, immersed depth of the vibrator, setting time, slump consistency, permeability of the form, and size and shape of the form. Schojdt's method did not receive acceptance due to its complexity and the requirement of determining the shear strength properties of fresh concrete.

2.1.3 ACI models

The American Concrete Institute (ACI) Committee 622 [1958] (currently designated as ACI 347) "*Formwork for Concrete*" proposed that the lateral pressure diagram is assumed to be trapezoidal in shape: the diagram is presumed to be a triangular distribution from the upper free surface of the casting down to some limiting depth, beyond which the value of pressure reached is considered constant until the bottom of the formwork. The significant variables considered in the ACI recommendations are the placement rate and method, consistency of concrete, coarse aggregate concentration, aggregate nominal size, concrete temperature, smoothness and permeability of the formwork material, size and

shape of the formwork, consolidation method, pore-water pressure, content and type of cement, as well as the depth of the concrete placement, or concrete head.

The ACI equations are reported along with the limitation of use, in the following paragraphs.

For wall elements:

R < 2.14 m/h

$$P_{max} = 7.19 + \frac{785R}{17.78 + T} < 95.8 \text{ or } 23.5\,H$$ ……………………….. (4)

2.14 < R < 3 m/h

$$P_{max} = 36 + \frac{244\,R}{T + 17.78}$$ ……….…………………….. (5)

$$P_{max} = 7.19 + \frac{1156}{T + 17.78} + \frac{244\,R}{T + 17.78} < 95.8 \text{ or } 23.5\,H$$ ……..…….. (6)

R > 3 m/h

$$P_{max} = 23.5\,H < 95.8$$ ………………..…….. (7)

For column elements

$$P_{max} = 7.19 + \frac{785R}{17.78 + T} < 143.7 \text{ or } 23.5\,H$$ ……..…….. (8)

For walls and columns

$$P_{max} = \gamma_c.H$$ …………………………......…….. (9)

where P_{max} : maximum lateral pressure, kPa;

R   : rate of placement, m/h;

T   : concrete temperature, °C; and

H   : head of concrete, m.

Notes: 1- These formulas are used only for normal internal vibration, immersion of vibrator ≤ 1.2 m in fresh concrete, Type GU cement, no pozzolans or admixtures, γ_c = 2,400 kg/m^3, slump ≤ 100 mm at time of casting, and any required re-vibration is allowed only in plastic stage;

2- Eq. (6) and term of [23.5 H] were added in 1963;

3- Eq. (7) was added in 1978; and

4- Eq. (9) was added in 1988 for all types of concrete.

In 2002, Hurd recognized that such equations are too conservative to be adopted nowadays, thus resulting in more expensive formwork. This is due to evolution in the composition of concrete mixtures, mainly with the introduction of chemical admixtures and portland cement replacements. Consolidation and placement techniques have also undergone significant changes with the use of fluid and highly fluid concrete. Hurd [2002] proposed applying some coefficients to the ACI equations [1958] in order to take into account different unit weights that can be encountered on the job-site, as well as the chemical admixtures and supplementary cementitious materials.

For walls and columns

$$P_{max} = C_W \, C_C \left(7.19 + \frac{785R}{17.78 + T} \right) \qquad \begin{array}{c} 30\,C_w \ \ (\text{kPa}) \ \leq \ P_{max} \ \leq 150C_w\,C_c \ (\text{kPa}) \\ P_{max} \ \leq \gamma_c H \end{array} \qquad \text{........ (10)}$$

where γ_c : unit weight of concrete, kg/m^3;

    H : head of concrete, m;

    P_{max} : maximum lateral pressure, kPa;

    R : rate of casting, m/h

    T : concrete temperature, ºC;

    C_W : Unit weight coefficient calculated as follows:

$$C_w = 0.5 \left(1 + \frac{\gamma_c}{23.2} \right) \quad but \geq 0.8 \quad for \quad \gamma_c < \ 2240 \ \ kg/m^3$$

$$C_w = 1.0 \qquad\qquad\qquad\qquad for \quad 2240 \ \ kg/m^3 < \ \gamma_c < \ 2400 \ \ kg/m^3$$

$$C_w = \frac{\gamma_c}{23.2} \qquad\qquad\qquad for \quad \gamma_c > \ 2400 \ \ kg/m^3$$

   C_c : chemistry coefficient calculated as follows:

    $C_c = 1.0$ for cement Type GU or HE without retarder

    $C_c = 1.2$ for blended cement without retarder (blended means: Type GU cement with < 70% slag or < 40 % fly ash replacements).

    $C_c = 1.4$ for blended cement with retarder (retarder refers to set retarder, water-reducing agent, or superplasticizer).

2.1.4   Adam et al.'s models [1963]

Adam et al. [1963] conducted laboratory tests on a large form measuring 3 m in height, 2.5 m in length, and of variable widths. Adam et al. [1963] studied the effect of cement type, additives, aggregate size, casting rate, slump consistency, and vibration on form pressure. The results of this study are summarized as follows:

For R < 2 m/h $P_{max} = 19.6 + 12.3\,R$ T < 5 ºC   ….................... (11)

$P_{max} = 19.6 + 9.8\,R$ T = 15 ºC   ….................... (12)

$P_{max} = 19.6 + 8.3\,R$ T > 25 ºC   ….................... (13)

For R > 2 m/h $P_{max} = 40.1 + 1.96\,R$ T < 5 ºC   ….................... (14)

$P_{max} = 35.3 + 1.96\,R$ T = 15 ºC   ….................... (15)

$P_{max} = 32.4 + 1.96\,R$ T > 25 ºC   ….................... (16)

where; P_{max} : maximum lateral pressure, kPa;

R   : casting rate, m/h; and

T   : concrete temperature, °C;

2.1.5   Models of German Standard [DIN 18218, 1980]

DIN 18218 presented a series of equations to calculate the limiting lateral pressures of internally vibrated concrete made with various consistency levels and temperature of 15 °C [Eq. (17) or Eqs. (18)]. In order to adjust for variable concrete temperatures, it is recommended to decrease the limiting pressure (developed for concrete at 15 °C) by 3% for every degree above 15 °C and to increase it by 3% for every degree below 15 °C.

- For concrete cast at T = 15 ºC:

$$\boxed{P_{max} = \gamma_c\,C_2\,K_t\,(0.48\,R + 0.74)} \qquad\qquad ….................... (17)$$

$$\begin{pmatrix} P_{max} = 21 + 5\,R & \text{for stiff mixtures} \\ P_{max} = 19 + 10\,R & \text{for soft mixtures} \\ P_{max} = 18 + 14\,R & \text{for fluid mixtures} \end{pmatrix} \qquad ….................... (18)$$

- For concrete cast at T < 15 ºC: 3 % increase in P_{max} for each degree below 15 ºC.

- For concrete cast at T > 15 ºC: 3 % decrease in P_{max} for each degree above 15 ºC.

where P_{max} : maximum lateral pressure, kPa;

γ_c :   unit weight of concrete, kg/m^3:

C_2 : added coefficient;

K_t : temperature coefficient $= (145 – 3\ T)/100$

R : rate of placement, m/h; and

T : concrete temperature, °C.

2.1.6 CIRIA models [1965 - 1978]

The Construction Industry Research and Information Association (CIRIA) sponsored a large-scale field investigation of formwork pressures carried out by the Cement and Concrete Association and published in 1965. The CIRIA study proposed a lateral pressure design method that involved consideration of the rate of placement, concrete temperature, slump, concrete constituent materials, concrete unit weight, formwork dimensions and shape, and continuity of vibration. The CIRIA design procedure considered that lateral pressure envelope is hydrostatic up to a maximum value (P_{max}) limited by the lesser of concrete stiffening and arching effects, as given by the two equations below. In narrow sections, it was found that the wall friction can significantly limit the maximum exerted pressure [CIRIA, 1965]. In 1978, CIRIA published a two-page design chart to replace these equations.

- For arching criterion

$$\boxed{P_{max} = 14.37 + 0.094\ d + 3.14\ R \quad < \quad 24\ H \quad or \quad 143.7}\ \ ……................. (19)$$

- For stiffening criterion or concrete hardening

$$\boxed{P_{max} \; = \; \frac{\gamma_c RT}{1 \, + \, c\left(\dfrac{t}{t_{max}}\right)^4} \; + \; \left(4.6 - 1.89R\right) < \; 24\,H \quad or \quad 143.7}\ \ .... (20)$$

- General formula

$$P_{max} = \gamma_c\left[C_1\sqrt{R} + C_2 K\sqrt{H - C_1\sqrt{R}}\right] \; \not> \gamma_c.h \quad (kPa) \qquad\qquad ……................. (21)$$

where P_{max} : maximum lateral pressure, kPa;

d : minimum formwork dimension, mm;

R : rate of placing, m/h;

T   : fresh concrete temperature, ºC;

t   : time after start of placing, h;

t_{max} : stiffening or hardening time, h;

c   : vibrating time;

γ_c : unit weight of concrete, kg/m³;

H   : vertical formwork height, m;

h   : height of fresh concrete above the point considered, m;

C_1 : coefficient depending on the size and shape of formwork (= 1.0 at the wall);

C_2 : coefficient depending on the constituent materials of concrete (= 0.3 - 0.6);

K   : temperature coefficient taken as $\left(\dfrac{36}{T+16}\right)^2$; and

(c and t_{max} are defined in empirically derived charts).

2.1.7   Gardner's models [1980 - 1984]

Gardner [1980] carried out series of laboratory studies using a large instrumented form. The variables considered by Gardner [1980] were the depth of vibration, power of vibrator, casting rate, concrete temperature, member dimension, and concrete slump. For formwork design purposes, Gardner [1980] considered that the lateral pressure envelope is bilinear. The envelope is hydrostatic from the free surface to a maximum value and becomes constant thereafter until the bottom. The proposed equations are as follows:

$$P_{max} = 24\,h_i + \frac{3000\,HP}{d} + \frac{d}{40} + \frac{400\,\sqrt{R}}{18+T} + \frac{S-75}{10} < 24\,H \qquad \text{.......................... (22)}$$

where P_{max} : maximum lateral pressure, kPa;

H   : total height of formwork, m;

h_i : immersed depth of vibrator not to be less than 1 meter, m;

d   : minimum formwork dimension, mm;

HP : horsepower of vibrator;

R   : rate of placement, m/h;

T   : concrete temperature, ºC; and

S   : slump after application of superplasticizer, mm.

A subsequent investigation using the same apparatus, Gardner [1982, 1984] investigated the effect of incorporating superplasticizers and supplementary cementitious materials; Class F fly ash, and blast furnace slag on lateral pressure. It was found that partial cement replacement of portand cement by fly ash or blast furnace slag can increase the mobility of the concrete and decreases the rate of strength gain at early age, thus resulting in an increase in formwork pressure. An additional factor was introduced in the above equation to account for fly ash and slag substitutions. The equation was shown to give conservative design values for fly ash concrete.

$$\boxed{P_{max} = 24\,h + \frac{3000\,HP}{d} + \frac{d}{40} + \frac{400\,\sqrt{R}}{18+T}\left(\frac{100}{100-\%F}\right) + \frac{S-75}{10} < 24\ H}$$ .... (23)

where   F   : percent substitution of cement by Class F fly ash or blast furnace slag.

2.1.8   Models of French Standard [NFP 93-350, 1995]

The French Standard [NF P93-350, 1995] reported that the formwork must be designed to withstand forces in the elastic domain due to the placing of ordinary concrete with a density of 2,400 kg/m^3. The exerted maximum lateral pressure is given by the following equation:

$$\boxed{P_{max} = 2,400\ g\ H}\ \ngtr\ 72\ kPa\ \text{at the bottom of a 3-m high form}$$ ....……........ (24)

where   g: gravitational acceleration;

H: formwork height, m.

A comparison of the lateral pressure envelopes that can be obtained from design equations offered by DIN 18218, CIRIA 108, and NF P93-350 models for conventional vibrated concrete with flowable consistency is made in Fig. 2. These results are plotted for fresh concrete having a unit weight (γ_c) of 2,500 kg/m^3, temperature (T) of 15 °C, and an end of solidification time (t_E) of 5 h cast at placement rates of 1 to 25 m/h in a wall element measuring 20 m in height. The data show the influence of the casting rate on the pressure envelope. According to the DIN 18218 model, the increase in casting rate from 1 to 12.5 and 25 m/h would lead to linear design pressure envelope equal to hydrostatic pressure in the upper 1.5, 9, and 18 m portions of the wall, respectively. These values were approximately 1.5, 6, and 8 m, respectively, for the CIRIA 108 design model.

13
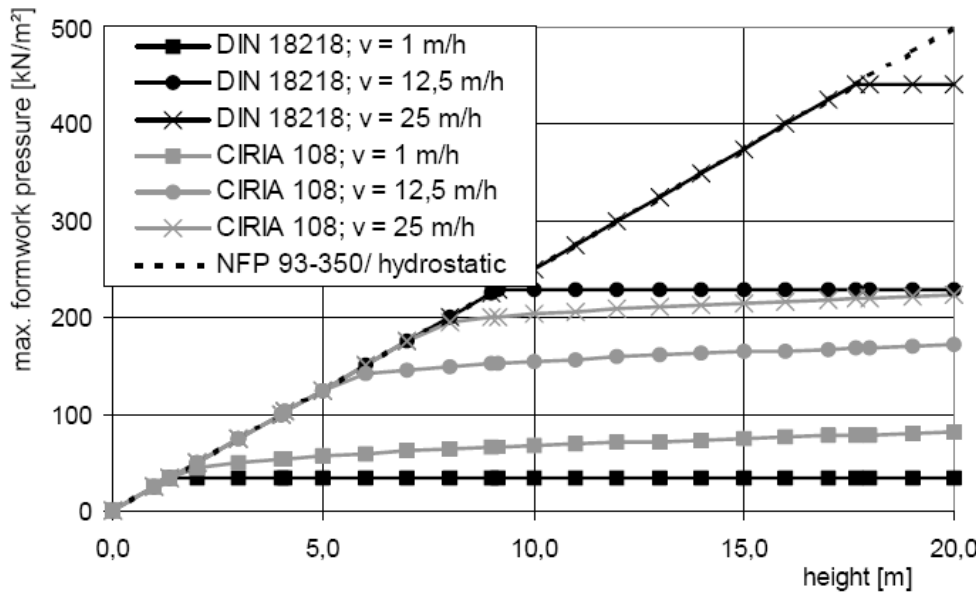
Fig. 2 - Formwork pressure - DIN 18218 (D), CIRIA 108 (GB), and NF P93-350 (F)
[Proske and Graubner, 2002]

2.2 Theoretical models to predict formwork pressure

2.2.1 Shear strength properties of fresh concrete using soil mechanics principles

Several researchers carried out experimental investigations based on soil mechanics principles for assessing shear strength properties of fresh concrete and their influence on lateral pressure. Ritchie [1962A] used the triaxial test approach to determine the effect of coarse aggregate-to-cement mass ratio on the angle of internal friction of plastic concrete. Different mixtures having aggregate-to-cement mass ratios varying between 1:3 and 1:6 were evaluated. The corresponding *w/c* ranged between 0.45 and 0.81, and the consistency varied from low to high. Undrained triaxial tests were performed on 100 × 200 mm cylindrical samples at a strain rate of 2.1% per min until the specimens were seen to fail or the strain exceeded 20%. Cell pressures ranging from 35 to 420 kPa were used. The angle of the tangent line determined from Mohr circle diagrams was taken as the angle of internal friction. The author concluded that:

— For a given compacting factor, internal friction in plastic concrete was reported to increase with the increase in the aggregate-to-cement ratio;

14

— The decrease in *w/c* was found to reduce the level of lubrication of the paste layer among coarse aggregate particles, hence increasing internal friction.

Olsen [1968] attempted to relate the magnitude of formwork pressure to the undrained shear strength of fresh concrete. The author measured the variations in undrained shear strength with time using triaxial testing and related the stress-strain relationships of the concrete to the strains and corresponding pressures imposed on the formwork. A standard mixture with 0.40 *w/c* and cement:sand:coarse aggregate ratio of 1.0:1.5:1.5 was used. The undrained triaxial tests were performed for set times ranging from 20 to 180 min following the initial contact of cement with water and under confining pressures ranging from 140 to 560 kPa.

From Olsen's results, the following generalized conclusions can be made:

— For mixtures with low set time, the shear strength of fresh concrete consists mainly of cohesive bond in the cement paste;

— As the setting continues, the cement paste becomes less plastic, and the mobility of the aggregate particles decreases causing an increase in the angle of internal friction;

— Cohesion steadily increases with set time as cement hydration takes place to form the binding medium.

Alexandridis and Gardner [1981] evaluated the shear strength characteristics of fresh concrete through the use of a triaxial compression apparatus. Cylindrical samples measuring 100 mm in diameter and 200 mm in height were tested. The confining pressures varied between 0 and 140 kPa, and the tests were carried out at two temperatures (4 and 21 °C) and at different periods after the initial contact between cement and water ranging from 40 to 160 minutes. The concrete mixture had a cement:sand:coarse aggregate mass ratio of 1.0:1.5:3.0, a *w/c* of 0.57, and a slump of 50 mm. The authors concluded that:

— Fresh concrete, as in the case of soil, can be considered to be a particulate system composed of particles weakly bonded together and submerged in a liquid medium. Such system possesses shear strength properties as a result of internal friction and cohesion.

— The shear strength properties can be expressed in fundamental terms using soil mechanics principles. The results are found to be in agreement with both the Mohr-Coulomb and Rowe theories.

— Immediately after mixing, the magnitude of shear strength of concrete is mainly due to the development of internal friction that remains constant with setting time and temperature change. Internal friction results from the frictional resistance and interlocking between aggregate and cement particles; internal friction requires some strain to be mobilized.

— The hardening of concrete with setting time is due mainly to the development of cohesion as a result of the hydration process. Cohesion is due to bonding of aggregate particles by the cement hydration products.

— Cohesion results from cement hydration, and therefore depends on the elapse time following contact of water with cement as well as on temperature at which the concrete is allowed to hydrate. At lower temperatures, hydration is retarded and cohesion develops at a slower rate causing the fresh concrete to behave like a fluid for a longer period of time.

2.2.2   Computer-based model of concrete pressures on complex-shaped wall formwork [Tah and Price, 1991]

Tah and Price [1991] proposed a computer-based model, based on the CIRIA report 108 [1985], to calculate the pressure envelopes of concrete on complex-shaped walls for formwork design. The model can allow several simulations to be quickly performed to investigate the magnitude of maximum concrete pressures resulting from changes in temperature at concrete placement and variations in the casting rate of concrete. The main steps considered in predicting the lateral pressure envelopes are as follows:

1- *Split the pour into horizontal levels (the top and bottom edges in each section are parallel) at the changes in cross-section, or with the vertical distance between each level of 1 m or less*

Figure 3 shows a complex-shaped wall and its subsections at the changes in the cross section. Individual subsections are numbered sequentially from the top to the bottom of the wall. Each sub-section can be identified by the co-ordinates of its four vertices, (X,Y). The vertices of each subsection are numbered from the bottom-left vertex clockwise to the bottom-right vertex. In the case of trilateral subsections shown in Fig. 3-b, the top vertices numbered 2 and 3 are coincident in section 1 and the bottom vertices numbered 1 and 4 are coincident in section 3.

2- *Calculate the plan area at each level*

The plan area $(A_{i,j})$ = cross-sectional width $(w_{i,j})$ × length of wall pour (L)

A) Calculate the slopes of the left edge λ_i and right edge ψ_i of a wall subsection:

$$\lambda_i = \frac{Y_{i,2} - Y_{i,1}}{X_{i,2} - X_{i,1}} \qquad \psi_i = \frac{Y_{i,3} - Y_{i,4}}{X_{i,3} - X_{i,4}} \qquad \text{…..................... (25)}$$

B) Using the slopes, compute the co-ordinates of the points of intersection, $a(X_{a_{i,j}}, Y_{a_{i,j}})$, $b(X_{b_{i,j}}, Y_{b_{i,j}})$ of the level concerned with the left and right edges, respectively.

$$X_{a_{i,j}} = X_{i,2} - \frac{d}{\lambda_i} \qquad X_{b_{i,j}} = X_{i,3} - \frac{d}{\psi_i} \qquad Y_{a_{i,j}} = Y_{b_{i,j}} = Y_{i,2} - d \quad \text{…..................... (26)}$$

C) Cross-sectional width, $w_{i,j} = |X_{a_{i,j}} - X_{b_{i,j}}|$ …..................... (27)

3- *Calculate the instantaneous rate or rise at each level*

At level j in subsection i, the rate of rise is given by:

$$R_{\text{level, i,j}} = \frac{\text{Uniform volume supply rate Q (m}^3\text{/h)}}{\text{Plan area at the level considered } A_{i,j}(\text{m}^2)} \qquad (m/h) \text{…............. (28)}$$
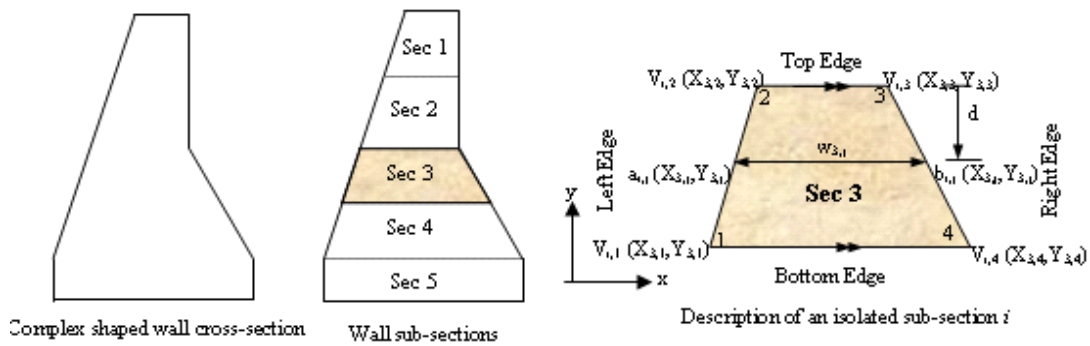
(A) Quadrilateral wall
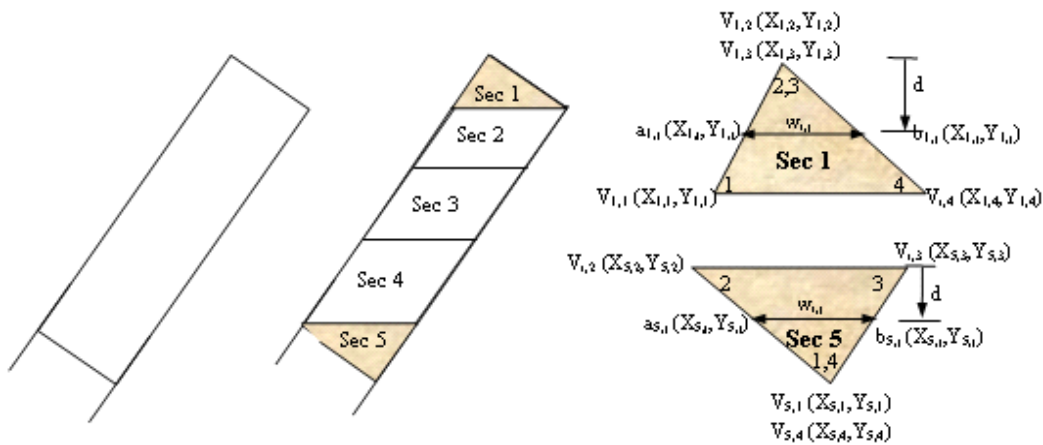
(B) Trilateral wall
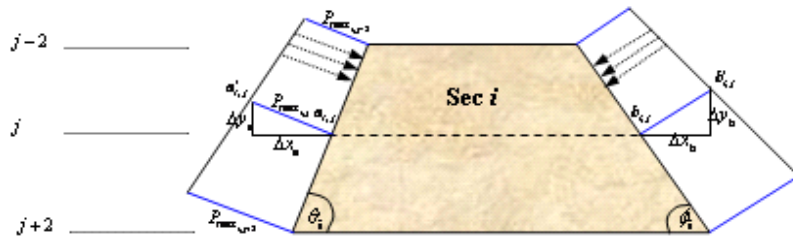
(C). Pressure envelope construction on subsection

Fig. 3 - Graphical representation of a wall-shaped structure

4- *Calculate the pressure at each level using the full height of the form, H, with the equation*

The maximum pressure at level j in the subsection i is given by:

$$P_{\max_{i,j}} = D[C_1\sqrt{R_{i,j}} + C_2K\sqrt{H - C_1\sqrt{R_{i,j}}} \leq Dh_{i,j} \quad (kN/m^3)$$

$$\text{when} \quad C_1\sqrt{R_{i,j}} > H \qquad \text{then} \qquad P_{\max_{i,j}} = Dh_{i,j} \quad (kN/m^3)$$

…............. (29)

where $h_{i,j}$ is the depth from the surface of the pour to level j in subsection i. General data about the concrete pour are required as follows: the concrete temperature at placing, unit weight of concrete, rate of concrete placement R, the shape and size of the form coefficient C_1, the constituent materials of concrete coefficient C_2, and the vertical form height H.

5- Produce the design pressure envelope acting at right angles to the forms

Having obtained the maximum pressures at each level as $P_{max_{1,1}}$ to $P_{max_{N,N}}$, these can be scaled down by a convenient scaling factor F, and the pressure envelope plotted. The pressure at any level acts perpendicular to the sides of the wall pour. The calculations of points $a'_{i,j}$ and $b'_{i,j}$ on the pressure envelope (Fig. 3-C) are as follows:

$$\theta_i = \tan^{-1}(\lambda_i) \qquad and \qquad \phi_i = \tan^{-1}(\psi_i)$$
$$\Delta x_a = P_{max_{i,j}} \sin(\theta_i)F \quad and \qquad \Delta x_b = P_{max_{i,j}} \sin(\phi_i)F \qquad \text{................ (30)}$$
$$\Delta y_a = P_{max_{i,j}} \cos(\theta_i)F \quad and \qquad \Delta y_b = P_{max_{i,j}} \cos(\phi_i)F$$

Therefore, the co-ordinates of point $a'_{i,j}$ and the co-ordinates of point $b'_{i,j}$ are given by:

$$
\begin{aligned}
X_{a'_{i,j}} &= X_{a_{i,j}} - \left|\Delta x_a\right| & \qquad X_{b'_{i,j}} &= X_{b_{i,j}} - \left|\Delta x_b\right| \\
Y_{a'_{i,j}} &= Y_{a_{i,j}} + \left|\Delta y_a\right| \quad for \quad \lambda_i > 0 & \qquad Y_{b'_{i,j}} &= Y_{b_{i,j}} + \left|\Delta y_b\right| \quad for \quad \psi_i > 0 \\
&= Y_{a_{i,j}} \qquad\qquad for \quad \lambda_i = 0 & &= Y_{b_{i,j}} \qquad\qquad for \quad \psi_i = 0 \\
&= Y_{a_{i,j}} - \left|\Delta y_a\right| \quad for \quad \lambda_i < 0 & &= Y_{b_{i,j}} - \left|\Delta y_b\right| \quad for \quad \psi_i < 0
\end{aligned}
\qquad \text{........... (31)}
$$

6- Computer implementation

The implementation of the data model described above has been coded into a computer program called WalPress. It runs alongside the ProCAD drafting package on a microcomputer. The ProCAD drafting package has a toolkit consisting of several routines that provide access to the information in the drafting software database. These routines are programmed via the PASCAL programming language and interfaced with the drafting software. This method allows digitized entry of the co-ordinates of the wall cross-section by means of a mouse and graphical display of the pressure envelope.

The results can be displayed on the monitor in tabular text form, saved on a disc file, printed or plotted. The pressure envelope plot can be saved in the drafting software database for later retrieval.

2.2.3 Vanhove and co-authors' model [2004]

Vanhove et al. [2004B] selected the silo geometry from the Janssen models [Janssen, 1885] for soil mechanics and applied it to a model aimed at predicting formwork of fresh concrete. The approach treats the granular medium as one that is continuous. The approach assumes perfect frictional contact with the wall. The lateral pressure $P'(h)$ (Fig. 4) is proportioned to the vertical pressure $P(h)$, as follows:

$$P'(h) = K.P(h) \qquad \text{….............. (32)}$$

where K is a phenomenological coefficient, which depends on the internal friction angle φ of the material [Ritchie, 1962A]. As lateral pressure is measured on site at the end of casting, the at-rest state can be applied. In this case, the phenomenological coefficient K may be expressed by:

$$K = 1 - \sin \varphi \qquad \text{….............. (33)}$$

Triaxial tests established that φ for SCC was equal to approximately 5°. The wall friction, according to Janssen's models, can be expressed as follows:

$$\tau(h) = \mu . P'(h) \qquad \text{….............. (34)}$$

Janssen assumes that, at all points, pressure is at the slip threshold, which is taken in its Coulomb form, and for a general approach, equation (34) should be rewritten as follows:

$$\tau(h) = \mu . P'(h) + \tau_o \qquad \text{….............. (35)}$$

where τ is the friction stress (or tangential stress), τ_o is the threshold friction stress, and μ is the friction coefficient, which is assumed to be constant in Janssen's model. A tribometer was designed to find μ, [Djelal, 2001; Vanhove et al., 2004A].
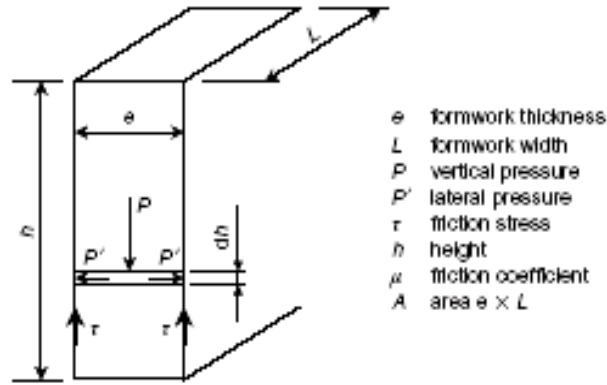
Fig. 4 - Schematic representation of stress in a formwork system [Vanhove et al., 2001]

It is therefore possible to write the equilibrium equation between forces exerted by the material on the walls and the vertical forces as follows:

$$A(P+dP) + \mu.K.P'.(2e+2L)dh = \rho.g.A.dh + A.P \qquad \text{…............. (36)}$$

where A is the area, e is the thickness of the structure, L is the width, ρ is the density of the granular material, and g is the gravity acceleration. According to equations (32) and (36):

$$P'(h) = \frac{\rho.g.A}{(2e+2L).\mu.K} \times \left(1 - e^{\left(\frac{(2e+2L).\mu.K}{A}\right)h}\right) \qquad \text{…............. (37)}$$

This calculation concerns totally relaxed stacking and represents a long-term model. Equation (37) was found to underestimate real lateral pressure exerted by fresh concrete on formwork. Unlike the materials studied by Janssen, fresh concrete has a shear threshold [Tattersall and Bloomer, 1979] and [Hobbs, 1976].

Tests carried out in the granular medium have shown that it is often necessary to apply a coefficient taking into account physical phenomena, which are difficult to quantify. A friction coefficient α is placed in front of the parameters describing grain-to-grain or concrete-to-wall friction.

$$P_{concrete} = \frac{\rho.g.A - \alpha.\tau_o.(2e+2L)}{\alpha(2e+2L).\mu.K} \times \left(1 - e^{-\left(\frac{\alpha(2e+2L).\mu.K}{A}\right)h}\right) \qquad \text{…............. (38)}$$

By analyzing the site results obtained at the end of the concrete casting, it was possible to estimate the coefficient α as 0.15 for SCC cast from the top of the formwork and 0.34 for SCC pumped from the bottom [Vanhove et al., 2004B]. Equation (38) can then be

used to determine the lateral pressure exerted by fresh concrete on formwork by knowing the friction coefficient μ of the concrete against the wall. The authors obtained a good fit between the on-site tests and the tribometer results.

2.2.4 Roussel and Ovarlez's model [2005]

The model proposed by Roussel and Ovarlez [2005] considered that SCC is characterized by a yield stress (τ_o), which is a growing function of resting time. For the sake of simplicity, the authors considered that the yield criterion is a Tresca criterion, i.e. τ_o is the maximum shear stress sustainable by an internal plane. Moreover, below this yield stress, it behaves as an elastic material.

The elastic theory gives, for an isotropic elastic material and in the limit of small deformations, a linear relationship between the stress tensor components σ_{ij} and the strain tensor components ε_{ij}:

$$E\varepsilon_{ij} = (1+\nu_p)\sigma_{ij} - \nu_p\delta_{ij}\sigma_{kk}$$ …............ (39)

where E is the Young's modulus, and ν_p the Poisson's ratio. Roussel and Ovarlez used the coordinates x, y, and z in the directions shown in Fig. 5; the walls are the planes $x = \pm L/2$ and $y = \pm e/2$. The authors recalled a general framework of homogeneous isotropic linear elasticity, and then predicted the behavior of an elastic material of density ρ confined in a rigid rectangular formwork, i.e. displacements:

$$u_x(\pm L/2, y, z) = u_y(x, \pm e/2, z) = 0$$ …............ (40)

The authors imposed a Tresca boundary condition at all points at the walls:

$$\sigma_{xz}(L/2, y, z) = \sigma_{yz}(x, e/2, z) = \tau_o$$ …............ (41)
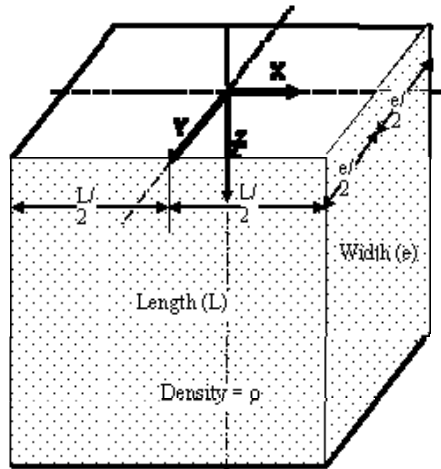
Fig. 5 - Sketch for the formwork wall

Using the stress-strain relationship (39) and internal equilibrium relationship $\partial_i \sigma_{ij} = -\rho\, g_j$, the authors found:

$$\sigma_{zz}(z) = \left(-\rho g + 2\tau_o\left(\frac{1}{L} + \frac{1}{e} \right) \right) z \qquad \ldots\ldots\ldots\ldots(42)$$

$$\sigma_{xx}(z) = \sigma_{yy}(z) = K\left(-\rho g + 2\tau_o\left(\frac{1}{L} + \frac{1}{e} \right) \right) z \qquad \ldots\ldots\ldots\ldots(43)$$

$$\left.\begin{aligned} \sigma_{xz}(x,y,z) &= -\tau_o\left(\frac{x}{L/2} \right) \\[2mm] \sigma_{yz}(x,y,z) &= -\tau_o\left(\frac{y}{e/2} \right) \end{aligned}\right\} \qquad \ldots\ldots\ldots\ldots(44)$$

Comments on the model

(1) Roussel and Ovarlez's Eq. (43) was found to be like the Janssen model [Janssen, 1885] expressed by $\sigma_{xx} = \sigma_{yy} = K\sigma_{zz}$. In the Janssen model, the parameter K is defined as the ratio of horizontal to vertical stresses and is related to the Poisson's ratio, v_p:

$K = v_p / (1 - v_p)$.

(2) The shear stress at the walls can take any value between 0 and τ_o, and the normal stresses at the walls correspond to a value between the profile described by Eq. (43) and the hydrostatic pressure.

(3) Ovarlez et al., [2003] have shown that Janssen's model agrees well with experiments performed in granular columns. However, there is no need for force chains, as in granular materials, for writing such proportionality between vertical and radial stresses.

(4) There is a limitation of the model for low values of K; however, in the case of SCC with standard air contents, this is not the case.

(5) The TRESCA condition at $z = 0$ is not compatible with a free top surface for which
$$\tau_o(L/2, y, z) = \tau_o(x, e/2, z) = 0$$

(6) The vertical displacement is parabolic, which is not compatible with a flat displacement imposed by a rigid base. The solution may be slightly modified near the bottom of the column.

(7) The TRESCA condition may be satisfied somewhere in the bulk if the material is compressible (i.e. $K \neq 1$), e.g., at the center of the formwork where $x = y = 0$. The maximum shear stress on an internal plane is:

$$\tau_m = \frac{1}{2\sqrt{2}} \frac{1-2v_p}{1-v_p}\left(\rho g - 2\tau_o\left(\frac{1}{L}+\frac{1}{e}\right)\right)z \qquad \text{…............. (45)}$$

<u>General case</u>

Boundaries on stresses at the walls may be computed out of any mechanical model (the material may be elastic or not), simply by considering it as a TRESCA material.

a)—The TRESCA criterion imposes that the material cannot lean too much against the walls: $\sigma_{xz}(L/2, y, z) \geq -\tau_o$ and $\sigma_{yz}(x, e/2, z) \geq -\tau_o$

b)—Moreover, the material should not yield in the bulk, i.e.
$$\sigma_{xx}(x, y, z) - \sigma_{zz}(x, y, z) \leq \sqrt{2}\tau_o \quad \text{and} \quad \sigma_{yy}(x, y, z) - \sigma_{zz}(x, y, z) \leq \sqrt{2}\tau_o$$
here it is supposed that $\left|\sigma_{xx}\right|, \left|\sigma_{yy}\right| \leq \left|\sigma_{zz}\right|$

c)—The equilibrium equation of horizontal slices may be written:
$$\int_{-L/2}^{L/2}\int_{-e/2}^{e/2}\left(\frac{\partial\sigma_{zz}(x, y, z)}{\partial z}\right)dxdy = -\rho gLe - 2\int_{-e/2}^{e/2}\sigma_{xz}(L/2, y, z)dy - 2\int_{-L/2}^{L/2}\sigma_{xz}(x, e/2, z)dx$$

d)—The authors assumed that $\sigma_{xx}(x,y,z)$ and $\sigma_{yy}(x,y,z)$ did not vary much with x and y so that:

$$\int_{-L/2}^{L/2}\int_{-e/2}^{e/2} -\sigma_{yy}(x,y,z)dxdy = -\sigma_{yy}(z)Le \ and \ \int_{-L/2}^{L/2}\int_{-e/2}^{e/2} -\sigma_{xx}(x,y,z)dxdy = -\sigma_{xx}(z)Le$$

e)—Combining Eqs. given in a, b, and c, the authors obtained a lower boundary on normal stresses at the walls close to the one obtained with elasticity, without any assumption on the mechanical modeling of the material.

$$\left. \begin{array}{l} -\sigma_{yy}(z) \geq \rho gz - 2\tau_o z(1/L+1/e) - \sqrt{2}\tau_o \\ -\sigma_{xx}(z) \geq \rho gz - 2\tau_o z(1/L+1/e) - \sqrt{2}\tau_o \end{array} \right) \qquad \text{…............. (46)}$$

The main difference with lateral pressure prediction given by Eq. (43) is that for sections where the depth is on the order or less than that of the width, the boundary could be lower than in the case of the elastic model. In such an approach, the shear stress at the walls can vary between 0 and τ_o, depending on the local deformation. Even if the yield stress of the material is evolving, there should not be any change at the walls as there is no deformation. In the case of concrete, this deformation can occur as the material slightly consolidates under its own weight [Khayat and Assaad, 2005B], and a surface settlement can be obtained. This means that the assumption that the yield shear stress is fully mobilized at the wall is licit and remains licit as the yield stress increases with the resting time.

Comparison with experimental measurements

The above approach was compared to a field experiment where concrete was used to fill formwork measuring 10 m in height, 5.44 m in length, and 0.20 m in width. The concrete had a unit weight (ρ) of 2,265 kg/m^3 and was pumped from the bottom of the formwork at high casting rate (R) of 43.5 m/h. Pressure sensors mounted at 0.55, 1.95, and 3.36 m from the bottom were used to determine lateral pressure. From Eq. (43), the shear stress τ_i between depths z_i and z_{i+1} can be computed as follows:

$$\tau_i = \frac{1}{2}\left(\frac{\sigma_{xx}(z_{i+1}) - \sigma_{xx}(z_i)}{z_{i+1} - z_i} + \rho g\right)\frac{1}{(1/L+1/e)} \qquad \text{…............. (47)}$$

The calculated shear stress and the measured yield stress evolutions are compared in Fig. 6 and show quantitative agreement despite the uncertainty of yield stress measurement.
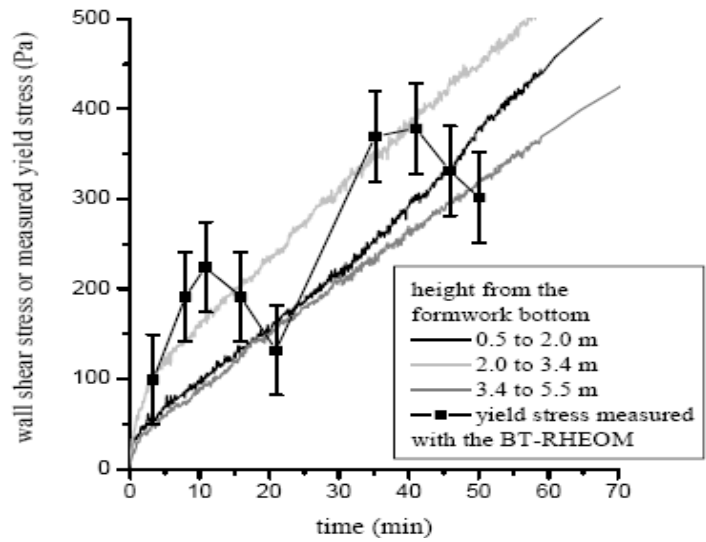
Fig. 6 - Comparison between calculated shear stress and measured yield shear stress in terms of resting time [Roussel and Ovarlez, 2005]

Practical application of the proposed model

(I) Evolution of apparent yield stress at rest

It can be assumed that the evolution of yield stress at rest is linear with time (at least at early age), and it may be described using Eq. (48) as:

$$\tau_o(t) = A_{thix}t \qquad\qquad ….............. (48)$$

where *t* is the resting time and A_{thix} is a flocculation coefficient.

(II) Computation of the maximum pressure during casting

It was assumed that:

(i) the casting rate (R) is constant (at a time *t* after the beginning of casting, $H = R.t$);

(ii) the vertical deformation of the concrete under its own weight is always sufficient for the shear stress to reach τ_o; and

(iii) at the bottom of the zone where concrete is at rest (everywhere in the formwork except in the upper layer of thickness *e*), the resting time is maximum = (H - e)/R.

Therefore, the yield stress of the concrete varies with the depth and needs to be integrated in order to compute the lateral stress at the bottom of the formwork, as follows:

$$\sigma_{xx} = \sigma_{yy} = \frac{K}{Le}\left(\rho gHLe - 2(L+e) \int_0^{H-e} \tau_o(z)dz \right) \qquad \text{…............. (49)}$$

Using Eq. (48), $H = R.t$, and with $L >> e$: Eq. (49) becomes

Rectangular formwork with width, e	Circular column with radius, r

$$\sigma_{xx} = \sigma_{yy} = K\left(\rho gH - \frac{(H-e)^2 A_{thix}}{eR} \right) \qquad \sigma_{xx} = \sigma_{yy} = K\left(\rho gH - \frac{(H-r)^2 A_{thix}}{rR} \right)$$

For $H >> e$ $\qquad$ For $H >> r$

$$\sigma_{xx} = \sigma_{yy} = KH\left(\rho g - \frac{HA_{thix}}{eR} \right) \text{......(50)} \qquad \sigma_{xx} = \sigma_{yy} = KH\left(\rho g - \frac{HA_{thix}}{rR} \right) \text{.....(51)}$$

The only parameter that is fitted in the predictions of the model is A_{thix}. This factor is estimated at 0.6 Pa/s for SCC tested by Billberg [2003]. This value is an average value as the additives were different from one concrete to another. $A_{thix.}$ is equal to 0.2 Pa/s for the SCC tested by Khayat and Assaad [2005B]. These values were in the same order of magnitude as those obtained for the SCC tested by the authors (0.1 - 0.2 Pa/s), which confirms the quantitative validity of the proposed approach [Roussel and Ovarlez, 2005].

The relative lateral stress $\sigma^{'}$ is defined as the ratio between the lateral stress and the associated hydrostatic pressure at that depth.

$$\sigma^{'} = \frac{\sigma_{xx}}{P_{hyd.}} = \frac{\sigma_{xx}}{\rho gH} = K\left(1 - \frac{HA_{thix}}{\rho geR} \right) \qquad \text{…............. (52)}$$

This critical casting rate fulfills the following condition:

$$\frac{\partial \sigma_{xx}}{\partial H} = K\left(\rho g - \frac{2HA_{thix}}{eR} \right) = 0 \qquad \text{…............. (53)}$$

and thus, the critical rate can be expressed as follows:

$$R_{crit} = \frac{2HA_{thix}}{e\rho g} \qquad \text{…............. (54)}$$

From Eq. (54), it becomes possible to decrease the lateral stress exerted on the formwork by reducing the casting rate to the critical value.

2.2.5   Graubner and Proske's model [2005A]

Graubner and Proske [2005A] also established a model to predict SCC lateral pressure against the formwork based on the Silo Theory by Janssen. An experimental column measuring 4.30 m × 0.30 m × 0.30 m with measurement points M1, M2, M3, and M4 at heights of 0.30, 1.30, 2.30, and 3.30 m from the base, respectively, was used for monitoring lateral pressure (Fig. 7). The assumed pressure distribution is shown in Fig. 8.

The steps followed to construct the model are as follows:

The equilibrium equation $\quad A.\sigma_v + \gamma_c.A.dh = A.(\sigma_v + d\sigma_v) + \tau_W.U.dh \qquad$ …............. (55)

Pressure ratio $\qquad\qquad \lambda(t) = \sigma_h / \sigma_v \qquad\qquad\qquad$ …............. (56)

Friction coefficient $\qquad \mu(t) = \tau_W / \sigma_h \qquad\qquad\qquad$ …............. (57)

$\qquad\qquad\qquad\qquad\qquad dh = dt\, v \qquad\qquad\qquad\qquad$ …............. (58)

Differential equation $\qquad \dfrac{d\sigma}{dt} + \sigma_v.\lambda(t).\mu(t).\dfrac{U}{A}v = \gamma_c v \qquad$ …............. (59)

Vertical pressure $\qquad \boxed{\sigma_v = e^{-\int \lambda(t).\mu(t)v.\frac{U}{A}dt} . \left(\int \gamma_c v\, .e^{\int \lambda(t).\mu(t)v.\frac{U}{A}dt} .dt + C \right)}$ … (60)

Horizontal pressure $\qquad \boxed{\sigma_h = \sigma_v .\lambda(t)} \qquad\qquad\qquad$ …............. (61)
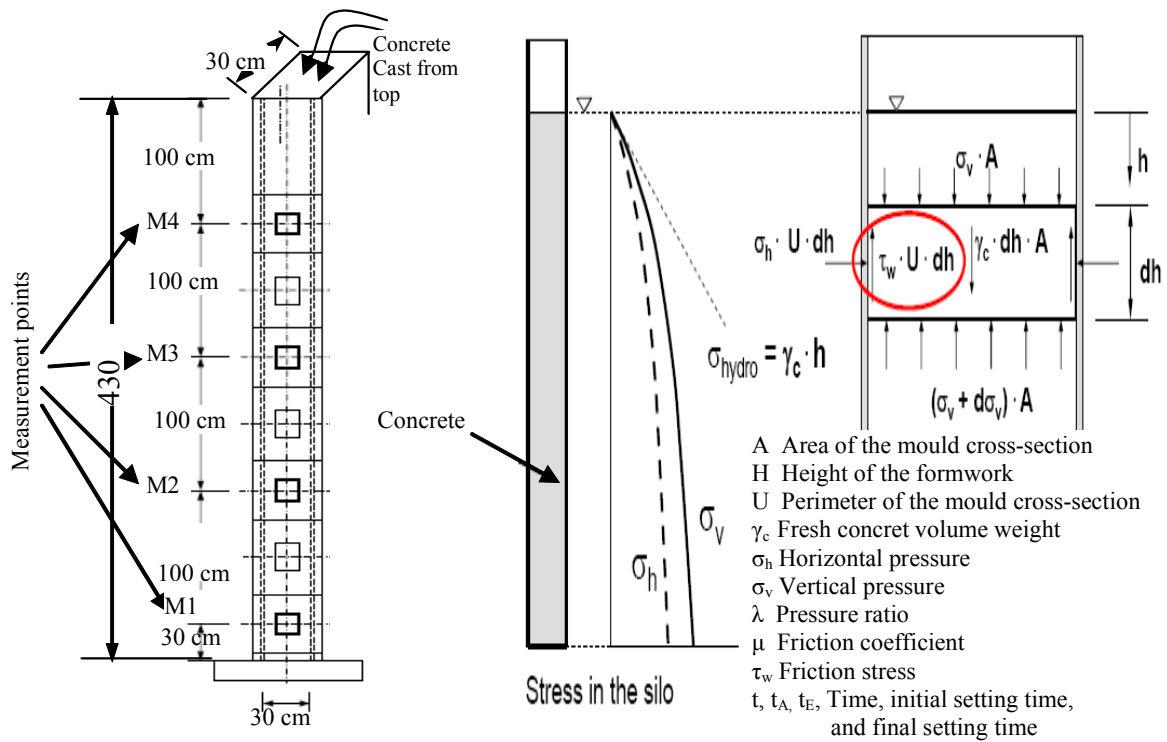
Fig. 7 - Experimental column and sketch for pressure calculations
[Graubner and Proske, 2005B]
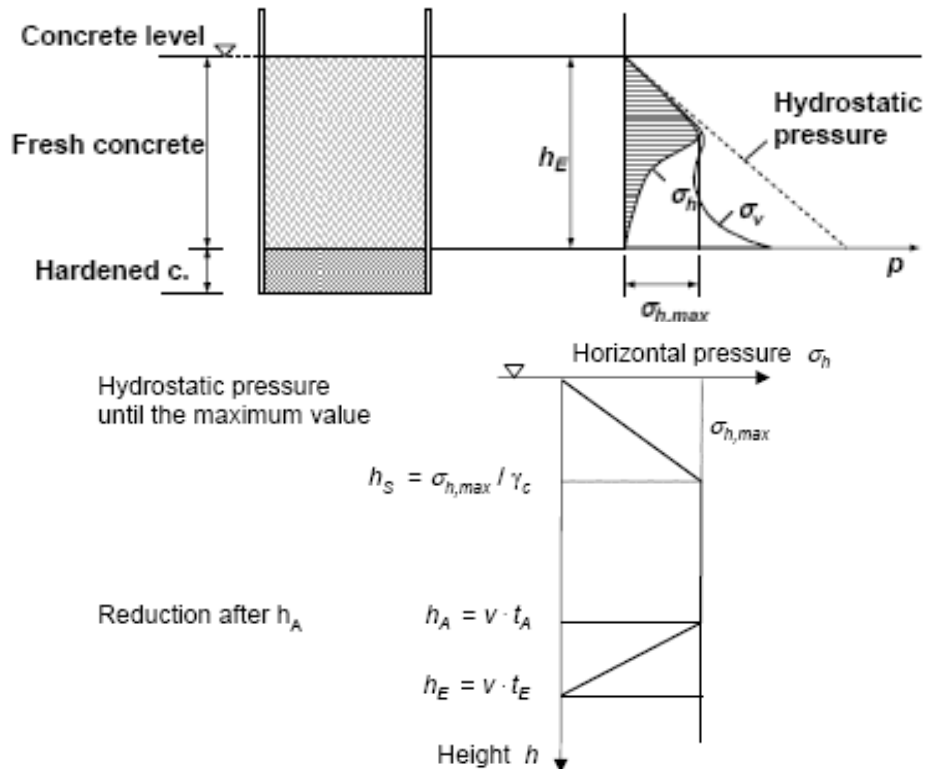
Fig. 8 - Pressure distribution [Graubner and Proske, 2005A]

Graubner and Proske used the testing machine shown in Fig. 9 to determine the model parameters.
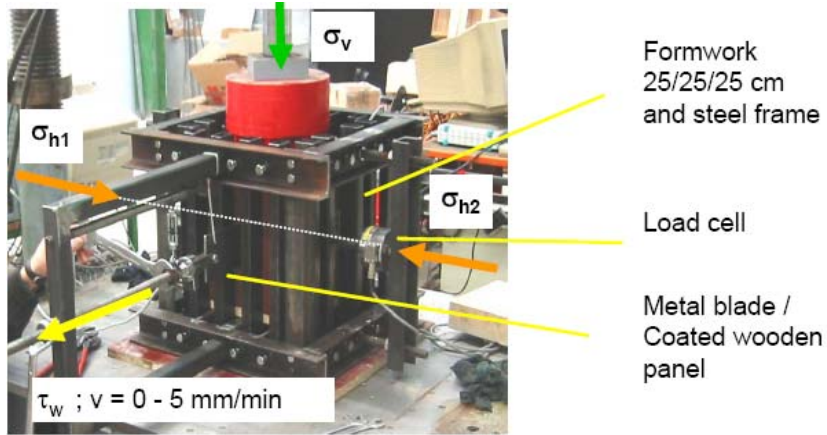
Fig. 9 - Testing machine used to determine model parameters
[Graubner and Proske, 2005A]

The pressure ratio (λ) and the friction coefficient (μ) for the calculation can be obtained from Eqs. (62) and (63) or from Fig. 10.

$$\lambda = 1 - 0.18(t/t_E) + 2.43(t/t_E)^2 - 9.14(t/t_E)^3 + 7.84(t/t_E)^4 - 1.79(t/t_E)^5$$

$\Rightarrow \sigma_v = 80 \text{ kN/m}^2$ …......... (62)

$$\mu = 0.23(t/t_E) - 1.093(t/t_E)^2 + 1.72(t/t_E)^3 + 0.002(t/t_E)^4 - 0.636(t/t_E)^5$$

$\Rightarrow \sigma_v = 80{\sim}170 \text{ kN/m}^2$ .... (63)
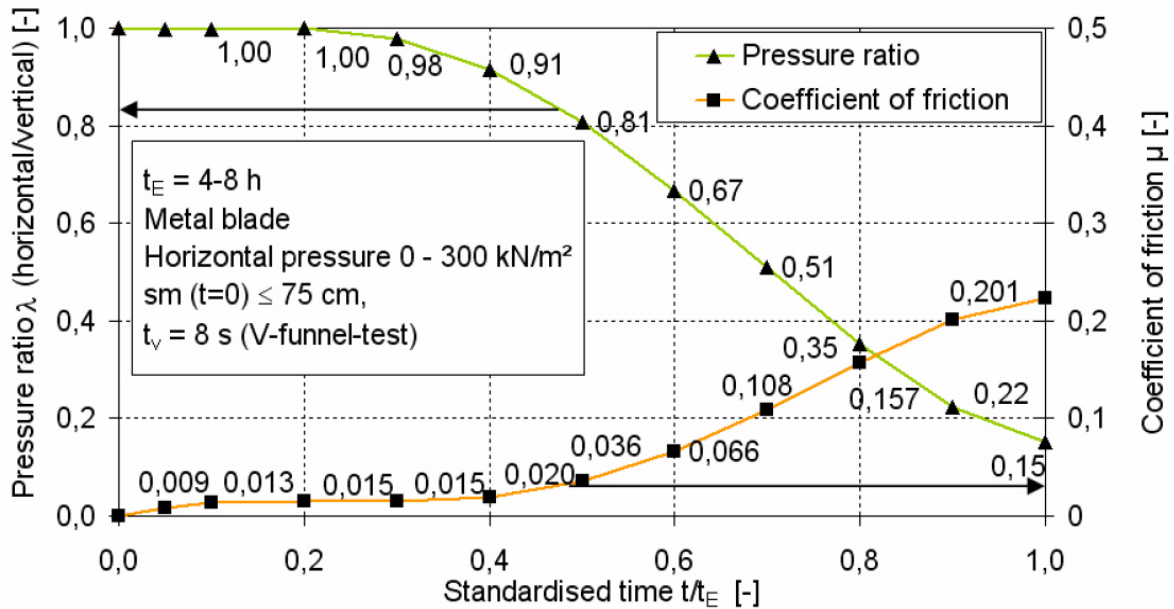
Fig. 10 - Pressure ratio λ and friction coefficient μ for the calculation of formwork pressure [Graubner and Proske, 2005A]

An example for the maximum lateral pressure distribution calculated using the Graubner and Proske's model given in Eqs. (60) and (61) which use the relationships of pressure ratio λ and friction coefficient μ of Eqs. (62) and (63), respectively, is illustrated in Fig. 11. In this figure, $b = (b_{s1} . b_{s2}) / (b_{s1} + b_{s2})$, where b_{s1} and b_{s2} represent the dimensions of the formwork cross-section. For wall elements and small cross sections: b is taken as the smallest width of the section.

Consideration of the setting time

$$t_A \leq 4h \quad \rightarrow \quad \sigma_{h,max}(t_A) = \sigma_{h,max}(chart) \qquad \text{…............. (64)}$$

$$t_A > 4h \quad \rightarrow \quad \sigma_{h,max}(t_A) = \sigma_{h,max}(chart).\frac{t_A}{4h} \qquad \text{…............. (65)}$$

Filling from bottom by pumping

In this case, hydrostatic pressure should be assumed.
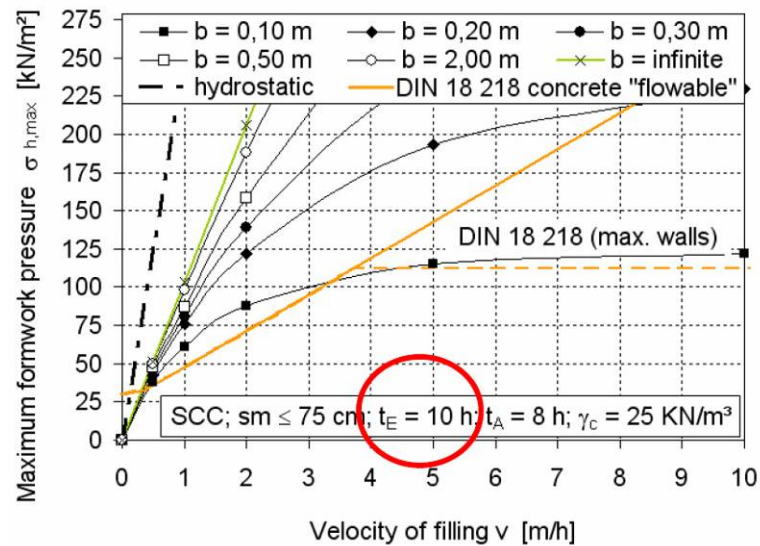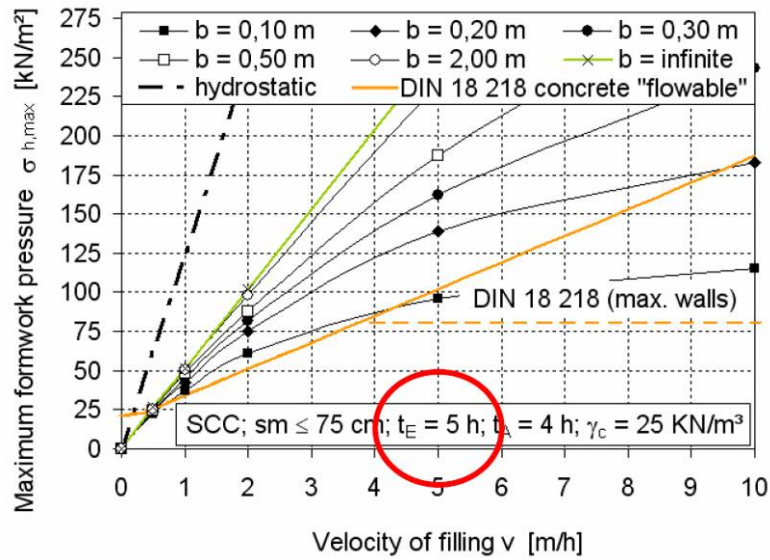
Fig. 11 - Calculated maximum pressure using Graubner and Proske's model [2005A]

Figure 12 shows a comparison between the data calculated from the model and the data measured.
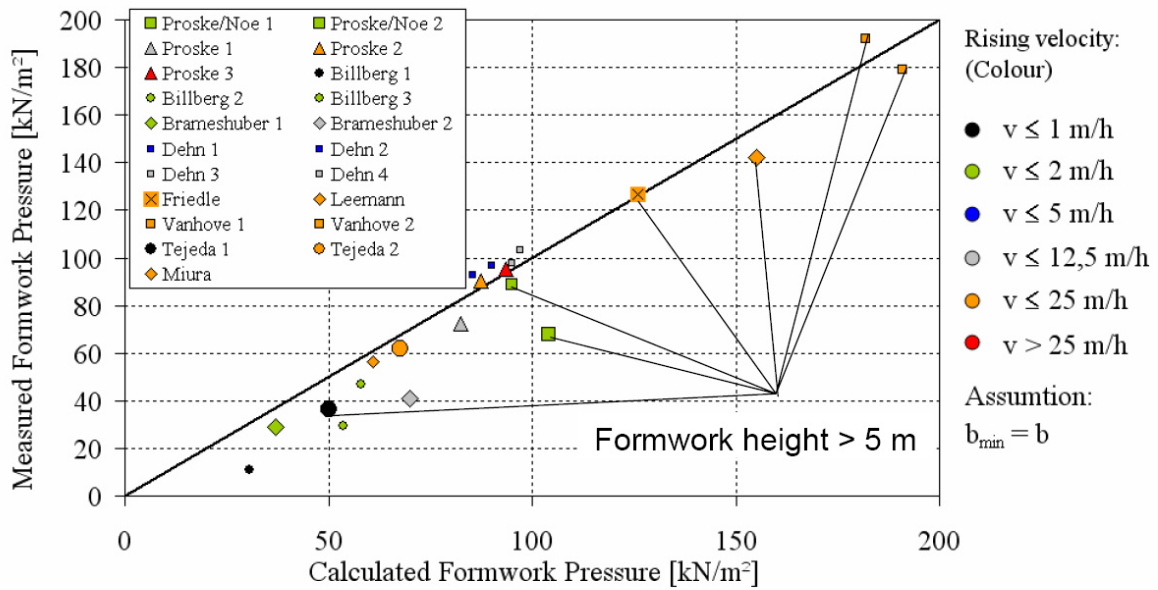
Large symbols: Setting time is known
Small symbols: Setting time is estimated
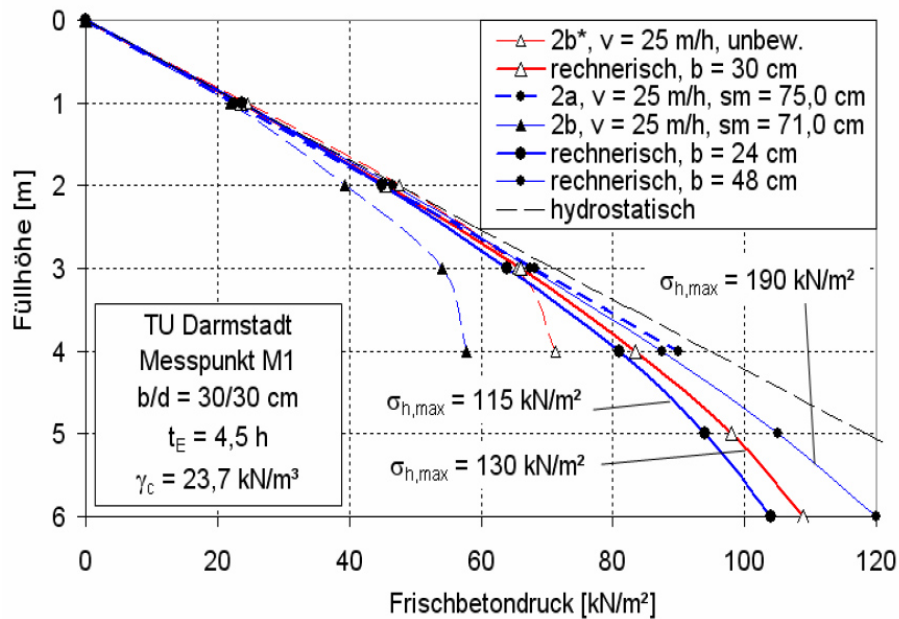
Fig. 12 - Comparison between the calculated data using Graubner and Proske's model and
the measured data – Influence of reinforcement [Graubner and Proske, 2005B]
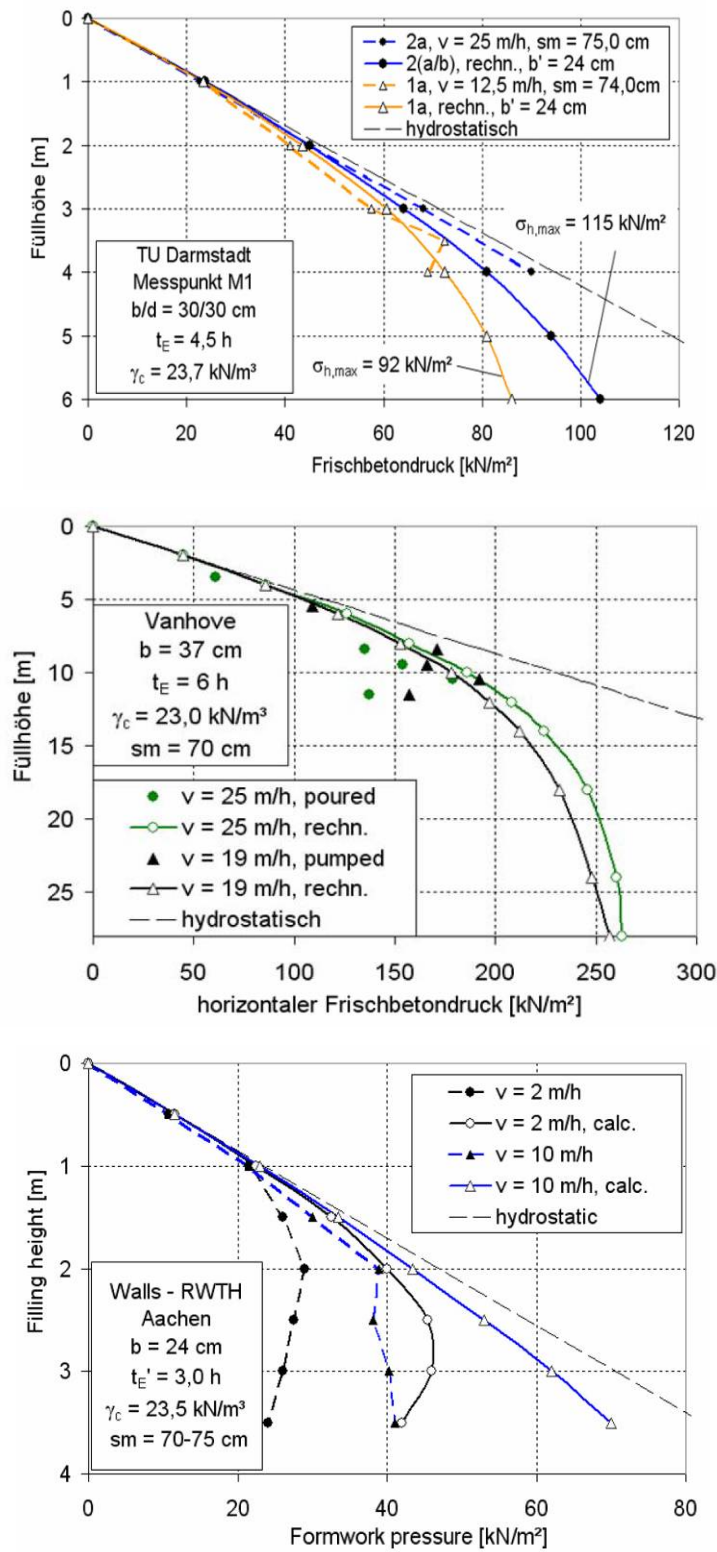
33

Fig. 12 (cont.) – Comparison between the calculated data using Graubner and Proske's
model and the measured data – Influence of casting speed
[Graubner and Proske [2005B]
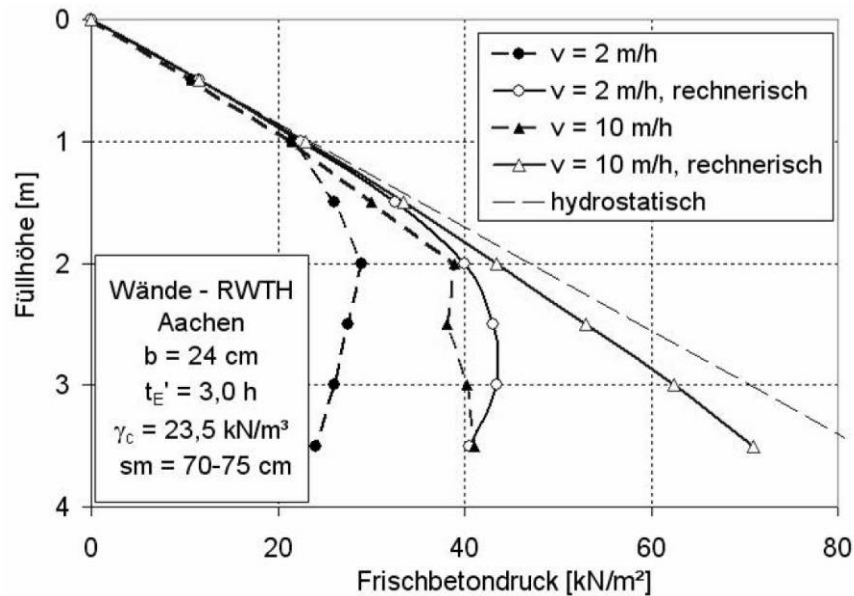
34

Fig. 12 (cont.) – Comparison between the calculated data using Graubner and Proske's model and the measured data [Graubner and Proske, 2005B]

From the results presented in Graubner and Proske's model, the following can be concluded:

1. Considering the time dependent behavior of the concrete, the Silo theory describes approximately the real stress state.

2. In general, the assumption of hydrostatic pressure is not warranted.

3. The maximum formwork pressure depends significantly on the casting rate, setting time of the concrete, and formwork width. The smaller the formwork width, the lower the formwork pressure would be.

2.2.6 Khayat and Assaad's model [2005A]

An extensive investigation was carried out by the authors to determine the key factors affecting formwork pressure of SCC. The thixotropy of the SCC has been shown to have considerable influence on both the initial lateral pressure and the pressure decay. SCC with high degree of thixotropy is shown to exert lower initial lateral pressure and higher rate of pressure drop in time compared to those with low thixotropy. Khayat and Assaad [2005A] used an instrumented PVC column measuring 0.20 m in diameter and 2.8 m to monitor the variations in lateral pressure of SCC soon after casting. A similar column measuring 1.1 m

35

in height was used to monitor pressure decay until the cancellation of pressure, which corresponds to setting. The columns were cast by discharging the SCC continuously from the top at a rate of rise of 10 m/h, for the most part, and without any mechanical consolidation.

In total, 70 SCC mixtures made with different mix designs and material constituents were prepared to derive the pressure prediction models. The mixtures had slump flow consistencies, temperatures, unit weights, and air volumes of 650 ± 15 mm, 20 ± 3 °C, $2{,}200 \pm 200$ kg/m³, and $7\% \pm 2\%$, respectively. The breakdown area (A_b) determined from structural breakdown curves (see Section 4.2.2) was used to determine thixotropy at time intervals. The values A_{b1}, A_{b2}, and A_{b3} were determined at time intervals of T1 (0-30 min), T2 (60-90 min), and T3 (120-150 min) [Assaad et al., 2003A].

Relationship between thixotropy and relative lateral pressure

The relationship between thixotropy (A_b) and the relative lateral pressure (K) obtained near the bottom of the 2.8-m-high column is illustrated in Fig. 13 for all tested SCC mixtures. The relative lateral stress K is defined as the ratio between the lateral stress and the associated hydrostatic pressure at that depth. The equations enabling the estimate of K at different time intervals with respect to thixotropy can be expressed as follows:

K_0 (%) = $-$ 0.047 A_{b1} + 105.8   (R^2 = 0.89)   .... (66)

K_{100} (%) = $-$ 0.099 A_{b2} + 112.2   (R^2 = 0.85)   .... (67)

K_{200} (%) = $-$ 0.125 A_{b3} + 116.8   (R^2 = 0.84)   .... (68)

where,

  K : relative pressure = $P_{maximum}$ / $P_{hydrostatic}$ (pressure in kPa)

  K_0, K_{100}, and K_{200}: relative pressures determined at elapsed times of 0, 100, and 200 min after the end of casting, respectively; and

  A_{b1}, A_{b2}, and A_{b3} structural breakdown areas determined at T1, T2, and T3 time intervals, respectively.
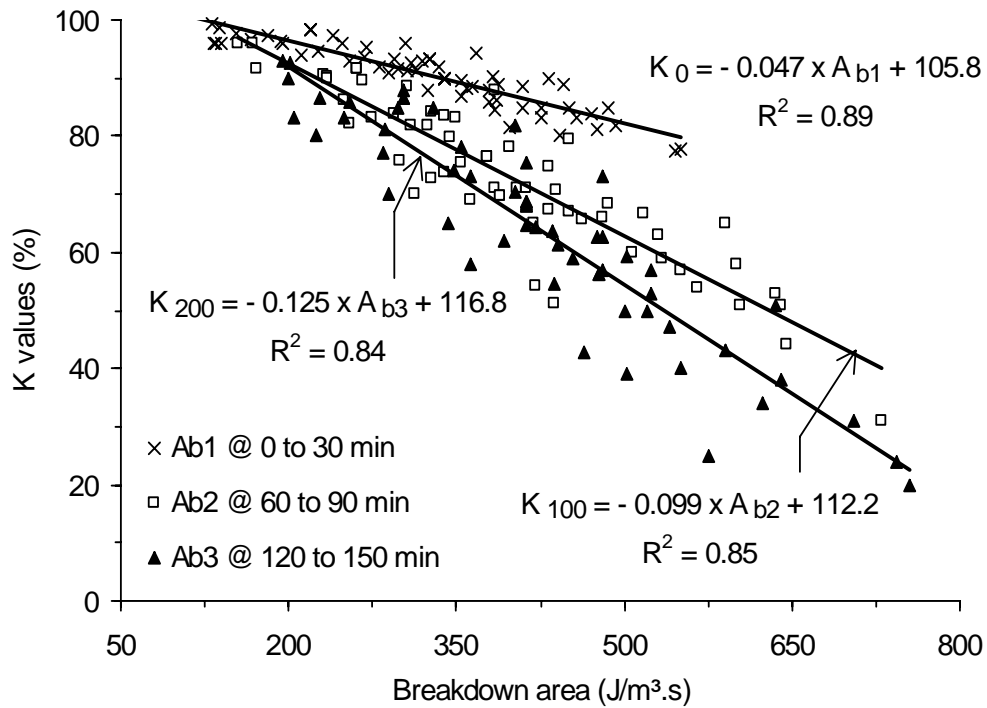
Fig. 13 - Ab vs. relative lateral pressure measured initially, and after 100 and 200 min [Khayat and Assaad, 2005A]

The K_{100} and K_{200} values can be estimated from the A_{b1} index since A_{b2} and A_{b3} values showed good correlations to the A_{b1} value, as demonstrated in Fig. 14.

$$A_{b2} = 1.14 \ A_{b1} \qquad\qquad (R^2 = 0.96) \qquad \text{................................. (69)}$$

$$A_{b3} = 1.29 \ A_{b1} \qquad\qquad (R^2 = 0.90) \qquad \text{................................. (70)}$$

By substituting Eq. (69) and (70) into Eq. (67) and (68), the K_{100} and K_{200} values can be estimated from the breakdown area determined initially at the time interval T1 (0-30 min), as follows:

$$K_{100} \ (\%) = - \ 0.113 \ A_{b1} + 112.2 \qquad (R^2 = 0.83) \qquad \text{................................. (71)}$$

$$K_{200} \ (\%) = - \ 0.161 \ A_{b1} + 116.8 \qquad (R^2 = 0.81) \qquad \text{................................. (72)}$$
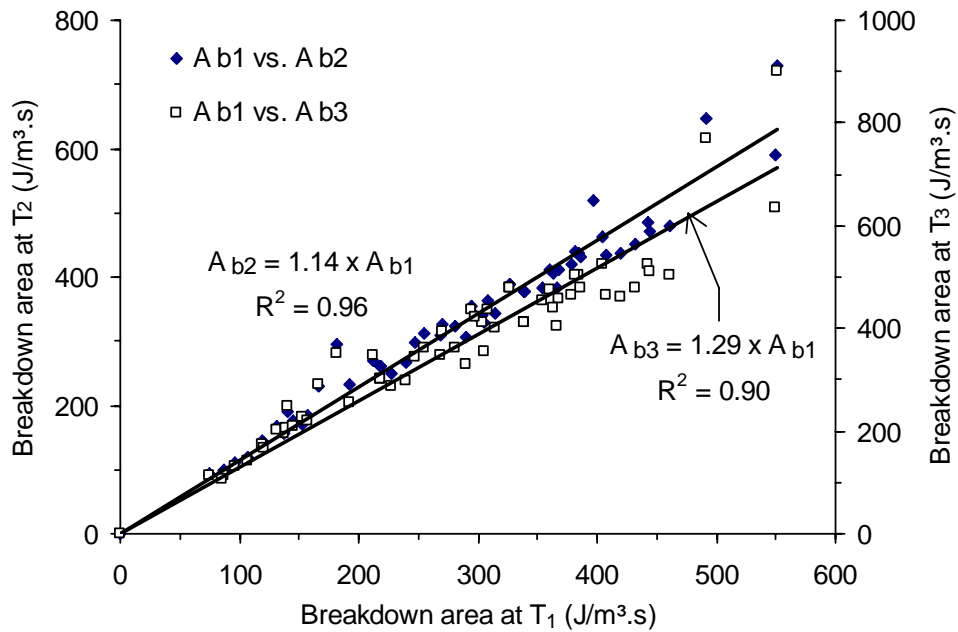
Fig. 14 - Relationship between breakdown areas determined at various time intervals
[Khayat and Assaad, 2005A]

Relationship between drop in apparent viscosity and K values

The drop in apparent viscosity was also determined to estimate lateral pressure. This value is calculated as: $\Delta\eta_{app} = (\tau_i - \tau_e) / \gamma$, where γ refers to the shear rate (s^{-1}) corresponding to a given rotational velocity. Variations in $\Delta\eta_{app}$ determined at 0.3 and 0.9 rps during (0-30 min) with respect to K_0 are plotted in Fig. 15. The equations relating K_0 values with $\Delta\eta_{app}$ determined at 0.3 and 0.9 rps during (0-30 min) were as follows:

For N = 0.3 rps, K_0 (%) = $-$ 0.112 $\Delta\eta_{app}$ + 103.9   (R^2 = 0.74) .... (73)

For N = 0.9 rps, K_0 (%) = $-$ 0.168 $\Delta\eta_{app}$ + 106.7   (R^2 = 0.82) .... (74)
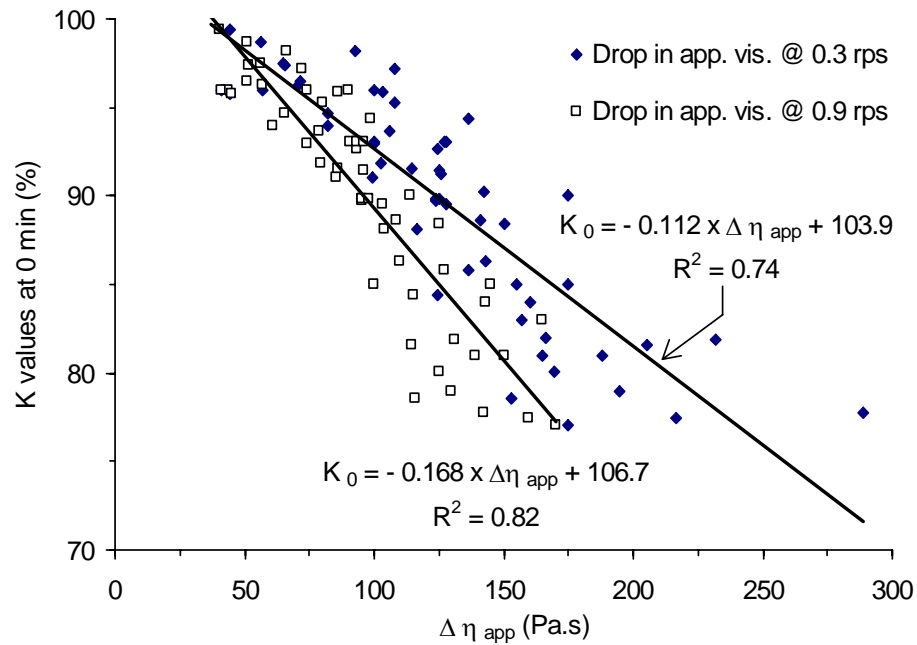
Fig. 15 - Drop in apparent viscosity vs. initial lateral pressure [Khayat and Assaad, 2005A]

Effect of concrete head on lateral pressure

In order to evaluate the effect of concrete head on the initial pressure, the K_0 values were determined at various heights along experimental columns filled with concrete to heights of 1, 1.3 2, 2.4, and 2.8 m. Fig. 16 presents the relationships between concrete head and K_0 values for SCC with different thixotropy values for mixtures cast at 10 m/h. As expected, the relative pressure decreases with the increase in height given the longer time duration needed to fill the column sections.
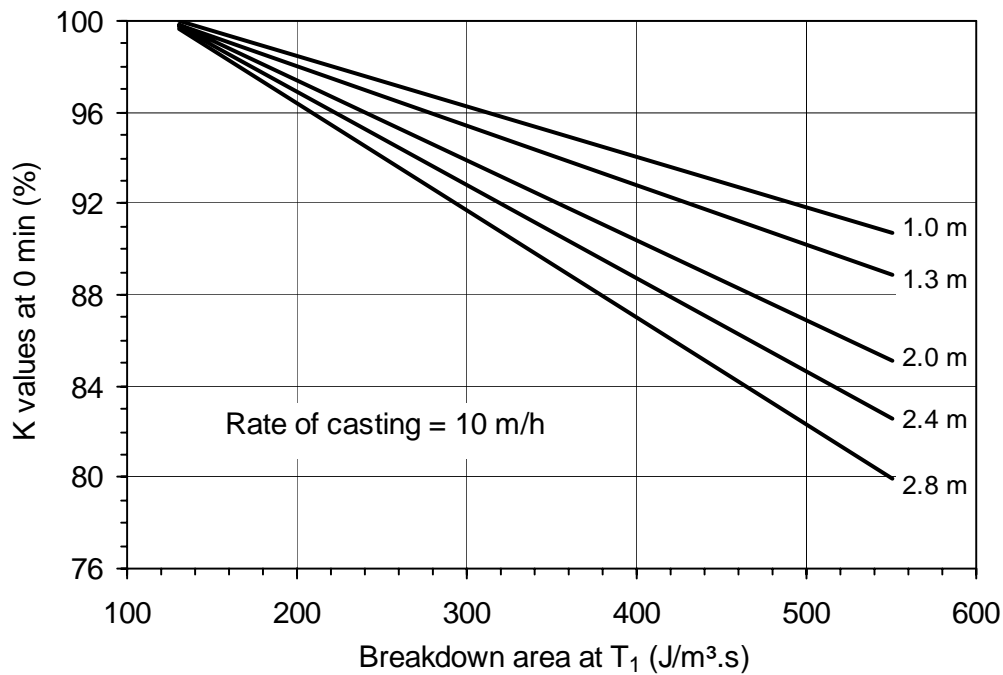
Fig. 16 - Effect of concrete head on variations of K0 values for mixtures having various degrees of breakdown areas [Khayat and Assaad, 2005A]

Effect of casting rate on proposed models

Casting rate (R) of used to derive the above pressure models were set to 10 m/h. In order to evaluate the effect of changes in R on the prediction models, a reference SCC mixture was cast in the 2800-mm high column at R values of 5, 15, 25, and 30 m/h. Based on the results, the following model was proposed to account for variations in casting rate:

$$K_0 \ (\%) = 9.254 \ Ln \ (R) + 66.5 \qquad (R^2 = 0.95) \qquad \text{........................} \ (75)$$

The K models established earlier for R of 10 m/h can then be modified as follows:

$$K_0 \ \text{at any given R (m/h)} = K_0 \ \text{determined at 10 m/h} + \Delta \ K_0 \qquad \text{........................} \ (76)$$

where $\Delta \ K_0$ is the spread of K_0 from values predicted for R = 10 m/h. A number of $\Delta \ K_0$ values are given in Table 1 for various casting rates.

Table 1 - Spread in pressure from relative pressure determined at casting rate of 10 m/h

Casting rate (R), m/h	5	7	10	13	15	17	20	23	25	30
$\Delta \ K_0$ (%) from Eq. 76	-6.1	-3.1	0	2.3	3.6	4.7	6.1	7.3	8.0	9.6

Relationship between measured and predicted K values

The relationships between K values measured directly from the 2800-mm experimental column (K_M) and those predicted (K_P) using Eq. (66) and (68) are plotted in Fig. 17 for the tested SCC. Good correlation can be established between the two values.
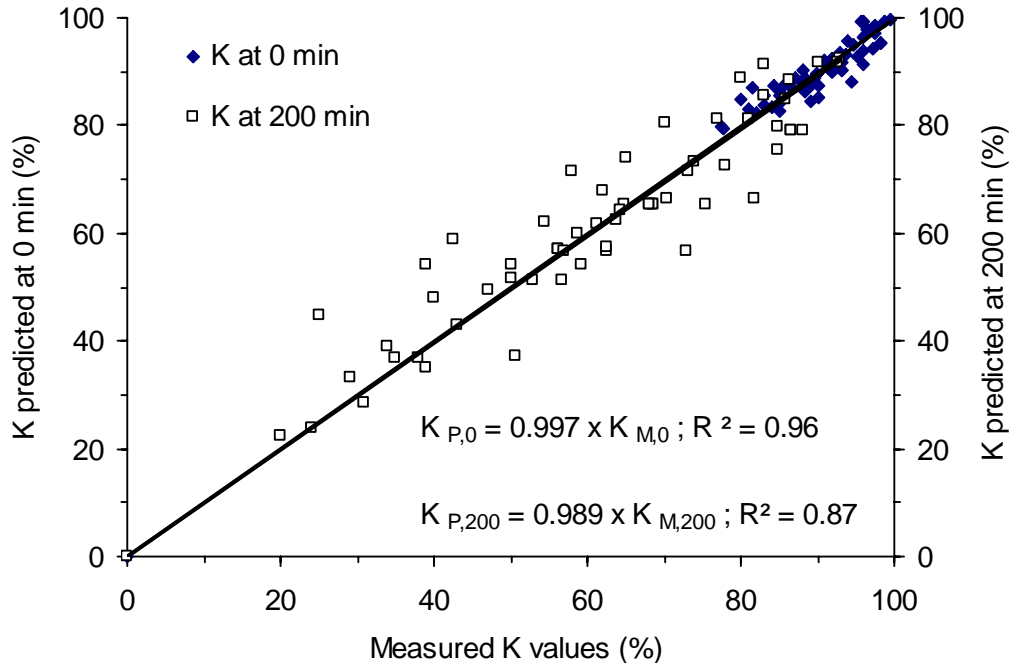
Fig. 17 - Relationship between predicted and measured K [Khayat and Assaad, 2005A]

3. RELATIONSHIP BETWEEN FORM PRESSURE AND RHEOLOGY OF SCC

3.1 Thixotropy of cement-based materials

As illustrated above, form pressure developed by SCC can be related to the degree of structural build-up of the material after a given period of rest. In cementitious materials, this structural build-up is a function of both the reversible structural changes from the thixotropic phenomena and the irreversible structural changes due to hydration mechanisms altering the resulting microstructure. Barnes et al. [1989] defined thixotropy as a decrease in time of viscosity under constant shear stress or shear rate, followed by a gradual recovery when the stress or shear rate is removed. The transition of the material from the at-rest state to shearing conditions, and vice versa, is illustrated in Fig. 18 [Barnes, 1997].

Oftentimes, thixotropy is confused with shear-thinning behavior of non-Newtonian fluids. It is important to point out that thixotropy is related to Non-Newtonian time-dependent changes, whereas shear-thinning refers to Non-Newtonian time-independent changes. In a plot of viscosity versus time (for a given shear rate), a shear thinning fluid will have a constant viscosity for any given time, whereas a thixotropic fluid will display a decrease in viscosity. In actuality, nearly all shear-thinning materials are thixotropic because it takes time for the microstructure to realign itself.
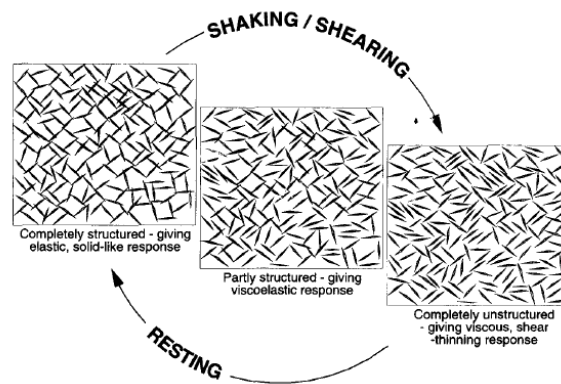
Fig. 18 - Breakdown and build-up of a 3-D thixotropic structure [Barnes, 1997]

Thixotropy of cement-based systems is strongly dependent on mixture composition and processing parameters, such as mixing and vibration. Tattersall and Banfill [1983] reported that cement characteristics, such as packing density, fineness, and chemical composition can significantly affect thixotropy. Struble [1991] suggested that thixotropy and the yield stress are dependent on both particle packing and interparticle links responsible for flocculation, while viscosity depends primarily on particle packing.

Thixotropic behavior typically occurs in heterogeneous materials, and it occurs due to the finite time that it takes for the microstructure to change from one state to another. The specific causation of thixotropy depends on interactions at the molecular level and unfortunately, these mechanisms are poorly understood. The decrease in apparent viscosity that is accompanied with thixotropy is believed to be due to the resulting flow altering the microstructure. When a specific microstructure is agitated, the viscosity will decrease with the shearing time until an equilibrium state (the lowest energetically possible state) is

achieved. Thus, the time scale in which the microstructural changes take place is an important parameter in the consideration of thixotropy [Ferron et al., 2006]. According to Barnes [1997], such structural changes can be attributed to two simultaneous processes: shear induced breakdown of the structure and build-up of the structure whereby the yield stress increases with increasing recovery time. Helmuth (as reported by Struble [1991]) suggested that mixing breaks down the flocculent structure responsible for thixotropic behavior. Thus, from a microstructural perspective, thixotropy is a result of structural degradation due to the rupturing of flocs of linked particles [Saak, 2000]. In cement paste, it is likely that thixotropy is governed by a combination of reversible coagulation, dispersion, and then re-coagulation of the cement particles [Wallevik, 2003]. When a cementitious suspension is sheared, its network structure is broken into smaller agglomerates and with continued shearing there is eventually an equilibrium state in which the agglomerates can not be broken into smaller fragments. When the suspension is at rest, the particles can form weak physical bonds and agglomerate into a network. The rheological behavior of the suspension is related to this network structure and the rate at which it can form.

The phenomenon demonstrating the effect of rest time on thixotropy for highly flowable concrete containing VMA is plotted in Fig. 19 [Assaad, 2004]. After 2 min of rest following placement of the concrete in the bowl of a rheometer, the concrete was subjected to constant rotational speed of 0.9 rps resulting in a continuous breakdown of the flocculated structure. Such breakdown with time under the imposed shear rate indicates the origin of thixotropy. An equilibrium structure is achieved after approximately 10 sec where a balance between flocculation and deflocculation is reached. This results in a constant viscosity ($\eta = \tau_e / \dot{\gamma}$, where τ_e is the shear stress at equilibrium (Pa), and $\dot{\gamma}$ is the shear rate in (s^{-1})). In contrast, under static conditions, individual particles of the concrete begin to collide and flocculate causing progressive change in the microstructure through the formation of a gel structure and interparticle links. In other words, when the shear is stopped, and the material is allowed to rest for 4 min, the experiment conducted using the same rotational speed of 0.9 rps shows that the measured viscosity is initially higher, but that it decreases again to the same equilibrium shear stress noted after the 2-min rest period.
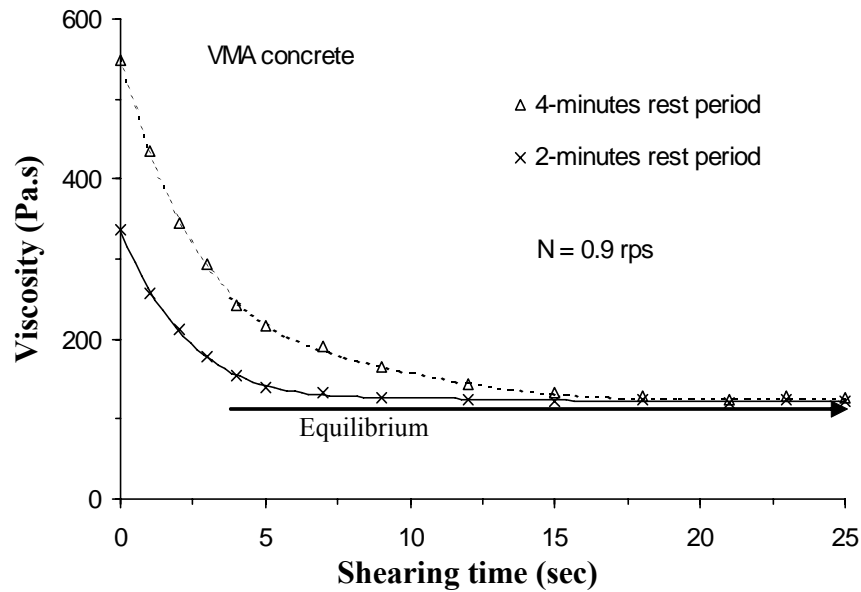
Fig. 19 - Variation of viscosity with time for VMA concrete following 2 and 4 min of rest, [Assaad, 2004]

The increased flocculation in cement-based materials can also be caused by hydrogen and ionic bonds that can develop between adjacent molecules leading to a rise in cohesiveness [Khayat et al., 2002A]. The longer the material is maintained at rest, the more the thixotropic structural build-up becomes significant, thus requiring higher initial yield stress to breakdown the structure. Once shearing occurs, the particle spatial distribution and alignment become asymmetrical in the flow direction, and the number of entanglements or associations decreases to the minimum. This leads, thereby, to similar values of viscosity at equilibrium [Khayat et al., 2002A].

Several attempts have been made to relate the experimental observations, such as those given in Fig. 19, to physical processes taking place in flocculated suspensions in order to propose physical models accounting for the breakdown phenomenon. The most quantitative theory was elaborated by Tattersall (summarized in [Tattersall and Banfill, 1983]) for describing the thixotropic behavior of cement paste. The basis of the structural breakdown theory is related to work done in a rotational viscometer to overcome normal viscous forces, to break existing linkages, and to maintain broken ones. The equation used to describe the decay in stress with time for a given shear rate can be expressed as:

$$\tau = \tau_e + (\tau_o - \tau_e)\, e^{-\beta.t} \qquad\qquad …............. (77)$$

where τ_e is equilibrium stress, τ_o is initial stress, β is breakdown constant, and t is time. The breakdown constant was shown to depend on the number and strength of interparticle links, as follows:

$$\beta = \frac{(2\,\pi\,K)\,w\,(w - w_1)}{n_o\,\psi} \qquad \text{…............. (78)}$$

where K and w_1 are constants, w is the angular velocity (equivalent to strain rate), n_o is the number of links at the beginning of the experiment, and ψ is the work required to breakdown each link.

3.2 Approaches to quantify thixotropy of concrete

There exist a number of test protocols that can be used to evaluate the structural build-up or the thixotropy of concrete. Measuring the rheology of cement paste gives an indication of the colloidal state and interactions that are occurring. There are no standard methods to measure thixotropy, but typical thixotropic experiments often consist of either rheological tests conducted at a constant shear rate (equilibrium flow curves) or using varied sheared rates (hysteresis curves) [Lapasin et al. 1983, Barnes, 1997, and Mewis, 1979].

3.2.1 Hysteresis curves

Thixotropic materials have typical hysteresis loops that are readily plotted from shear rate-shear stress experiments. Ish-Shalom and Greenberg [1962] used hysteresis measurements to characterize the flow properties of cement paste. In such tests, the shear rate ($\dot{\gamma}$) is increased from zero to some pre-defined maximum value and then decreased back to zero. When the shear stress (τ) is plotted as a function of shear rate, the up (loading) and down (unloading) curves can be obtained, as illustrated in Fig. 20. The enclosed area between the up and down curves (i.e. hysteresis) provides a measure of the degree of thixotropy in the sample [Tattersall and Banfill, 1979]. The down curve is normally linear and can easily fit to the Bingham model given as follows:

$$\tau = \tau_o + \mu\,\dot{\gamma} \qquad \text{…............. (79)}$$

where τ_o and μ are the Bingham yield stress and plastic viscosity, respectively.
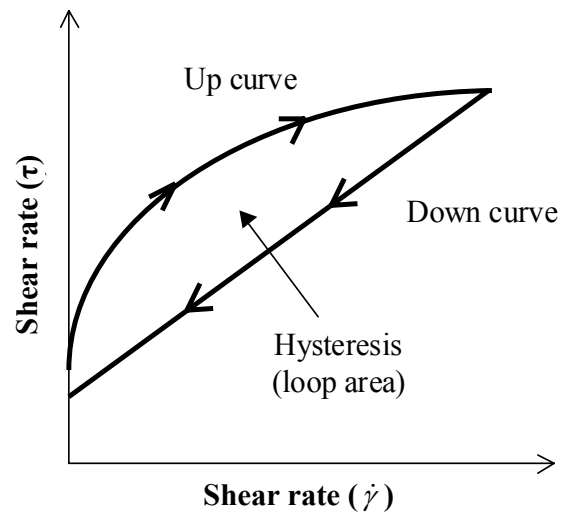
Fig. 20 - Hysteresis loop flow curve [Ish-Shalom and Greenberg, 1962]

Although the hysteresis loop testing procedure has been used for measuring the flow characteristics of cement paste, the shape of the hysteresis loop was criticized by several researchers. For example, Worral et al. (reported in [Banfill and Saunders, 1981]) showed experimentally that two suspensions of quite different thixotropic properties could give similar hysteresis loops. Barnes [1997] also reported that the hysteresis loop tests are not recommended for two main reasons. Firstly, the loop test is often carried out too quickly, and inertia effects due to the measuring head are introduced but not always accounted for. Secondly, a test where both shear rate and time are changed simultaneously on a material where the response itself is a function of both shear rate and time is not quite adequate. This is because the response cannot then be resolved into the separate effects arising from both variables.

When carefully run and interpreted, the use of the hysteresis loop can be useful for evaluating the structural build-up of cement-based materials. For example, Douglas et al. [2005] used this approach to show that structural build-up within the induction period of hydration is time dependent (Fig. 21) and is adversely related to the superplasticizer content in the mixture. The higher the superplasticizer dosage, the lower the thixotropy and the lower the rate of structural build-up.
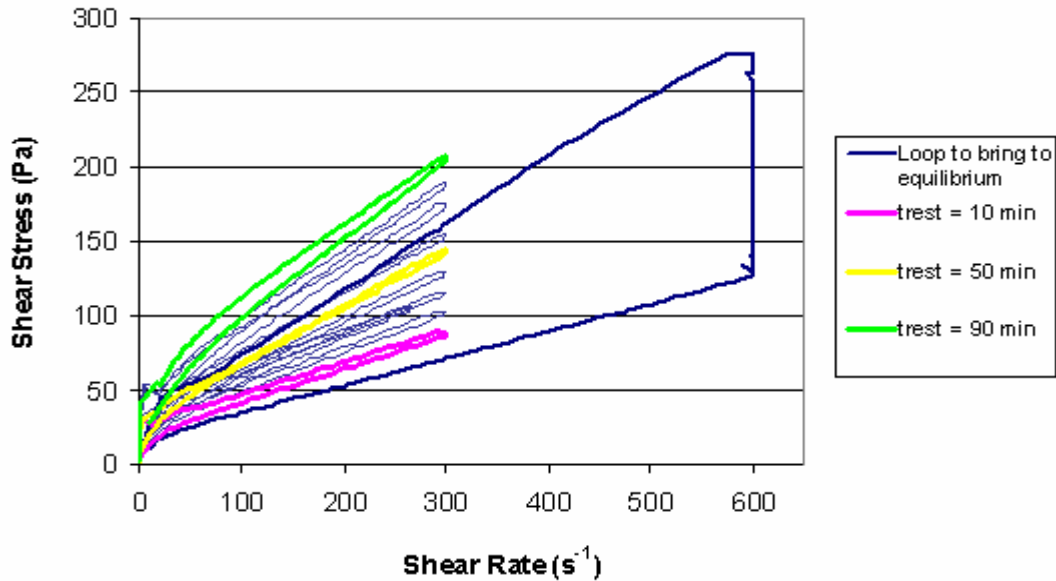
Fig. 21 - Effect of superplasticizer content and rest time on thixotropy and hysteresis loops
[Douglas et al., 2005]

3.2.2   Structural breakdown curves

The other method that can be used to characterize thixotropy of cement-based systems is the steady state, or equilibrium, approach illustrated schematically in Figs. 19 and 22. The steady state approach consists of measuring the behavior of shear stress versus time while fixing a constant shear rate. The initial shear stress necessary to breakdown the structure (τ_{peak}) is generally considered to correspond to the initial structural condition, [Shaughnessy and Clark, 1988]. On the other hand, the shear stress decay with time towards an equilibrium value (τ_{eq}) corresponds to an equilibrium condition that is independent of the shear history.

The steady state approach has been widely used for interpreting the effect of chemical admixtures as well as different forces existing in cement-based systems on the flow conditions ([Tattersall and Banfill, 1983] and [Ghezal et al., 2002]). In addition to its simplicity, this approach provides an advantage compared to the hysteresis loop tests as it enables measuring the entire shear stress range as a function of time for a given shear rate. Conversely, hysteresis loops normally measure transient flow properties somewhere in between the peak and equilibrium stresses for a given shear rate [Saak et al, 2001].
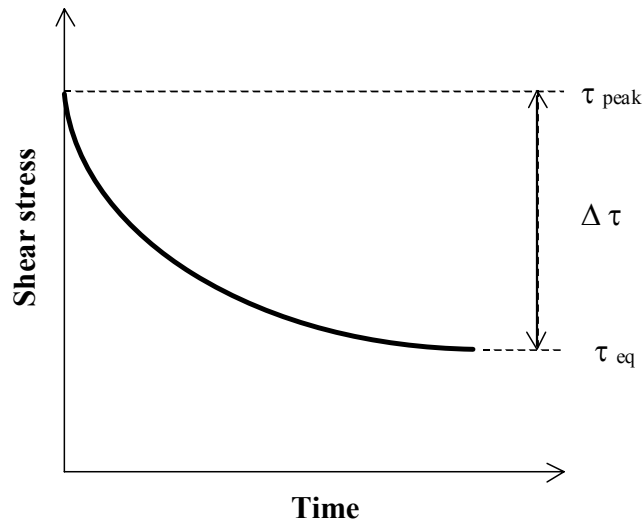
Fig. 22 - Steady state flow curve [Shaughnessy and Clark, 1988]

Assaad et al. [2003A] used the structural breakdown approach to evaluate the thixotropy of SCC. The concrete was subjected to constant rotational speeds of 0.3, 0.5, 0.7, or 0.9 rps. A typical set of structural breakdown curves is plotted in Fig. 23. The corresponding shear rates were calculated according to Legrand's approach by considering that the specially designed bladed vane rotates in an infinite medium [Legrand, 1971]. In this protocol, immediately after the vane drive mechanism is started, readings of the torque are noted as a function of time without delay. The first reading is considered as the initial maximum torque value (T_i) necessary to initiate the flow of the vane. This initial maximum torque is used to calculate the peak yield stress (τ_i), which corresponds to the initial structural condition. The mean of the five smallest measurements over the 25 sec duration at each rotational speed is taken as the equilibrium torque value (T_e). The equilibrium torque is used to calculate the shear stress at equilibrium (τ_e), which corresponds to an equilibrium condition that is independent of the shear history, for that speed. The rest period during which the concrete was not subjected to any shearing action prior to conducting each of the four structural breakdown tests was 5 min for the SCC. This period was found necessary to obtain sufficient spread between T_i and T_e values. In total, the time required to perform all of the rheological tests at the four rotational speeds was approximately 25 minutes.

The spread between τ_i and τ_e gives, for a given rotational speed, a measurement of the amplitude of the structural modifications inside the tested material. Lapasin et al. [1983]

suggested that the area comprised between the initial flow curves $[\tau_i (N)]$ and the equilibrium flow curve $[\tau_e (N)]$ can be used to quantify the thixotropic phenomenon. This area, called the "breakdown area (A_b)", provides a measure of the energy done per unit time and unit volume of concrete necessary to break the initial linkages and internal friction in order to pass from the initial state into a state of equilibrium.

The A_b can be calculated as:

$$A_b = \int_{0.3}^{0.9} \left(\tau_i (N) - \tau_e (N) \right) dN \qquad \text{…............. (80)}$$

Example of the variations in shear stress with shearing time and the calculation of the structural breakdown area between the τ_i vs. N and τ_e vs. N plots are shown in Figs. 23 and 24, respectively. These data are determined for SCC made with ternary cement containing silica fume (SF) and fly ash (FA) and a set-retarding admixture (RET).
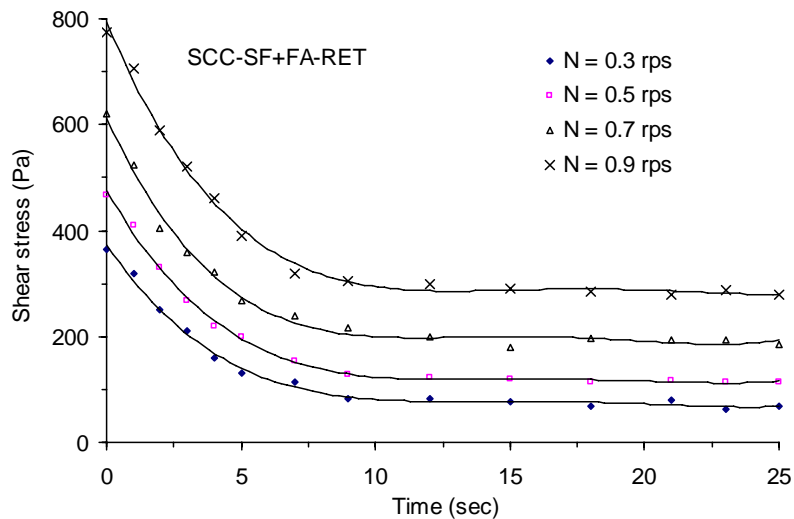
Fig. 23 - Typical example of structural breakdown curves for SCC [Assaad et al., 2003A]
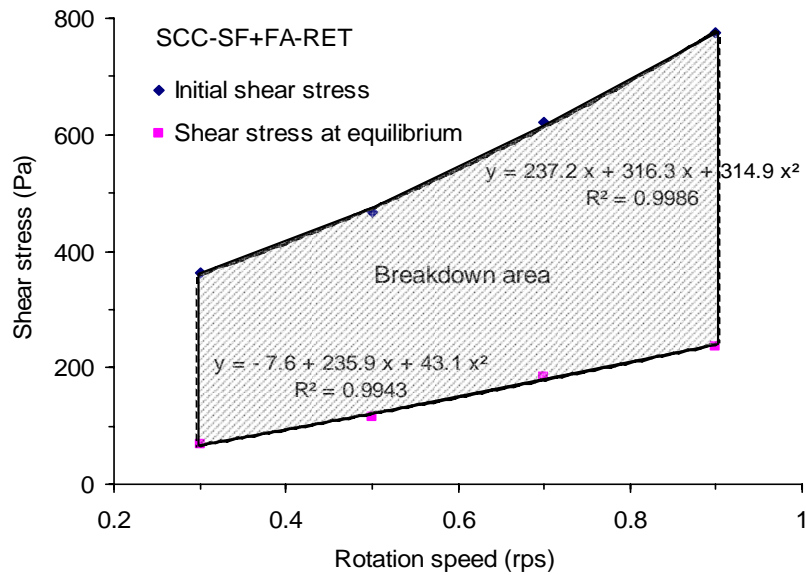
Fig. 24 - Typical example of structural breakdown area calculation [Assaad et al., 2003A]

3.2.3 Apparent viscosity

The drop in the apparent viscosity ($\Delta\eta_{app}$) can also be considered as an index for evaluation of the degree of thixotropy. The value of the drop in the apparent viscosity was used by Assaad et al. [2003A] at various shear rates to characterize thixotropy of SCC. At a given rotational speed, the concrete is sheared causing destruction of the links between the internal particles until equilibrium state is reached. The difference between the initial shearing stress representing initial destruction and the equilibrium shearing stress measured over the applied shear rate can be defined as the drop in apparent viscosity ($\Delta\eta_{app}$):

$$\Delta\eta_{app} = (\tau_i - \tau_e) / \dot{\gamma} \qquad \text{…............. (81)}$$

where,

τ_i : initial shear stress;

τ_e : equilibrium shear stress; and

$\dot{\gamma}$: applied shear rate.

3.2.4 Yield stress at rest

The yield stress can be used as measure of the strength and number of interparticle bonds that are ruptured due to the applied shear or stress [Tattersall and Banfill, 1983]. Tattersall and Banfill reported initial yield stress values for a normal consistency cement

paste ranging from 50 - 200 Pa [Tattersall and Banfill, 1983]. Similarly, the yield stress values for conventional concrete range from 500 Pa to a several thousands Pa, and for SCC these values tend to range from 0 - 60 Pa [Wallevik, 2003].

The protocol adopted for the determination of yield stress at rest (also referred to as static yield stress and shear-growth yield stress) consisted of applying a minute and constant rotational speed to a vane immersed in the fresh material and recording the resulting torque as a function of time. In the case of concrete shown in Fig. 25, the speed was set at 0.03 rps. This was chosen so that the maximum torque is not affected by the rotational speed of the vane. As the blades start rotating only when the applied shear stress exceeds the resistance created by the friction forces and bonds between the particles. The profile shows a linear elastic region followed by a yielding moment where the torque exerted on the vane shaft reaches a maximum value corresponding to the beginning of the microscopic destruction of the bonds between the particles and the suspension allowing the material to flow. Beyond this value, the torque decays towards a steady state region. It constitutes a new dynamic arrangement of the particles, offering an internal friction less than that resisted the first destruction. Therefore, the peak shear stress value is considered as the yield stress at rest.

The presence of such maximum torque response is an index of thixotropy that can be explained by the concept of structural deformation and breakdown of the bond in the flocculated system [Dzuy and Boger, 1985]. The maximum value during this profile corresponds to the yield shear stress at rest, $\tau_{o\ rest}$. The calculation of τ_o rest from the measured maximum torque (T_{max}) requires knowledge of the geometry of the yield surface and shear stress distribution on the surface.
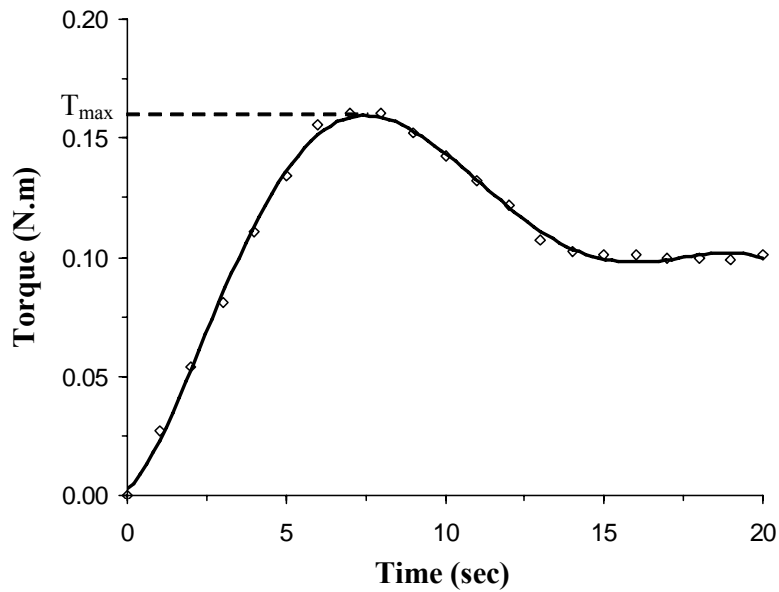
Fig. 25 - Typical torque-time profile for concrete with 200 mm slump
[Assaad et al., 2003A]

Dzuy and Boger [1985] assumed that the material is sheared along a localized cylindrical surface circumscribed by the vane. They also assumed that the shear stress is uniformly distributed over the cylindrical sheared surface. Hence, good approximation of the shear stress can be calculated as follows:

$$\tau_{o\ rest} = T_{max} / K \qquad\qquad \text{…............. (82)}$$

where, $K = \text{constant} = 2\,\pi\,R^2\,H + 4/3\,\pi\,R^3 = 0.001939\ m^3$

H and R are the height and radius of the vane (H = 130 mm and R = 45 mm for the vane used in this study), respectively.

The variation in yield stress at rest with time of restructuring of the mixture with rest can also be used to determine the degree of thixotropy expressed as the rate of gain in yield stress with time (Pa/sec), as discussed in Section 3.2.4.

3.2.5 Billberg's protocol [2006]

Billberg [2006] used a Physica MCR 300 rheometer to assess thixotropy of micro mortar where only sand fines sieved passing 0.125 mm are used. Five micro mortars made with CemII/A-LL 42.5 R (Swedish cement for housing) and *w/c* ranging between 0.34 and

0.42 were tested. As shown in Fig. 26, the testing protocol was carried out to measure the dynamic rheology before and after a given resting period to find the magnitude of the irreversible structural change with time. After the resting period and before the last dynamic rheology measurement, the structure is broken down with relatively large shear rate loop.

The Bingham model is used to determine the dynamic yield stress and plastic viscosity at shear rates of 10 to 30 s^{-1} using the down-curves of the first and last loops. During the resting period between the first and last dynamic tests, the time-dependent static yield stress is determined. After successive resting periods of 10 min, the micro mortar is subjected to an increasing stress from 0 to 300 Pa at a rate of 3.33 Pa/s until the structure breaks and the measurement is cancelled. The criterion for this cancellation is when the shear rate reaches 0.5 s^{-1}, i.e., when the deformation due to the broken structure increases. The results of each are shown in Fig. 27. The area between the static and dynamic curves represents the reversible structure, i.e., total structural build-up minus the irreversible structure over time.
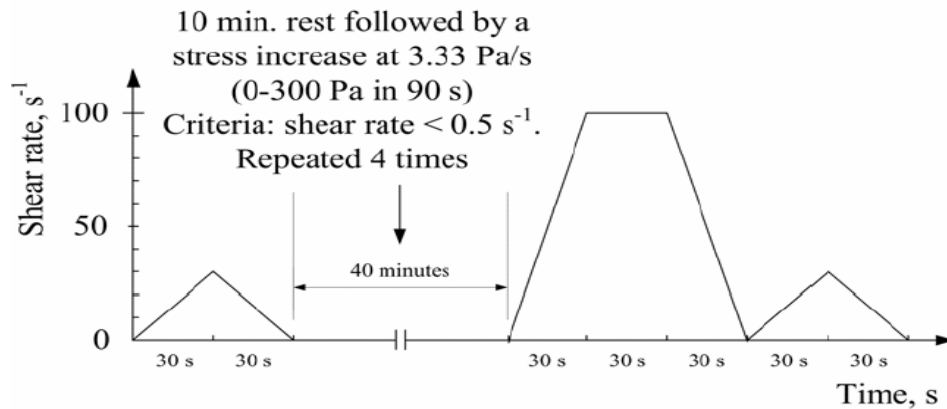
Fig. 26 - Configuration of rheometer for tests on micro mortar [Billberg, 2006]
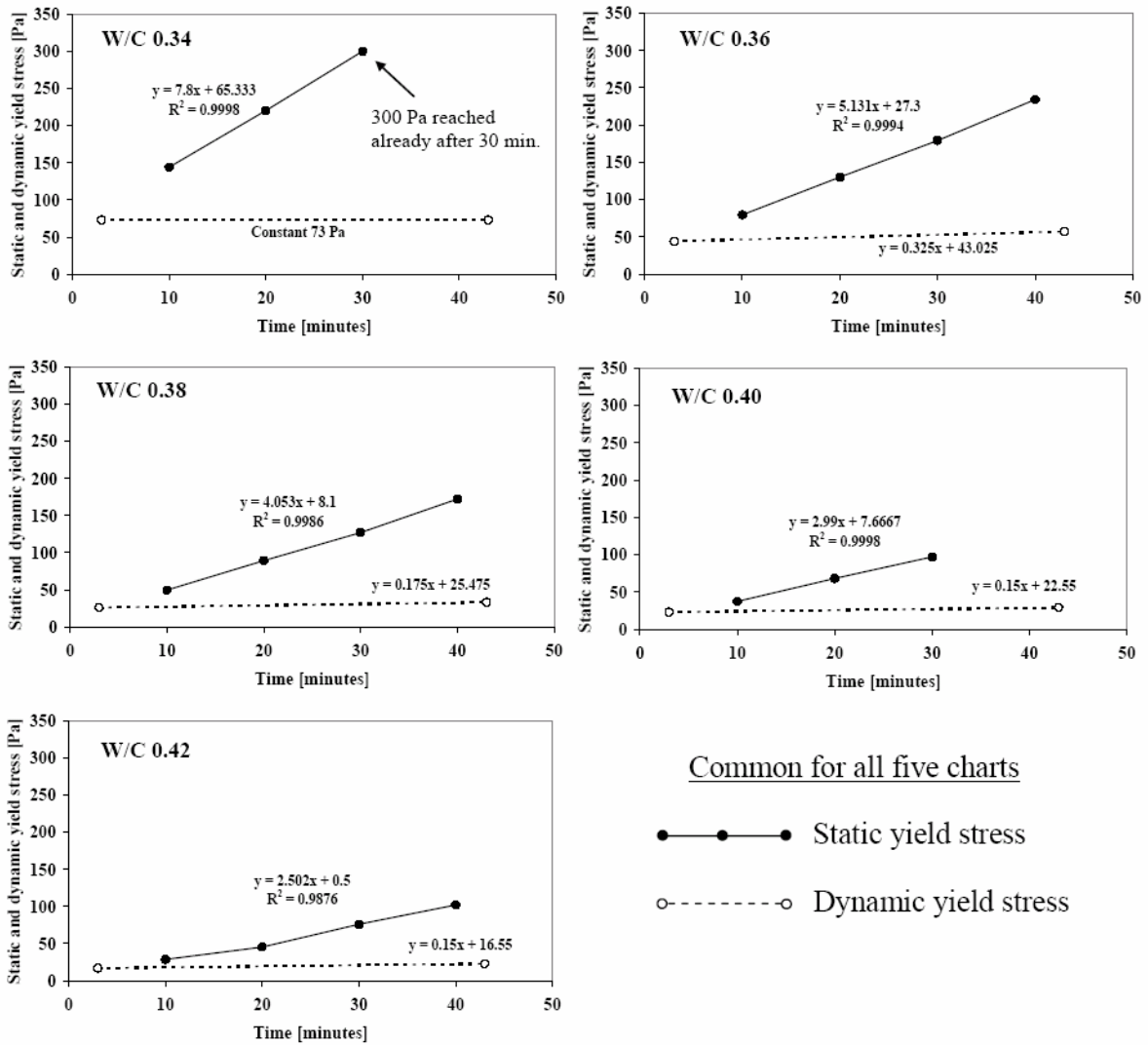
Fig. 27 - Results of dynamic yield stress development and structural build-up of micro mortars made with w/c ranging from 0.34 to 0.42 [Billberg, 2006]

3.3 Relationships of lateral pressure and rheological properties

It is reasonable to presume that the lateral pressure envelope for SCC can be attributed to the same combination of physical factors and mixture characteristics that apply to normal-consistency concrete. The rate of restructuring of concrete should have a significant influence on changes in pressure distribution with time. The restructuring phenomenon is considered to be mainly due to the development of internal friction and attractive forces among solid particles at rest as well as to an increase in the degree of physical and chemical bonds during cement hydration. The evolution of the restructuring of the cement-based material can be indirectly assessed by observing thixotropy, which describes the

54

destructuring phenomenon. Concrete that can exhibit faster degree of restructuring can develop greater cohesiveness soon after casting, thus acting as a cohesive body exerting less pressure than its full hydrostatic pressure.

Khayat and Assaad showed that formwork pressure exerted by SCC could be directly related to the magnitude of thixotropy. The greater the degree of thixotropy, the lower the initial lateral pressure can be and the faster is the rate of pressure drop with time. Concrete with higher degree of thixotropy was found to develop lower initial lateral pressure and higher rate of pressure drop with time. This is attributed to the stiffening effect, which enables the material to re-gain its shear strength when left at rest without any shearing action [Khayat and Assaad, 2005B].

Changes in both the initial lateral pressure and pressure determined after 100 and 200 minutes after concrete casting in 2.8-m high PVC column measuring 200 mm in diameter were shown (Fig. 13) to increase with the thixotropy of the SCC. The SCC mixtures had slump flow consistencies of 650 ± 10 mm. The thixotropy was determined using the breakdown area approach evaluated at different time intervals (Section 4.2.2). As expected, the most thixotropic mixtures were shown to exhibit the lowest relative initial pressure and the highest rate of drop in pressure with time. For example, SCC with high breakdown area of 450 J/m³.s can develop approximately 60% of hydrostatic pressure near the bottom of the 2.8-m high experimental column after 200 min, whereas a less thixotropic mixture with low breakdown area 180 J/m³.s can maintain a high relative pressure of 95%.

Billberg et al. [2006] also showed that the increase in structural build-up at rest of SCC can result in shaper rate of drop in formwork pressure that was determined during the first hour after casting (Fig. 28). The formwork pressure was determined at a height of 50 mm from the bottom of tube measuring 1.5 m in height and 200 mm in internal diameter. The structural build-up at rest was monitored at 10-min intervals was evaluated as per the procedure described in Sections 4.2.4 and 4.2.5.
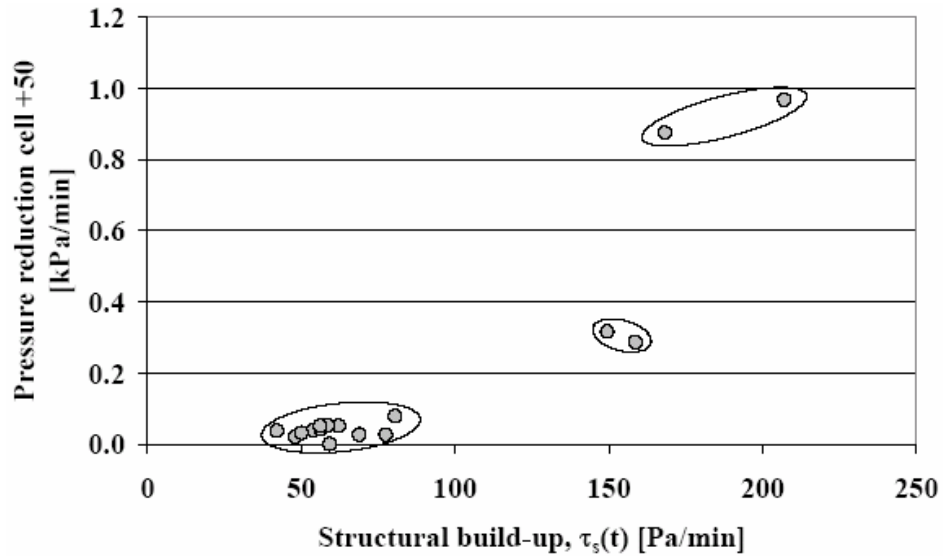
Fig. 28 - Influence of structural build-up on pressure loss pressure during the first hour after casting [Billberg et al., 2006]

4. PARAMETERS AFFECTING FORMWORK PRESSURE AND THIXOTROPY

Since the early 1900s, numerous laboratory and field investigations were carried out to provide broad understanding of the variables that can affect lateral pressure of fresh concrete. ACI Committee 622 [1958] studied all published field and laboratory investigations of lateral pressure developed on formwork. From these results and those reported latter in the literature [Rodin 1952, Schojdt 1955, Adam et al., 1963, Gardner 1980, CIRIA 1985, Assaad 2004, etc.], key factors that can influence lateral pressure of concrete are summarized in Table 2. These factors are discussed in below with special emphasis, whenever possible, on formwork pressure exerted by SCC as well as thixotropy and structural build-up characteristics.

Table 2 - Factors influencing formwork pressure

Material properties	Consistency level	Placement conditions	Formwork characteristics
- Cement type and content - Use of supplementary cementitious materials and fillers - Size, type, and content of coarse aggregate - Water content - Chemical admixtures - Unit weight of concrete		- Placement rate - Height of concrete - Placement method - Height of pouring - Consolidation method - Vibration magnitude and duration - Impact during placing - Ambient and concrete temperatures - Setting time - Time needed for formwork removal	- Formwork dimension - Case of reinforcement - Formwork surface material - Permeability and drainage of formwork - Formwork surface roughness - Demolding agent characteristics

4.1 Material properties

4.1.1 Composition and content of binder

Cement content, type, and use of supplementary cementitious materials and fillers have significant influence on the development of lateral pressure exerted by conventional vibrated concrete and SCC. Roby [1935] investigated a series of rich, normal, and lean mixtures made with different cement:sand:coarse aggregate mass ratios of 1:1.25:2.25, 1:2:3.5, and 1:2.5:5, respectively (Fig. 29). An ordinary portland cement was used, and the slump values of the mixtures varied between 50 and 150 mm. The author reported that the cement content has a significant effect on lateral pressure since rich mixtures developed 40% greater pressure than the normal mixtures, which in turn, developed about 15% greater pressure than that of the lean mixtures.
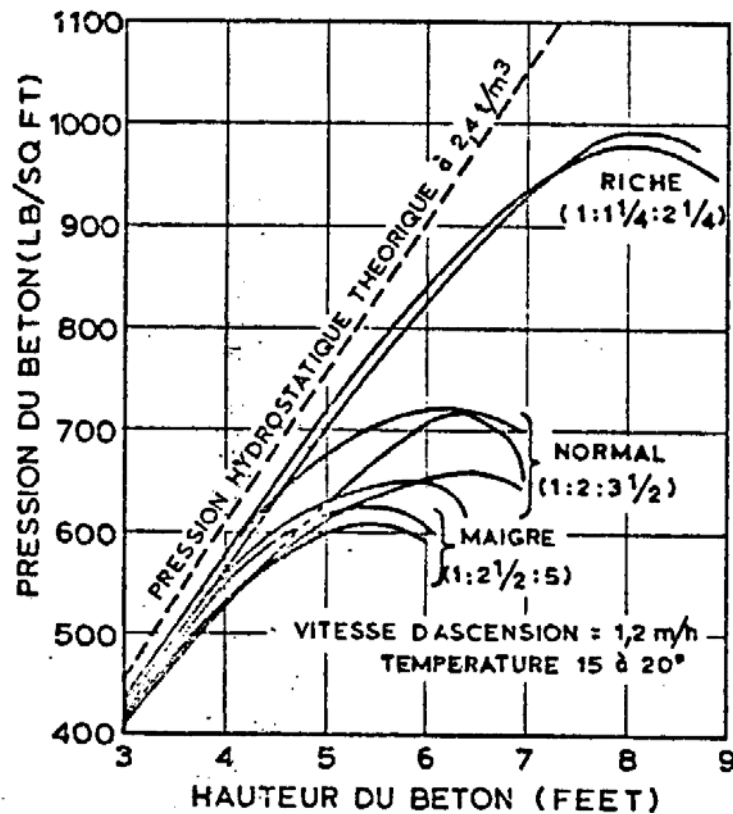
Fig. 29 - Effect of cement content on lateral pressure [Roby, 1935]

Similarly, Ritchie [1962B] attempted to determine the effect of portland cement on the lateral pressure envelope for conventional mixtures having 100 mm slump cast at a rate of 3 m/h. The cement content varied from 200 and 640 kg/m³. As indicated in Fig. 30, mixtures prepared with higher cement content developed greater lateral pressure. Roby [1935] and Ritchie [1962B] concluded such increase in lateral pressure resulting from the use of more cement can be indirectly related to the fact that such concrete contains lower volume of coarse aggregate. Interference caused by high aggregate particles can increase the degree of internal friction. This in turn can reduce the mobility of the plastic concrete and thereby the transformation of vertical load to lateral pressure.
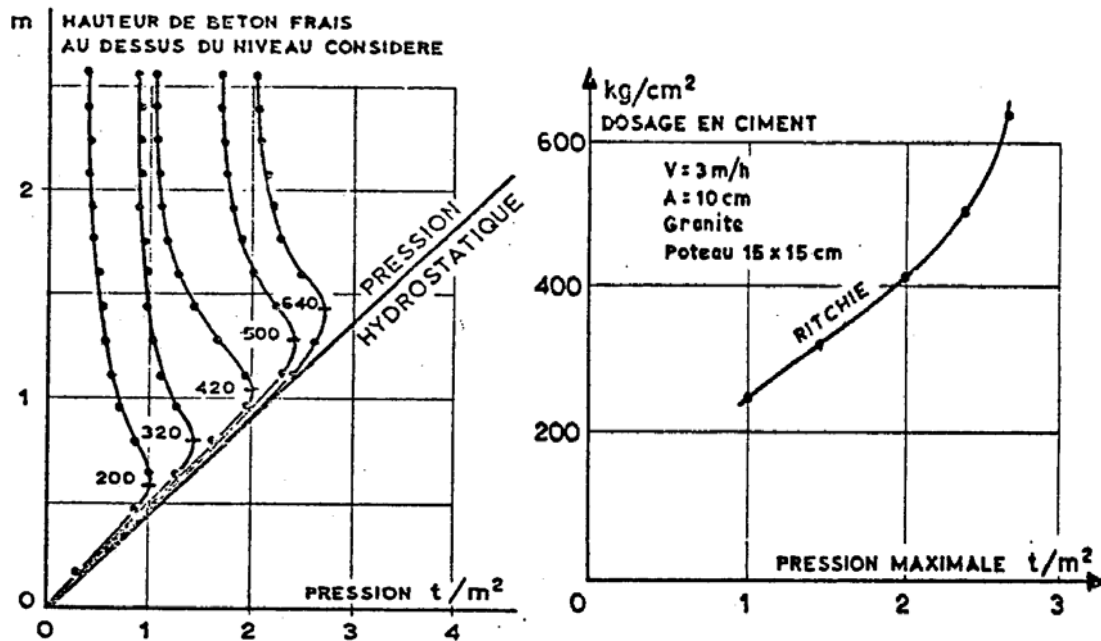
Fig. 30 - Effect of cement content on lateral pressure [Ritchie, 1962B]

Gardner [1984] investigated the influence of cement replacement by fly ash for conventional concrete with slump values ranging between 65 and 115 mm. The fly ash replacement varied between 0 and 50%. Concrete mixtures containing fly ash were found to develop higher lateral pressure than similar concrete prepared with only Type GU cement. The incorporation of fly ash is suggested to increase the mobility of the plastic concrete and reduce the rate of strength gain, thus leading to higher lateral pressure development.

Assaad and Khayat [2005A, 2005B] investigated formwork pressure exerted by SCC prepared with different binder contents and types. The binder content varied between 400 and 550 kg/m³. Type GU (T GU) and Type HE (T HE) CSA Canadian cements were used along with three blended cements. The blended cements included a binary cement (BIN) containing 8% silica fume (SF) and 92% T GU cement, a ternary cement (TER) made with 6% SF, 22% Class F fly ash (FA), and 72% T GU cement, and finally a quaternary cement (QUA) containing SF, FA, and granulated blast-furnace slag (GBFS) at combined substitution of 50% of T GU cement. A fixed content of 450 kg/m³ was employed for the mixtures made with T GU and T HE cements. The w/c remained constant at 0.40 for all tested mixtures, and the sand-to-total aggregate ratio was set at 0.46, by mass. The dosage of liquid-based viscosity-modifying admixture (VMA) was set at 260 mL/100 kg of binder.

59

The dosage rates of the high-range water reducing admixture (HRWRA) and air-entraining agent (AEA) were adjusted to secure initial slump flow of 650 ± 15 mm and air content of 6% ± 2%. An instrumented PVC column measuring 2.8 m in height and 200 mm inner diameter was used to determine lateral pressure. As in the case of conventional vibrated concrete, the initial lateral pressure and its rate of drop are significantly affected by the binder type for SCC.

As illustrated in Fig. 31, SCC made with Type GU cement exhibited the highest initial pressure and the lowest rate of drop in pressure than other mixtures made with the same binder content of 450 kg/m³. On the other hand, SCC prepared with Type HE cement had the lowest initial pressure and the highest rate of pressure drop. The authors concluded that for a given binder type, higher initial pressure can be obtained for mixtures containing greater binder contents; this is due to the lower coarse aggregate volume as elaborated earlier. For longer elapsed times, lateral pressure variations depend significantly on the development of cohesion resulting from the binder phase. Therefore, the increase in binder content leads to sharper pressure decay, as illustrated in Fig. 32. For SCC made with the same binder content, the thixotropy was also shown to be higher in the case of ternary cement than binary cement Assaad and Khayat [2005A]. This was attributed to the increase in contact points and inter-granular forces when substituting cement by cementitious materials with finer particles, such as fly ash and silica fume.

Andreas et al. [2005] studied the influence of binder type on SCC lateral pressure. Two different types of ordinary portland cements (CEM I 42.5 N according to European Standard EN 197-1) were used. SCC mixtures were also prepared with either fly ash or limestone filler at 33% volume replacement of cement. The SCC was cast from the top of a formwork measuring 0.20 × 0.20 × 0.975 m. The partial substitution of ordinary portland cement (OPC 2) with fly ash or limestone powder can accelerate the pressure decrease. The acceleration was more pronounced when using fly ash. This is attributed to decrease in grain size leading to higher surface area and smaller inter-particle distance. This causes greater build-up of internal structure and accelerated pressure decay.
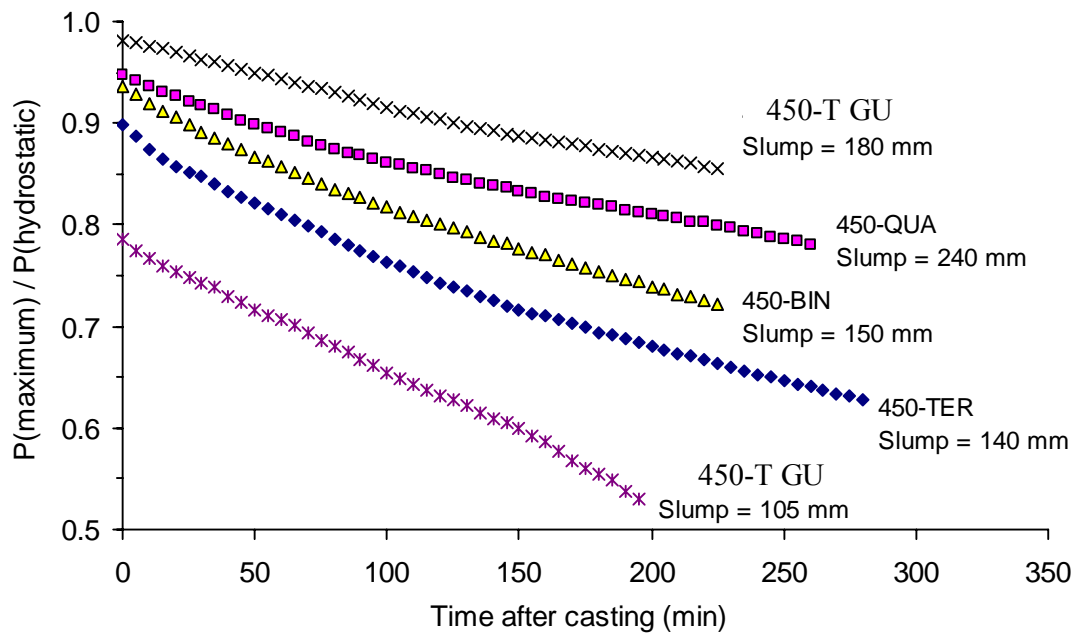
Fig. 31 - Variations in relative lateral pressure for SCC made with 450 kg/m³ of various binder; slump values are those determined at the end of pressure monitoring [Assaad and Khayat, 2005A]
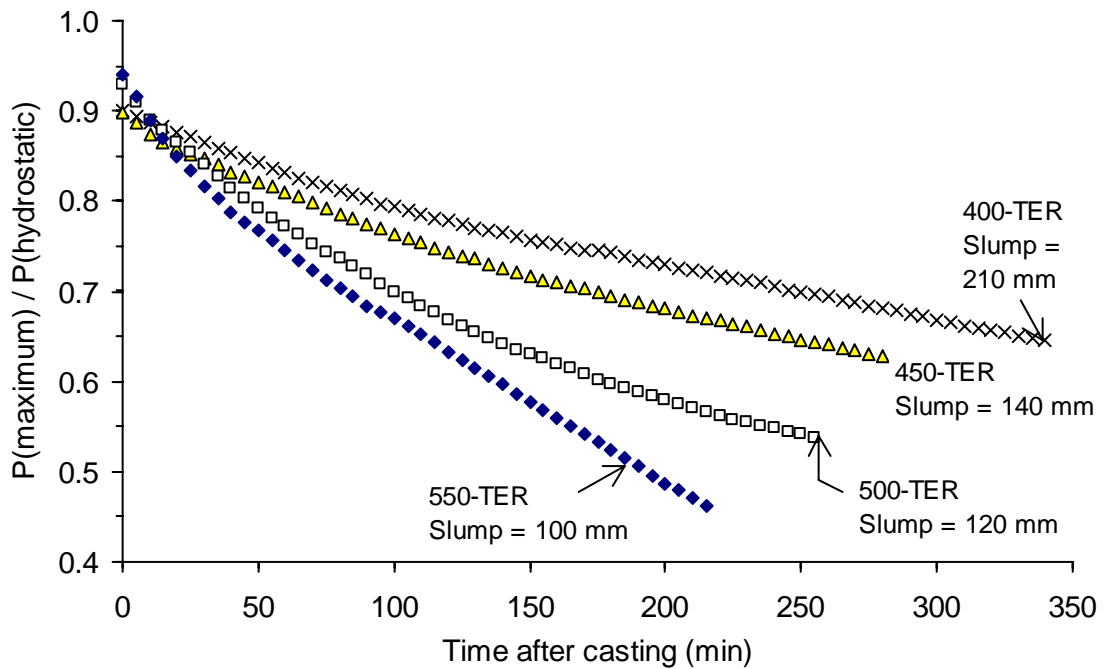
Fig. 32 - Variations in relative lateral pressure for SCC made with various contents of ternary binder [Assaad and Khayat, 2005A]

4.1.2 Characteristics of coarse aggregate

Gardner and Ho [1979] found that the increase in maximum-size of aggregate (MSA) from 10 to 20 mm had no significant influence on lateral pressure exerted by conventional concrete with slump of 50 to 100 mm. Amziane and Baudeau [2000] reported that the use of discontinuously-graded aggregate with MSA of 30 mm can lead to higher lateral pressure for conventional vibrated concrete than continuously-graded aggregate with MSA of 7 mm.

Amziane and Baudeau [2000] considered that concrete is a two-phase heterogeneous material composed of cement paste and coarse aggregate. The paste possesses a rheological behavior that is exclusively viscous, whereas the granular phase contributes to the resistance to shear stress through aggregate friction. Conventional concrete mixtures made with *w/c* of 0.5, various aggregate contents, MSA, slump values of 50 to 250 mm were evaluated. The lateral pressure was determined using steel formwork measuring 1650 mm in height, 1350 mm in length, and 200 mm in width. Full hydrostatic pressure was obtained in the case of cement paste. The maximum lateral pressure divided by the pressure obtained for the cement paste mixture (P_m/P_p) was shown to decrease with the increase in coarse aggregate volume until the volumetric ratio of the paste-to-coarse aggregate (V_p/V_{agg}) approached one. As indicated in Fig. 33, the variation in P_m/P_p with V_p/V_{agg} is linear between A and B that correspond to mixtures having aggregate concentrations lower than 40%. Only a slight reduction in the P_m/P_p value was obtained despite considerably reduction in the V_p/V_{agg} value. The authors suggested that as long as the volume of mortar is dominant, the magnitude of internal friction remains limited resulting in considerably higher lateral pressure. The second slope (BC) corresponds to mixtures with aggregate concentration greater than 40%, and indicates that a significant decrease in the relative pressure can be obtained for a small decrease in the V_p/V_{agg} value. This suggested that the concrete tends to have a granular behavior enabling the development of shear strength mainly through aggregate inter-particle friction, hence leading to significant reduction in lateral pressure.
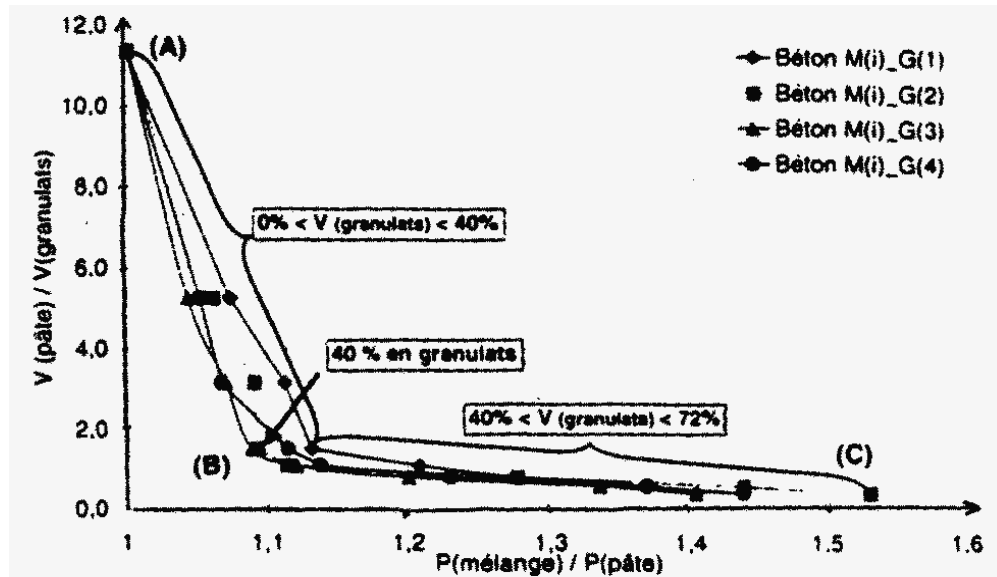
Fig. 33 -Variations of the Pm/Pp values with respect to coarse aggregate concentration [Amziane and Baudeau, 2000]

In the case of highly flowable mixtures with slump flow of 650 ± 15 mm, Assaad and Khayat [2005C] found that the increase in coarse aggregate volume could reduce the lateral pressure and increase the rate of pressure drop after casting. This was attributed to the increases of the degree of internal friction resulting from greater coarse aggregate content, which reduces the mobility of the concrete and the resulting lateral pressure. As illustrated in Fig. 34, the initial lateral pressure can decrease from 99% to 77% of hydrostatic pressure when the sand-to-total aggregate ratio (S/A) decreases from 1.0 to 0.30, respectively. The lateral pressure was determined near the bottom of a pressure column measuring 2.8 m in height in which concrete is cast at 10 m/h. The rate of drop in pressure with time was also found to be influenced by the S/A value. For example, for the 0.50-10-SCC and 0.30-SCC mixtures, the time required to reduce lateral pressure by 10% of hydrostatic value was 145 and 80 min, respectively (Fig. 34). In addition to lateral pressure, the decrease in S/A resulted in greater thixotropy, as illustrated in Fig. 35. For example, the breakdown area (A_b) is shown to increase from 130 to 340 J/m³.s and then to 550 J/m³.s during the first series of measurements (T1 time period) when the S/A value decreased from 1.0 to 0.46 and then to 0.30, respectively.
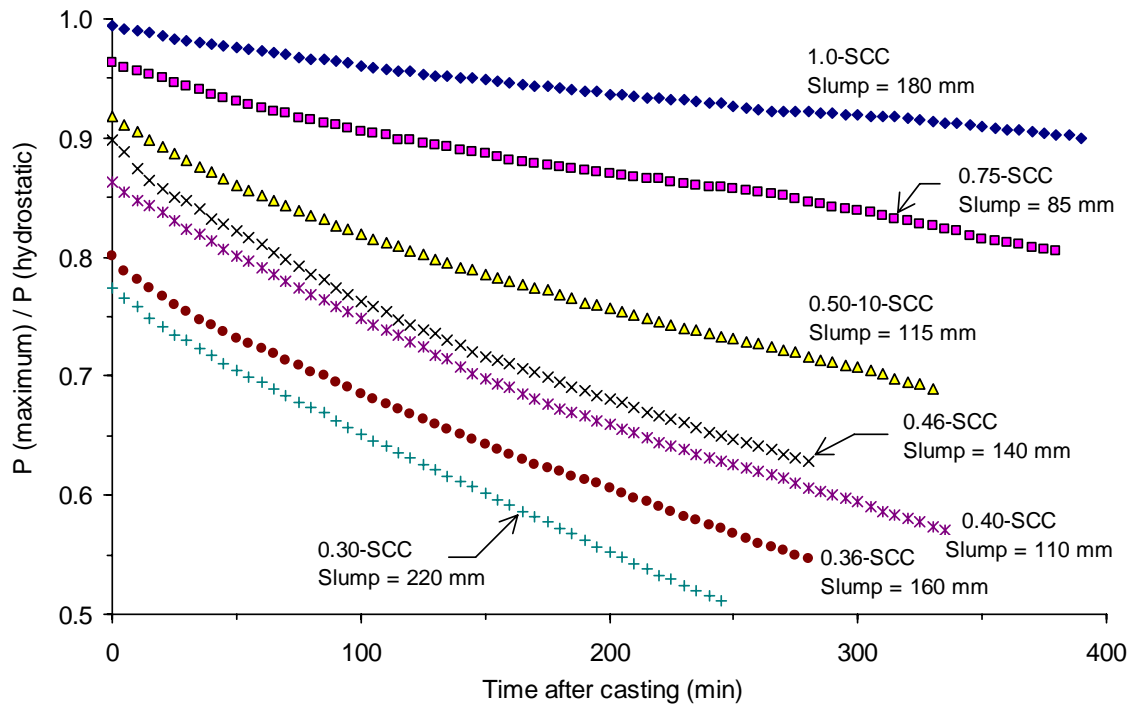
Fig. 34 - Variations of relative pressure with regard to elapsed time following casting for mixtures made with 10 mm MSA (slump values at end of pressure monitoring are noted) [Assaad and Khayat, 2005C]
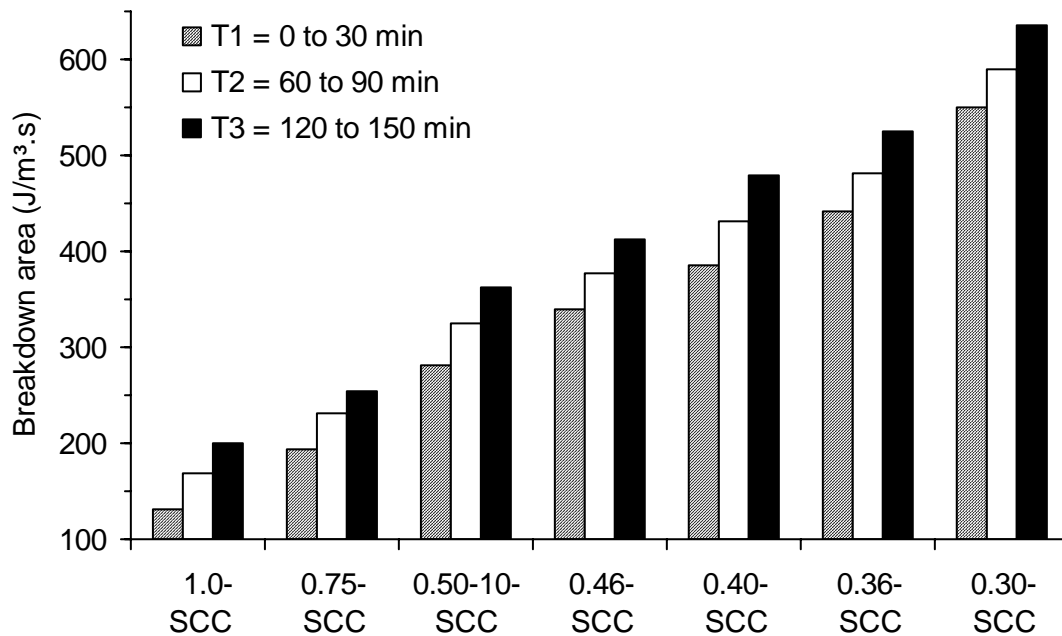
Fig. 35 - Variations of breakdown area for mixtures made with various coarse aggregate concentrations (MSA = 10 mm) [Assaad and Khayat, 2005C]

64

The MSA was also found to affect formwork pressure. The initial relative pressure was shown to decrease from 92% to 85%, and pressure decay was more pronounced when using 14 mm MSA compared to 10 mm MSA. Further increase of MSA to 20 mm had limited effect on pressure drop compared to the SCC with 14 mm MSA [Assaad and Khayat, 2005C].

4.1.3   Water content and *w/cm*

To determine the effect of water content on lateral pressure, Roby [1935] carried out series of tests using concrete mixtures with cement:sand:coarse aggregate ratio of 1:2:3.5. The *w/c* was varied from 0.86 to 0.91, and the slump consistency was changed from 80 to 180 mm. Concrete containing greater water content was reported to develop maximum pressure of 20% to 25% greater than that of dry concrete. The author attributed this behavior to the increased lubricating effect of the paste layer between the aggregate particles, thus decreasing internal friction and resulting in higher lateral pressure. Similar conclusion was drawn by Ore and Straughan [1968] concerning the effect of water content on formwork pressure determined for concrete with 75 to 100 mm slump. The authors noted that an excess amount of water added to a mixture containing only sand and coarse aggregate can result in pressure equivalent to that produced by the head of water. Such pressure can prevail until the excess water is drained out from the formwork.

In the case of SCC, Khayat and Assaad [2006] reported that changes in *w/cm* have significant effect on lateral pressure and thixotropy. For a given slump flow consistency of 550 mm, SCC proportioned with 0.46 *w/cm* exhibited lower thixotropy and slightly greater initial pressure compared to SCC made with 0.40 or 0.36 *w/cm* (Figs. 36, 37). This was attributed related to the increased water and paste contents and reduction in coarse aggregate volume, which lead to lower shear strength properties of the plastic concrete. Furthermore, the rate of drop in lateral pressure and gain in thixotropy with time were found to be considerably greater in SCC made with *w/cm* of 0.46 (Figs. 36, 37). The elapsed time to reduce the relative pressure by 25% decreased from 200 to 150 min with the decrease in *w/cm* from 0.40 to 0.36 for SCC made with PMS-based HRWRA. This is attributed to the lower HRWRA demand of the SCC made with the higher *w/cm*, which can present less

interference with the rate of structural build-up and development of cohesiveness than SCC with lower *w/cm* [Khayat and Assaad, 2006].
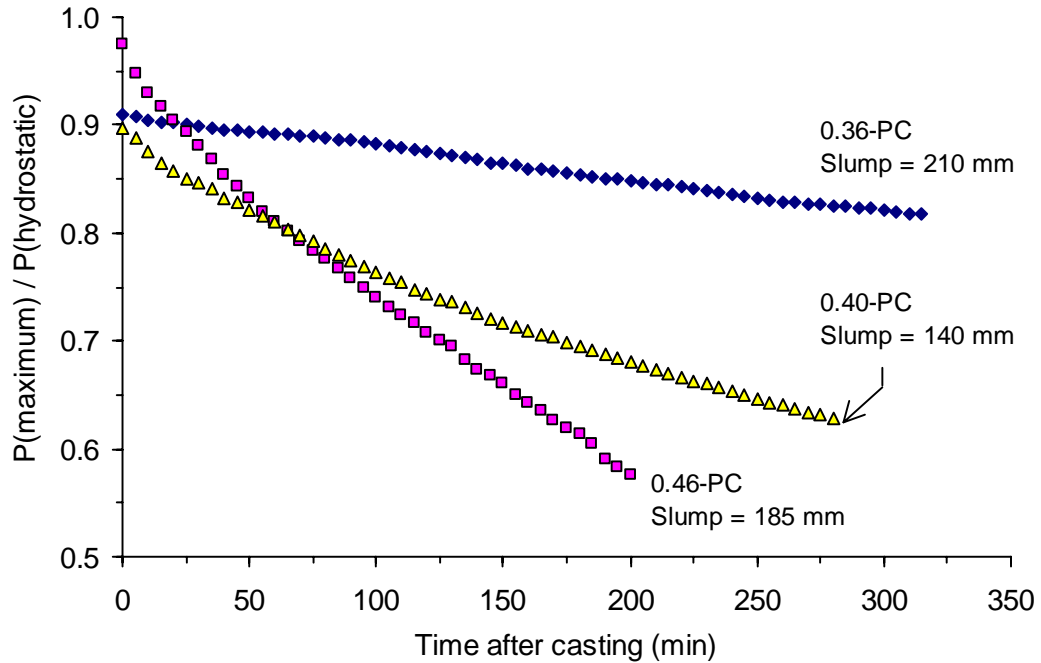
Fig. 36 - Effect of w/cm on relative pressure variations of SCC made with PC-based HRWRA [Khayat and Assaad, 2006]
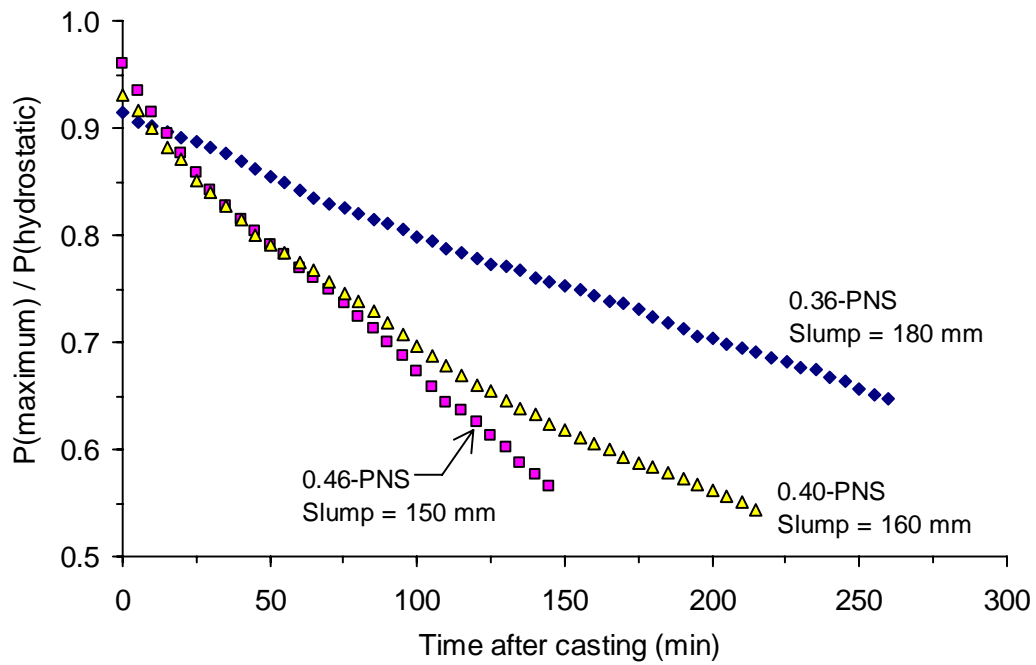
Fig. 37 - Effect of *w/cm* on relative pressure variations of SCC made with PNS-based HRWRA [Khayat and Assaad, 2006]

4.1.4   Chemical admixtures

Ore and Straughan [1968] reported that the effect of incorporating a water-reducing or set-retarding agent has limited influence on formwork pressure. The effect of adding HRWRA to enhance workability increased formwork pressure [Gardner, 1984]. However, the use of HRWRA to reduce the *w/c* for a given slump was found to develop similar formwork pressure envelope as that of concrete made without HRWRA of similar consistency.

Khayat and Assaad [2006] evaluated the effect of HRWRA type of formwork pressure characteristics of SCC cast in pressure column of 2.9 m in height cast at 10/m. Mixtures were prepared with polycarboxylate acid-based (PC), polynaphthalene sulphonate-based (PNS) and polymelamine sulphonate-based (PMS) HRWRAs. As shown in Fig. 38, for SCC made with 0.36 *w/cm*, the type of HRWRA has limited effect on the initial pressure. On the other hand, the type of HRWRA has considerable effect on pressure decay. Compared to SCC made with PNS- or PMS-based HRWRA, the use of PC-based HRWRA exhibits better fluidity retention which leads to lower gain in structural build-up and pressure decay. Similar results were obtained with SCC made with *w/cm* of 0.40 and 0.46.
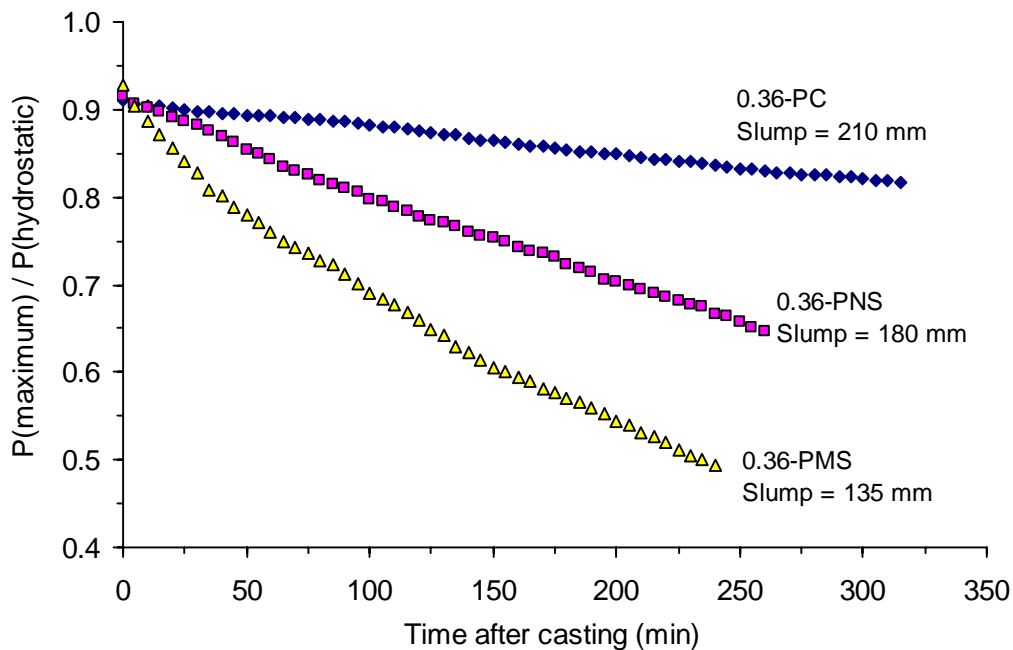
Fig. 38 - Effect of HRWRA type on pressure variations of SCC made with 0.36 *w/cm*
Khayat and Assaad [2006]

67

Andreas et al. [2005] evaluated the influence of VMA on SCC lateral pressure. The VMA types were microsilica, nanosilica slurry, high molecular ethylenoxide derivate, natural polysaccharide, and starch derivate. The SCC was cast from the top of a formwork measuring $0.20 \times 0.20 \times 0.975$ m. The addition of VMA can slightly accelerate pressure decrease; however, no difference was noted between the various VMAs. The decrease in HRWRA dosage and simultaneous increase in *w/cm* led to faster pressure drop.

Assaad and Khayat [2006] reported that the incorporation of cellulose-based VMA along with PC-based HRWRA in SCC can lead to greater thixotropy compared to mixtures containing polysaccharide-based VMA and PNS-based HRWRA. However, the former mixture exhibited lower rate of increase in thixotropy with time given of the use of PC-based HRWRA that enhances fluidity retention. A key finding pointed out in this study is the fact that regardless of the VMA type (cellulose-based or powder- or liquid polysaccharide-based VMA), the increase in VMA from relatively low to medium or high dosage could lead to considerably lower rate of pressure drop with time compared to concrete made with low concentration of VMA. This is attributed to the increase in HRWRA demand, which affects the rate of the development of structural build-up at rest [Assaad and Khayat, 2006]. This is illustrated in Fig. 39 for SCC made with 0.36 *w/cm* and 450 kg/m³ of ternary cement proportioned with polycarboxylate-based HRWRA and either cellulose-based or powder- or liquid polysaccharide-based VMA incorporated at relatively low (L) and high (H) dosage rates.

Ferron, et al. [2006] evaluated the influence of HRWRA and *w/cm* on the structural build-up of cement paste. In this study, the HRWRA dosage or *w/cm* was varied until the desired initial paste slump flow was obtained. It was determined that the adoption of a lower *w/cm* with a higher dosage of HRWRA is more effective in the rate of structural build-up than using a higher *w/cm* and a lower HRWRA dosage. Increasing the water content increases the thickness of the water layer around the cement particles. Therefore, the inter-particle distance increases, and the particle flocculation are reduced because the inter-particle coagulation forces decrease. In regards to HRWRA, particle aggregation is hindered by the presence of electrostatic repulsive forces and/or the steric hindrance effect that keeps the cement particles dispersed.

4.2 Consistency level

Most investigators reported that lateral pressure is expected to increase for mixtures having higher consistency level. This is due to the reduced degree of shear strength resistance that causes the material to behave like a fluid, thus resulting in greater lateral pressure. Rodin [1952] studied the coupled effect of slump consistency and rate of placement on the development of lateral pressure. Concrete mixtures having slump values varying between 0 and 250 mm were investigated. As shown in Fig. 40, the increase in slump results in greater lateral pressure for a given casting rate. Concrete subjected to internal vibration develops greater formwork pressure than that of hand placed concrete.
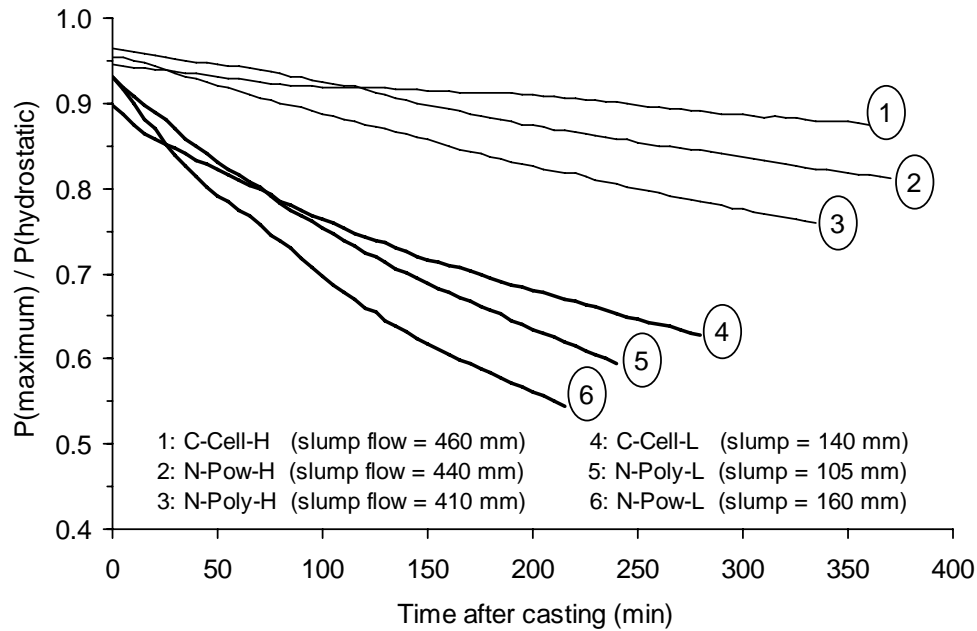
Fig. 39 - Effect of VMA type and dosage on pressure variations of SCC made with 0.36 *w/cm* Khayat and Assaad [2006]
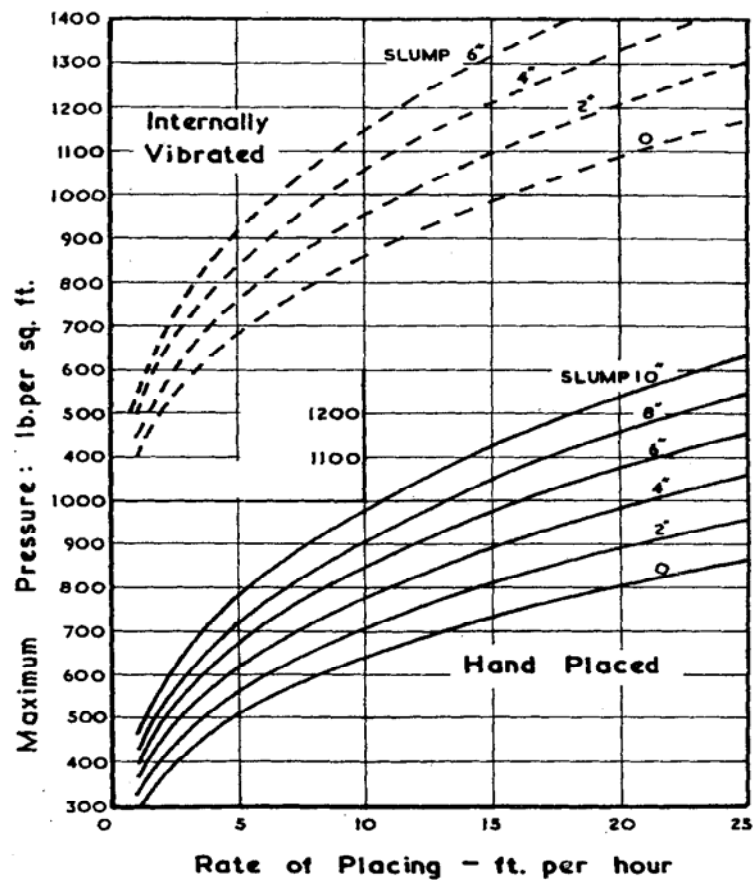
Fig. 40 - Maximum pressure related to workability and rate of placing [Rodin, 1952]

Ritchie [1962B] carried out a series of experiments on concrete with cement-to-total coarse aggregate ratios of 1:3 and 1:6. A fixed casting rate of 3 m/h was used, and the workability varied between low and high. Mixtures with lower workability were found to exert slightly greater pressures than those with higher workability. This behavior, in contradiction to what might be expected, was considered to be due to the fact that drier or lower-slump concrete requires more tamping and greater effort to be properly placed in the formwork, thus resulting in higher pressure.

Gardner [1980] found that for concrete with 170 mm slump cast at 6 m/h, the lateral pressure is equal, in some cases, or typically exceeds that of a concrete with 50 mm slump cast at much higher rate of 46 m/h. A 100-mm slump concrete cast at 46 m/h was found to develop 35% higher lateral pressure compared to a mixture with 50 mm slump, also cast at 6 m/h.

In the case of SCC, Assaad and Khayat [2006] investigated SCC mixtures prepared with 450 kg/m³ of binder and *w/cm* of 0.40. The mixtures had slump flow values of 550, 650, and 750 ± 15 mm, and incorporated VMA concentrations corresponding to 200, 260, and 350 mL/100 kg of binder, respectively. The sand-to-total aggregate ratio was held constant at 0.46 for all mixtures, and the air-entraining agent dosage was adjusted to ensure a fresh air content of 6 ± 2%. Variations of lateral pressure with time determined near the bottom of PVC column of 2.8 m in height and 200 mm in diameter are shown in Fig. 41 for concrete cast at 10 m/h. The results clearly indicate that the development of lateral pressure of highly flowable concrete (FC) and SCC are significantly affected by the initial consistency level. For a given mixture proportioning, concrete with higher dosage of HRWRA and consistency level was found to exert higher initial pressure and lower rate of pressure drop with time. For example, depending on the mixture consistency, the initial relative pressure can vary from 75% to 98% of hydrostatic and the time to reduce the pressure by 10% can range from 45 to 167 minutes. Studies by Ferron et al, [2006] also showed that the degree of thixotropy is strongly related to the initial fluidity of the paste. As the fluidity of the system is increased, thixotropy is decreased due to a reduction in the coagulation forces and inter-particle collisions.
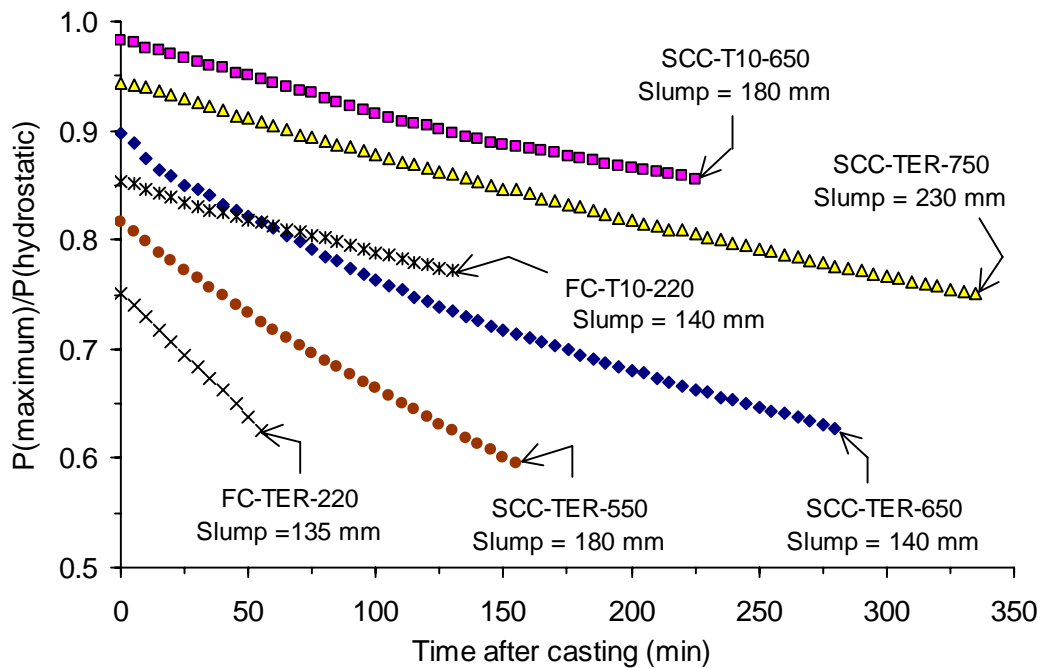
Fig. 41 - Effect of mixture consistency on relative pressure (consistency values are noted at the end of each test) [Assaad and Khayat, 2006]

4.3 Placement conditions

4.3.1 Placement rate

Several investigations were carried out to determine the influence of casting rate on the development of lateral pressure. Ritchie [1962B] conducted a series of experiments on concrete with cement-to-total coarse aggregate ratios of 1:3 and 1:6. Lateral pressure was determined on an experimental column measuring 2.4 m in height and 150 × 150 mm² cross-section. The casting rate varied from 1 to 20 m/h, as shown in Fig. 42. Irrespective of the composition and workability of the mixture, lateral pressure was found to increase with the casting rate. For example, for a 1:6 concrete mixture with high workability, the maximum lateral pressure decreased from approximately 38 to 24 and 10 kPa when the casting rate was reduced from 20 to 3.5 and 1 m/h, respectively.
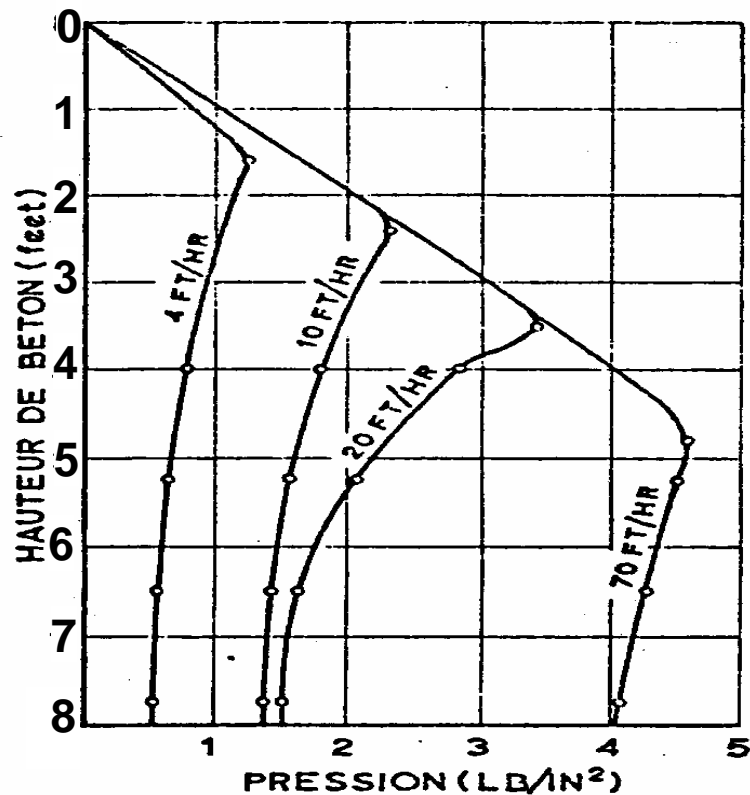
Fig. 42 - Effect of placement rate on lateral pressure [Ritchie, 1962B]

Similarly, Roby [1935] reported that the increase in placement rate from 0.3 to 3 m/h increases the lateral pressure developed by plastic concrete (Fig. 43). According to Gardner [1980], the time necessary to fill a formwork with a lower casting rates can increase the time available for the concrete to develop higher shear strength, thus resulting in reduced lateral pressure. Maxton (from [Rodin, 1952]) studied the coupled effect of casting rate and concrete temperature on the lateral pressure envelope. Different series of relatively low-slump concrete mixtures placed at casting rates varying between 0.6 and 2 m/h were investigated. The concrete temperature varied from 4.5 to 27 °C. The maximum lateral pressure was found to increase with the increase in the casting rate and/or decrease in concrete temperature. Irrespective of the above parameters, the pressure envelope was reported to be hydrostatic in nature from the free surface to a certain maximum value and remained constant thereafter until the bottom of the formwork. The author noted that such pressure distribution is applicable for vibrated concrete in widely spaced forms, such as those used for block construction on locks and dams. Whenever narrow formworks,

73

vibrators, and higher casting rates are used, the author recommended using pressure corresponding to the concrete hydrostatic pressure for the full depth of the formwork.
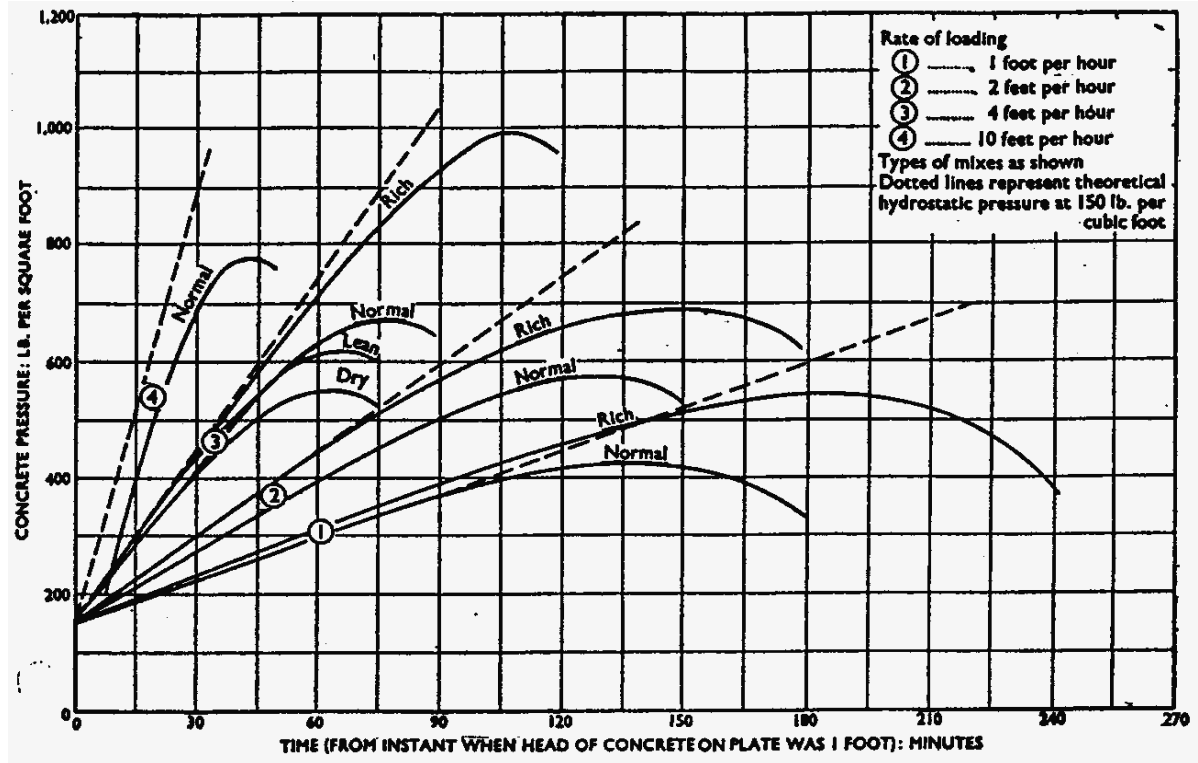
Fig. 43 - Effect of casting rate on lateral pressure [Roby, 1935]

Several studies established that the rate of casting could have marked effect on formwork pressure exerted by SCC (Vanhove et al., [2001], Khayat et al. [2002B], Leemann and Hoffmann [2003], Assaad [2004], Fedroff et al., [2004], Beitzel et al., [2004], and Tejeda-Dominguez et al. [2005]). When the pouring rate is so fast that no stiffening is allowed, (such as in small volume pours that can be completed in one single lift), SCC formwork pressure could well reach hydrostatic pressure. However, when formwork pressure measurements were done in larger structures where the pouring rate was indeed slower, the maximum pressure was considerably smaller than the hydrostatic pressure.

Billberg [2003] evaluated the formwork pressure exerted by SCC cast at relatively low placement rates of approximately 1 to 2.5 m/h. These rates of rise of concrete in the formwork may be obtained when casting SCC in relatively large sections, such as bridge

74

piers or long wall elements. Two different mix designs were employed for the SCC (SCC1 and SCC2 with *w/c* of 0.40 and 0.45, respectively) in addition to a conventional concrete (CC). The slump flow at the time of casting was 730 ± 50, 700 ± 50 for the SCC1 and SCC2, respectively. The concrete was dropped from 1 ± 0.5 m height over the concrete surface in formwork measuring 3 m in height. From the reported in Fig. 44, the correlation between casting rate and form pressure was found to be relatively linear for SCC.
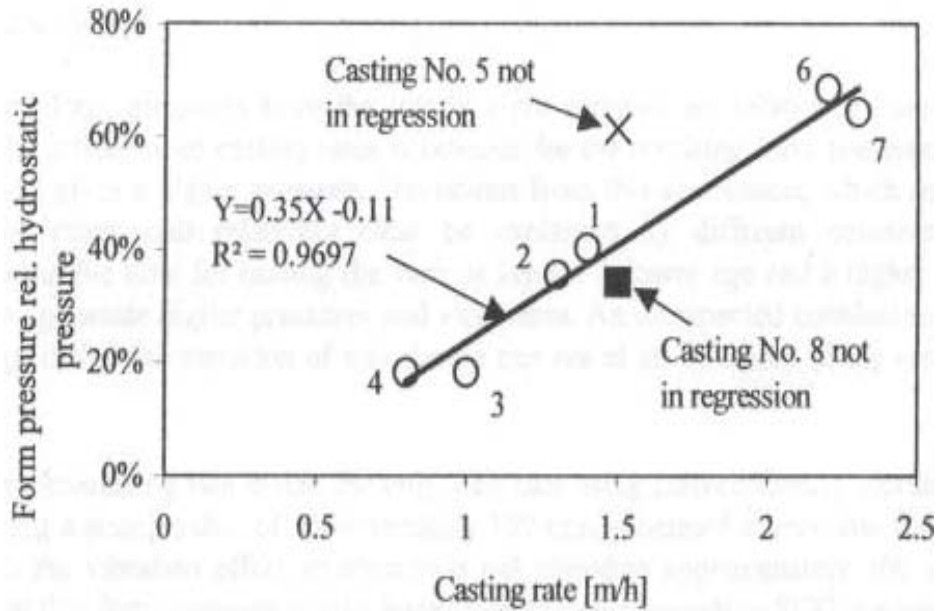
Fig. 44 - Variations of relative form pressure with casting rate for SCC [Billberg, 2003]

For SCC placed at relatively moderate-to-high casting rates, Assaad and Khayat [2006] evaluated the effect of casting of SCC using a pressure column measuring 2.8 m in height and 200 mm in diameter. As noted in Fig. 45, the decrease in casting rate from 25 to 5 m/h can reduce the maximum initial pressure by 15%; however, no significant effect was noted on the rate of pressure drop with time. The interruption of casting for 10 or 20 min between subsequent lifts at the middle of the placement was reported to lead considerable reduction in formwork pressure despite the fact that the casting rate was maintained at 10 m/h when placement was occurring [Assaad and Khayat, 2006].
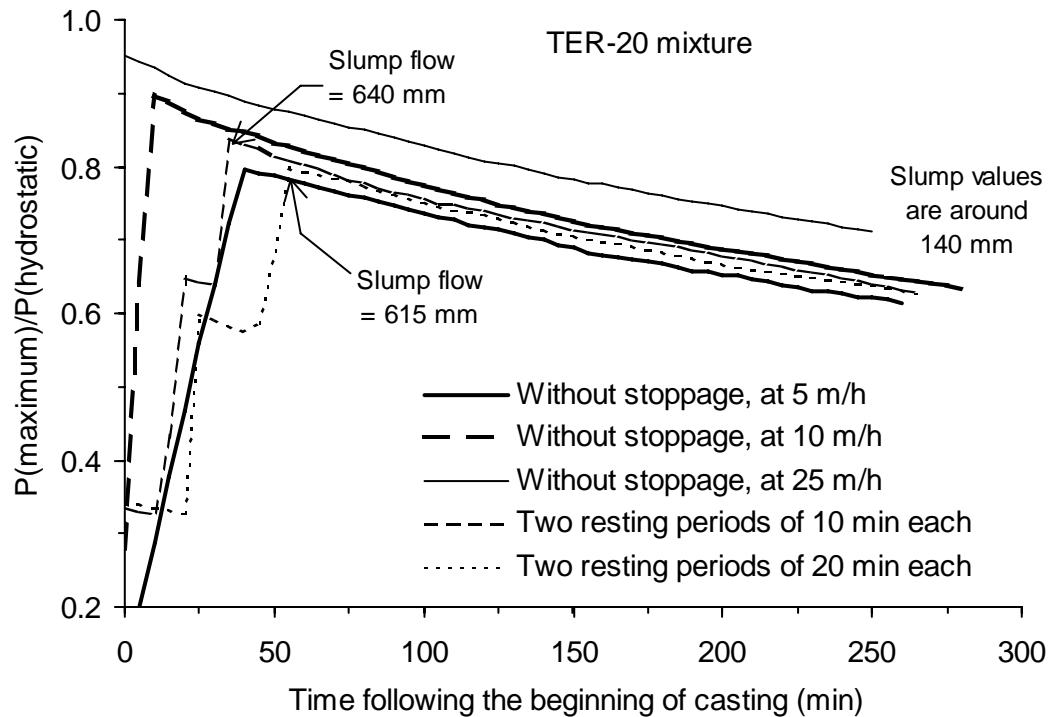
Fig. 45 - Effect of casting rate on relative pressure of SCC [Assaad and Khayat, 2006]

4.3.2 Placement method

Wolfgang and Stephan [2003] conducted an investigation on a model wall with h × w × d of 3.30 × 3.51 × 0.24 m, respectively. A complex configuration formwork was chosen (Fig. 46) to minimize boundary effects. Four walls were cast using SCC: two cast with buckets from the top and two with the concrete being pumped from the bottom at placement rates of 2 and 10 m/h. The fifth wall was cast using conventional vibrated concrete (VC) placed from the top with buckets with a placement rate of 7.5 m/h. As noted in Fig. 47, the vibrated concrete exhibited nearly hydrostatic pressure over the 3.3-m high wall element. Much lower lateral pressure distribution was obtained with the SCC cast from the top with a bucket. As expected, the decrease rate of placement resulted in lower lateral pressure for either the bucket and bottom injection placement methods. Hydrostatic pressure was obtained when placement was carried out from the bottom with concrete pump. The resulting lateral pressure was approximately twice that of SCC cast from the top at the same casting rate. Slowing down the casting rate at 2 m/h in the case of bottom injection was found to require higher pumping pressure.

76
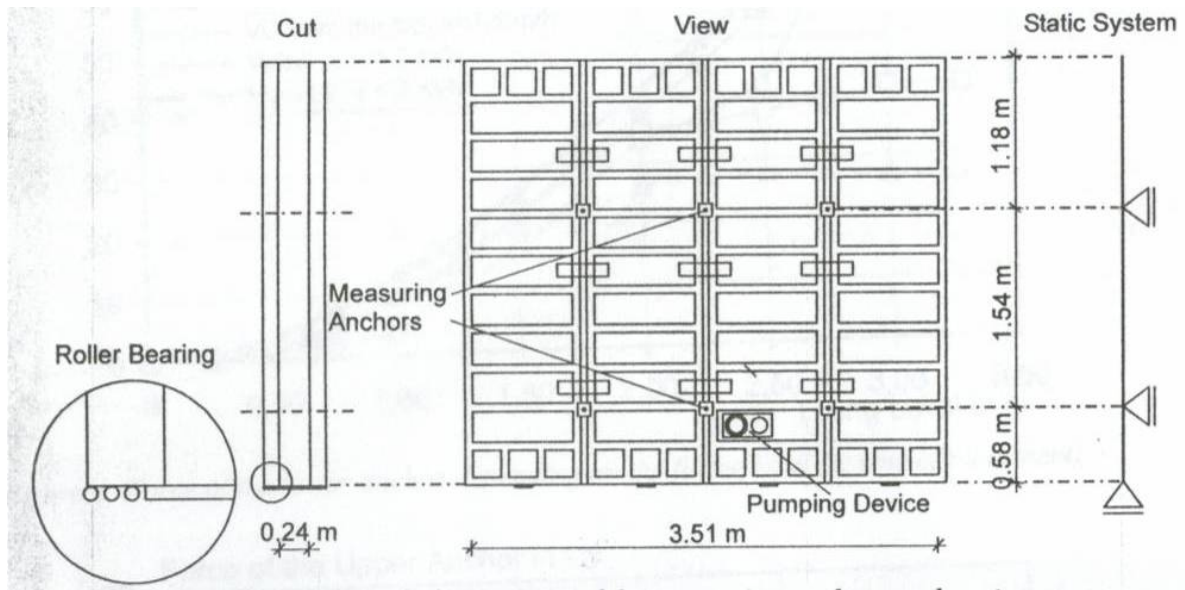
Fig. 46 - Test set-up with the position of the measuring anchors and static system [Wolfgang and Stephan, 2003]
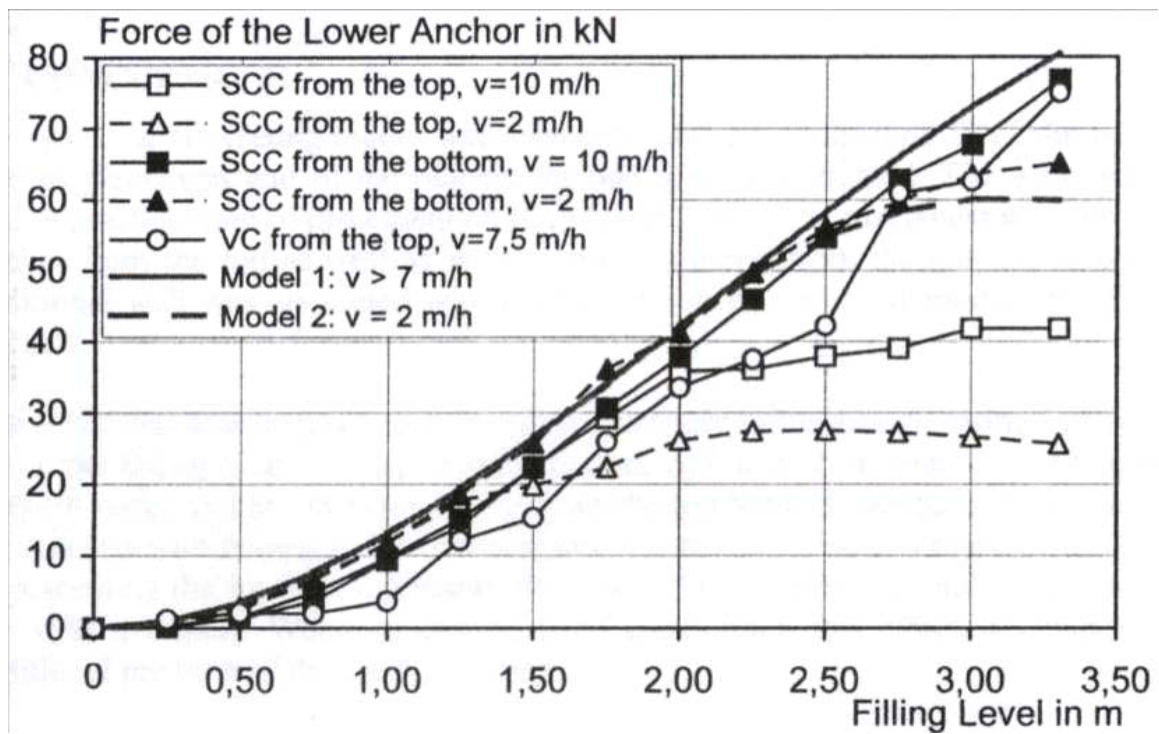
Fig. 47 - Force of the lower anchor depending on the filling level (v: rate of placement), [Wolfgang and Stephan, 2003]

4.3.3 Vibration magnitude and time of application for conventional concrete

Stanton [1937] reported the results of a series of tests made by the California Division of Highways to ascertain the effect of electrically-driven internal vibrator on concrete lateral pressure. The relationship between height of concrete above the pressure cell and the recorded pressure is plotted in Fig. 48. Measurements were made on retaining walls measuring 4.5 m in height, 650 mm in width at the bottom, and 450 mm in width at the top [Stanton, 1937]. The pressure cell was placed 1 m above the footing. Except in the instance noted in the diagram, the vibrator was embedded in the upper 600 mm. The readings indicated that full hydrostatic pressure acted until the head of concrete height reached 1.4 m, after which the concrete pressure steadily decreased except when the vibrator was lowered through the concrete to a point about 600 mm above the pressure cell for a period of 2 minutes.
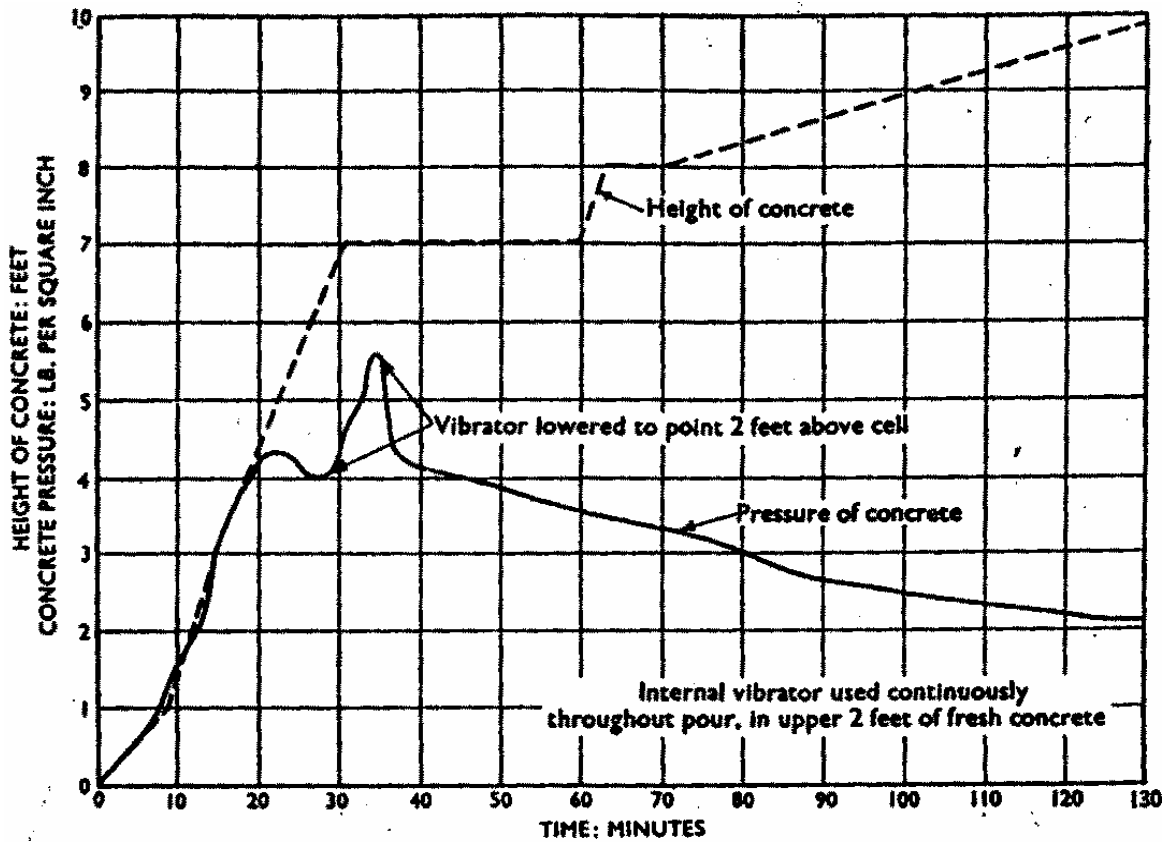
Fig. 48 - Pressure developed by vibrated concrete [Stanton, 1937]

78

Ore and Straughan [1968] reported that the maximum pressure for conventional vibrated concrete could drop from 100% to 40% of hydrostatic when the distance between the vibrator and the concrete-filled bottom of formwork is increased to 900 mm. When the concrete is re-vibrated, the pressure values could increase to 73% and 98% of hydrostatic, depending on the elapsed time between the placement and re-vibration. The authors concluded that the duration, magnitude, and location of the vibratory effort are more critical than any other factors considered in the development of pressure, and should therefore be consistent in formwork design.

Gardner [1984] reported that vibrated concrete behaves as a liquid having the same unit weight of concrete, with the pressure envelope tangential to the line of hydrostatic pressure. When the concrete head becomes sufficiently high (more than 2 m), the effect of the vibrator becomes considerably reduced or even cancelled. Concrete in the lowest part of the formwork can no longer be fluidized by the consolidation effort. The concrete will then start to develop shear strength and wall friction, and the lateral pressure at the bottom will start to deviate from the hydrostatic pressure. When the concrete head is again increased, the shear strength magnitude becomes more significant, and the lateral pressure reaches a maximum value at some elevation above the base of the formwork. Even with further increase in concrete head, the lateral pressure remains constant at a maximum value until the bottom of the formwork. The author concluded that the major parameters controlling the magnitude of lateral pressure are the depth of vibrated concrete, development of shear strength, and wall friction.

4.3.4 Ambient and concrete temperature

Roby [1935] showed that the pressure developed by concrete during hot weather is less than that obtained under moderate ambient temperature. For example, concrete mixture placed at 38 °C temperature was reported to develop maximum pressure of around 60% to 75% less than that exerted by the same mixture cast at a temperature of 16 °C.

The Portland Cement Association (from Rodin [1952]) studied the coupled effect of concrete temperature and casting rate for hand-placed concrete. Five casting rates varying from 0.5 to 2 m/h and concrete temperature of 10 to 21 °C were evaluated. For a given

casting rate, the increase in concrete temperature was reported to reduce the maximum pressure, as can be seen in Fig. 49.

The effect of concrete temperature on lateral pressure was also evaluated by Gardner [1984] on vibrated mixtures with slump values ranging between 65 and 115 mm. Concrete temperatures varying from 2 to 27 °C were tested. As reported earlier, the lateral pressure was found to increase with the decrease in concrete temperature. The author found that the mechanical properties of plastic concrete depend on the concrete temperature. For lower temperatures, the hydration of cement can be slowed down, and mechanical properties can develop at a slower rate resulting in higher lateral pressure. Gardner [1984] reported that lateral pressure is rather controlled by the concrete temperature, and not by the ambient temperature.
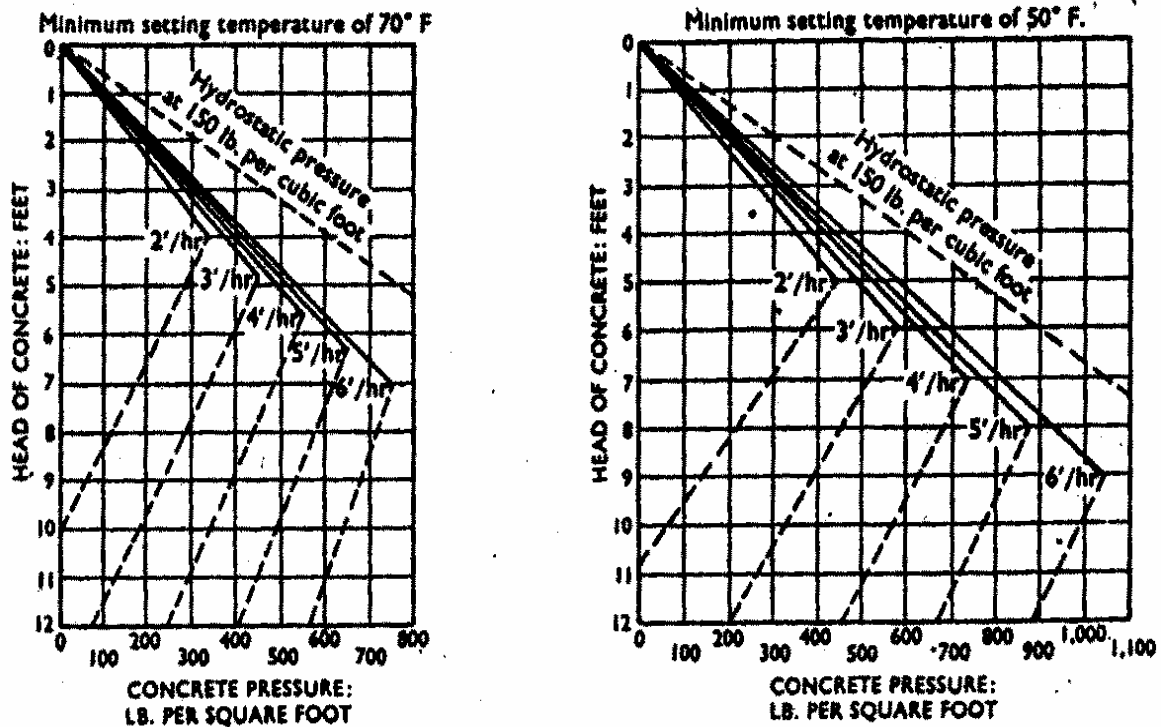
Fig. 49 - Effect of concrete temperature on lateral pressure [Rodin, 1952]

The effect of SCC temperature on lateral pressure variations was evaluated by Assaad and Khayat [2006]. The mixtures had a ternary binder content of 450 kg/m³, *w/cm* of 0.40, slump flow of 650 ± 15 mm, and air content of 6 ± 2%. They were prepared at 10, 20, and

30 ± 2 °C; these mixtures are referred to as TER-10, TER-20, and TER-30 mixtures, respectively, in Fig. 50. The variations of relative pressure of these mixtures cast at 10 m/h in PVC columns measuring 2.8 m in height and 200 mm in diameter are plotted in Fig. 50. The mixtures prepared with ternary cement at initial temperatures of 10, 22, and 30 °C develop similar relative pressures of 91% at the end of casting. On the other hand, the rate of pressure drop with time was significantly affected by the concrete temperature. For example, the elapsed time to reduce the relative pressure by 25% decreased from 400 to 250 and 160 min for the TER-10, TER-20, and TER-30 mixtures, respectively. Higher concrete temperature can result in greater rate of loss in consistency. For example, slump values of 170 and 180 mm were measured 5 and 3.5 hours after casting for the TER-10 and TER-30 mixtures, respectively. Pressure variations of SCC made with CSA Type 30 (HE) cement and ternary cement with set-accelerating admixture cast at 20 °C are also plotted in Fig. 50. As expected, the rate of pressure drop was faster for these mixtures given the accelerated rate of hydration leading to faster development of cohesion and reduction in lateral pressure.
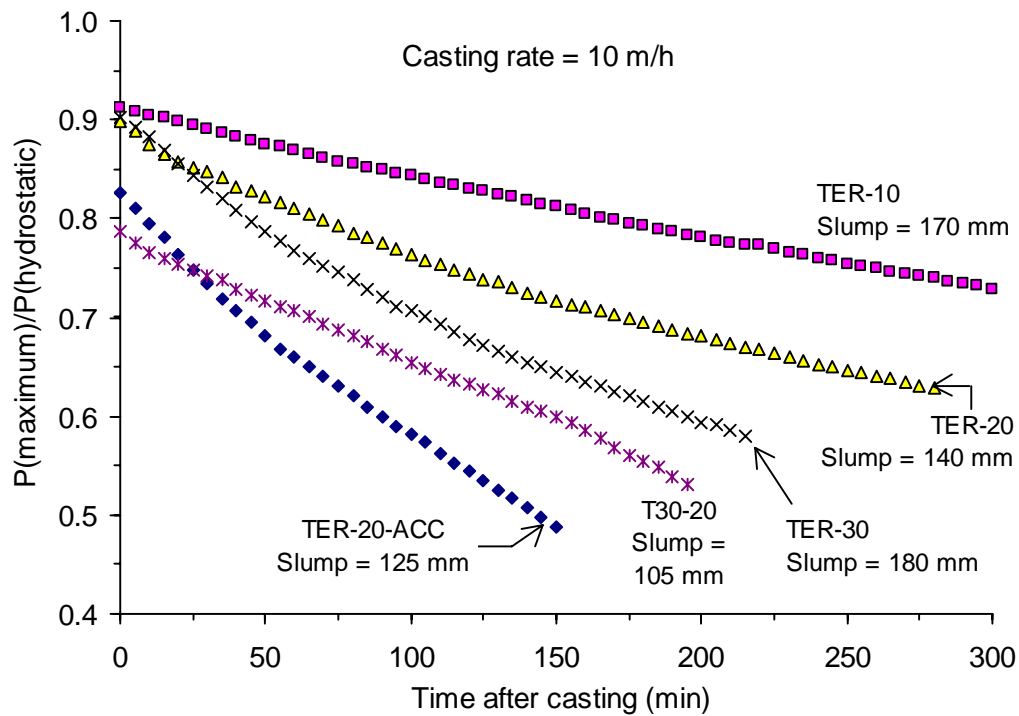
Fig. 50 - Effect of concrete temperature on variations in relative pressures determined at the bottom of the 2800-mm high column for SCC made with ternary cement (slump values determined at the end of pressure monitoring are noted) [Assaad and Khayat, 2006]

4.3.5 Time required before formwork removal

It is usually economical to remove formwork as early as possible, provided that the concrete is strong enough to support the imposed loading system when the formwork is struck. Therefore, it is important to decide on the minimum elapsed time after casting for formwork removal so that no damage occurs to the concrete. Premature removal might involve considerably more expense in remedial work than can be saved by an extra day's use of the formwork.

When the formwork is removed early from in-situ concrete, a number of potential problems need to be avoided. Harrison [1983] reported that the factors to be considered in setting the criteria for formwork removal can include collapse, deflection, freeze/thaw damage, mechanical damage to the concrete, moisture loss, color variation, durability, thermal cracking and shock, as well as some specific site requirements. The author found that the key parameter for assessing the time required for formwork removal is the characteristic *in-situ* compressive strength of the concrete.

Generally speaking, the minimum time for formwork removal depends on concrete strength and loading system to which the concrete would be subjected. According to Murdock and Blackledge [1968], a minimum time varying between 12 hours and 4 days would be necessary before the removal of formwork used to cast wall and column elements, respectively, depending on temperature and cement type. Such period can increase to 7 or even 14 days in the case of slab or beam horizontal elements of long spans where greater strength and rigidity developments would be required. The formwork could be removed earlier for mixtures having greater cement contents, especially those made with high early-strength cement.

Whenever the formwork must be removed at early age for particular circumstances, the British Standard (CP 114) stipulates that the concrete should attain a compressive strength corresponding to twice the total stress that is expected at the time of formwork removal [Taylor, 1965]. Such strength can be determined from control specimens or by means of non-destructive testing, such as the "Schmidt" spring hammer. The ACI Manual of Concrete Practice recommends that the evaluation of concrete strength can be

demonstrated by field-cured test cylinders or other approved procedures, such as penetration resistance (ASTM C 803), pullout strength (ASTM C 900), or maturity factor (ASTM C 1074).

4.3.6 Relating lateral pressure cancellation time and setting time of concrete

Final setting time is the time when the concrete reflects its transition from a plastic material to a solid one. Before final setting time, it is assumed that no stresses are developed because the concrete is in a plastic state. After final setting time, concrete become a rigid material, and deformations can translate into tensile and compressive stresses. The setting rate of concrete is affected by the characteristics of the concrete mixture as well as the prevailing conditions at the project site, including ambient temperature, humidity, and wind.

The times corresponding to initial and final settings are typically determined using mortars extracted from the concrete in compliance with ASTM C 403. These setting times are considered as suitable references to indicate the time at which the concrete can no longer be properly handled or placed. Even though they are based on purely arbitrary measurements, their evaluation can be of special interest to estimate the beginning of the stiffening phase [Jiang and Roy, 1991].

Khayat and Assaad [2005A] attempted to relate the standard ASTM C 403 setting times to the time required to cancel lateral pressure exerted by SCC. Relationships between the times corresponding to canceling of pressure (t2) and the initial and final setting times of mortars extracted from numerous SCC mixtures prepared with various material characteristics and mixture proportions are plotted in Fig. 51. As expected, mixtures exhibiting longer setting times necessitated longer periods after concrete placement prior to lateral pressure cancellation. Pressure cancellation was determined using a pressure sensor attached near the bottom of a 1.1-m high PVC column measuring 200 mm in diameter.
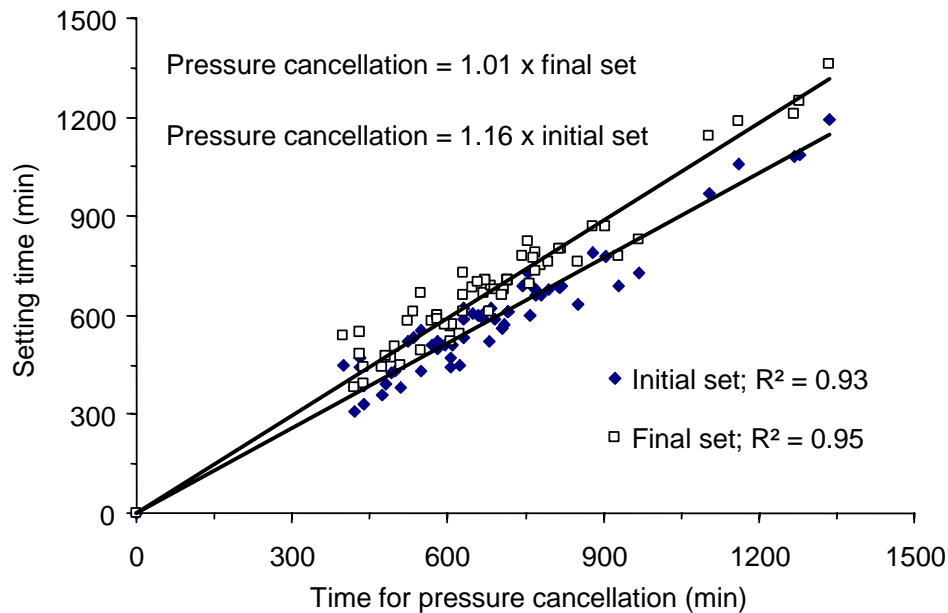
Fig. 51 - Relationship between initial and final setting times and elapsed time for lateral pressure cancellation [Khayat and Assaad, 2005A]

4.4 Formwork characteristics

4.4.1 Formwork dimension

Limited data exist regarding the effect of size and shape of the formwork on lateral pressure characteristics. Rodin [1952] reported that the general tendency indicates that the maximum pressure appears to be lower in formwork systems of smaller cross-sections. This can be attributed to the increased degree of the arching effect, which limits lateral pressure. Gardner [1980] demonstrated that the larger the dimension of the formwork, the larger the lateral pressure could be for conventional vibrated concrete.

Khayat et al. [2005A] studied the effect of column diameter on changes in lateral pressure. Two experimental formwork systems were used. A PVC tube of 2.1 m in height, 200 mm in diameter, and 10 mm in wall thickness was used for one system. The second column consisted of a sonotube measuring 3.6 m in height and 920 mm in diameter. The sonotube had an impermeable plastic liner and was adequately braced and reinforced. Lateral pressures were determined using pressure sensors located at various locations along the heights of the experimental columns. Both columns were cast at the same casting rate of 10 m/h. Fig. 52 illustrates the variations of relative lateral pressure determined at

approximately 2 m from the top of the formwork systems. Initially, the mixture placed in the larger column exhibited slightly greater relative pressure of 99% compared to 96% for the 200-mm diameter column. This can be due to an arching effect in the relatively restricted section. However, the rates of drop in pressure were significantly different. In the case of the concrete placed in the 920-mm diameter column, the time required to reduce lateral pressure by 5% of the hydrostatic value was 20 min, resulting in a rate of decay of 5.3 kPa/h. Conversely, for the 200-mm diameter column, this period was 38 min, or an initial rate of decay of 3.3 kPa/h.
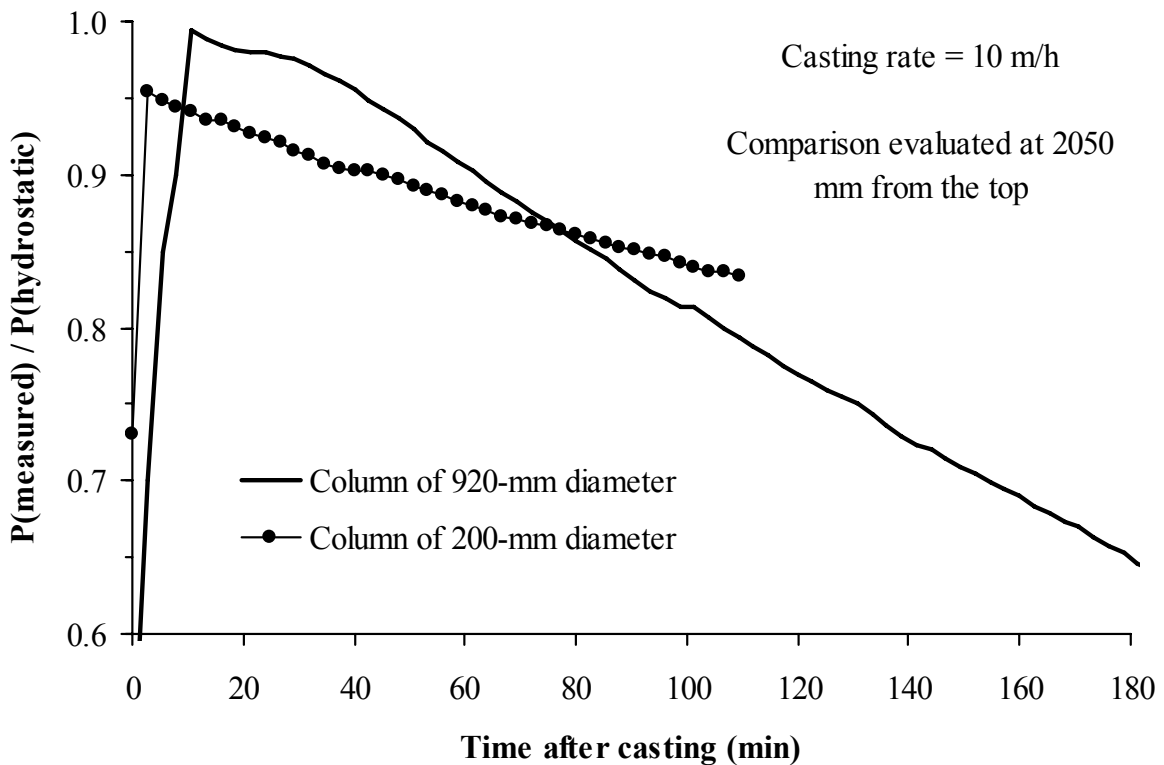
Fig. 52 - Effect of section width on lateral pressure [Khayat et al., 2005A]

4.4.2 Presence of reinforcement

The density of reinforcement in the formwork is an important item. The presence of reinforcing bars can be expected to carry part of the concrete load, and therefore have a beneficial effect on the formwork pressure. However, such beneficial effect might be

cancelled due to the increased level of tamping that could be required to distribute and consolidate the concrete between the reinforcements [Rodin, 1952].

4.4.3   Type of formwork surface material

In the study carried out by Arslan et al. [2005], seven wall forms with measuring 1 m in length; 2 m in height and 0.15 m in width were constructed. The surfaces of the forms were constructed using *populus nigra* and *pinus silvestris* timber, beech plywood, and steel sheet. The surfaces of all seven formworks were treated with mould oil. One of each pair of formworks, which were made from the same surface material, was watered before concrete placement. One surface of each form was fixed by welding to a supporting structure to make it stable during the concrete placement process. The other surface of the formwork was mounted by a pin at its upper point to allow it to rotate. The bottom part of this rotating surface sat on ball bearings in order to minimize friction, as shown in Fig. 53.

Table 3 summarizes the lateral pressure values measured during concrete lateral pressure experiments and indicates the limiting values (P_{max}), which are calculated by the equations of CIRIA [1965], DIN-18218 [1980], and ACI 347 [2001]. The recorded lateral pressure of all formworks increased continuously. However, the rate increase showed differences according to the surface materials of formworks, as shown in Fig. 54. Arslan et al. [2005] referred the lateral pressure increase to concrete swelling during setting time and to the wood formwork surface materials' swelling and its water absorption. The latter differs according to differences in formwork surface material in use. Thus, increases in the rate of lateral pressure were different [Dally et al., 1984]. The authors also concluded that the lateral pressure of steel formwork was equal to the limiting value of ACI 347 and larger than the lateral pressure obtained with *populus nigra* and *pinus silvestris* timber and plywood formwork. Lateral pressure of *pinus silvestris* formwork was the smallest. Watering the surface of the wood formworks was also found to increase lateral pressure of the plastic concrete on the formwork.
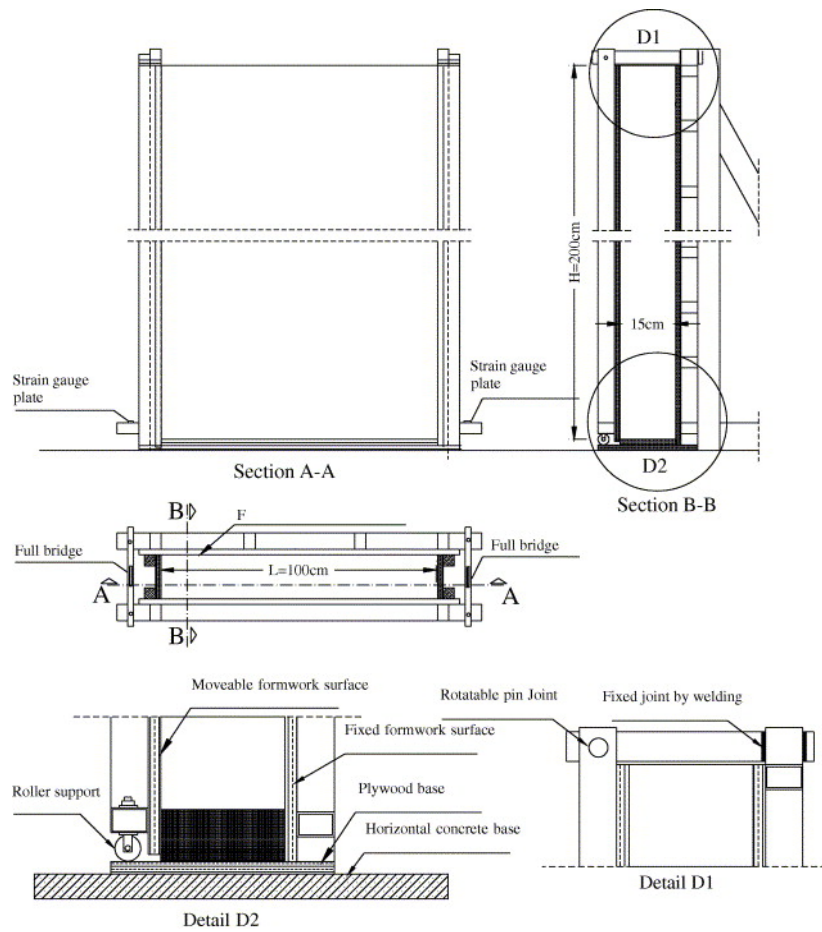
Fig. 53 - Formwork details of Arslan et al. [2005]

Table 3 - Concrete lateral pressure on formwork surface (kPa) [Arslan et al., 2005]

Formwork code and surface process	Mean pressure (kPa)	Min.	Max.
F1 *populus nigra* (watered)	22.85	21.77	23.74
F2 *populus nigra*	20.93	19.94	21.88
F3 *pinus silvestris* (watered)	23.68	21.39	25.11
F4 *pinus silvestris*	19.91	18.01	21.15
F5 plywood (watered)	24.55	22.47	25.96
F6 plywood	21.48	19.22	22.81
F7 steel	26.19	24.70	26.97
Limiting value of ACI 347			26.92
Limiting value of CIRIA			30.98
Limiting value of DIN-18218			30.98
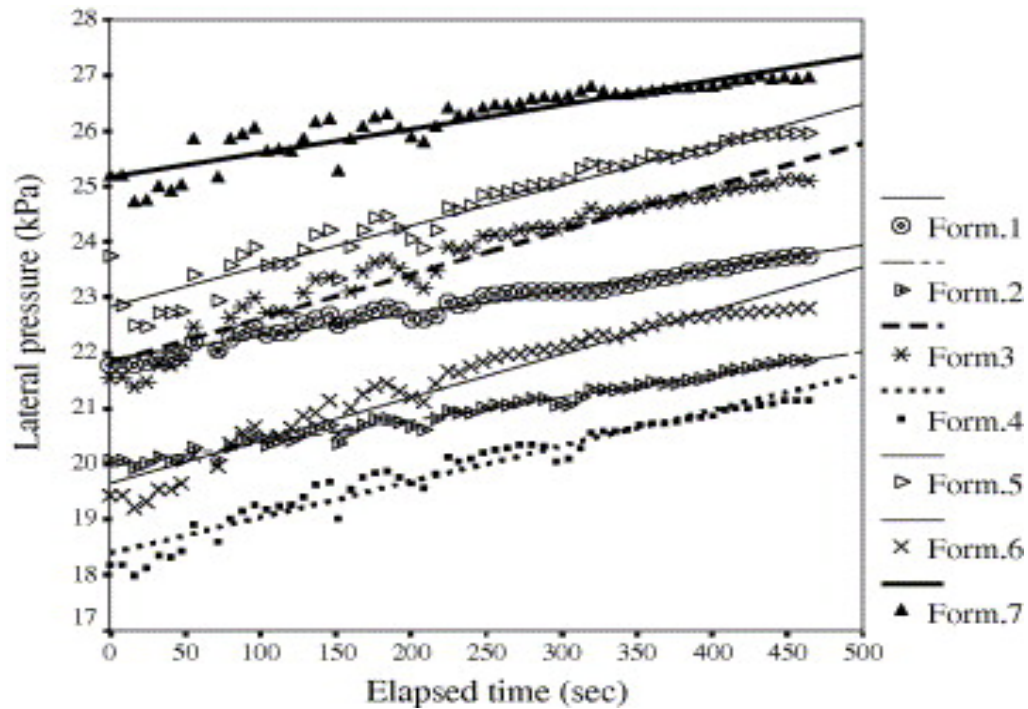
Fig. 54 - Variation of lateral pressure with elapsed time [Arslan et al., 2005]

Tejeda-Dominguez and Lange [2005] evaluated the effect of formwork material on SCC lateral pressure. Two different sonotube configurations were used (one without any modification [ST-1] and the second with an impermeable plastic liner to cover the interior wall [ST-2]). Also, two different formwork configurations of PVC columns were used (one without any modification or reinforcement [PVC-1] and the second cut along one side from top to bottom and reinforced with steel straps to keep it tightly closed [PVC-2]). All the columns have a diameter of 0.25 m and a total height of 3 m. For each column, two sensors were placed at 0.15 m from the bottom. All columns were filled from the top at an approximate rate of 27 m/h. The concrete was not vibrated or compacted by any means. The four tests showed that the lateral pressure characteristics of SCC were close to hydrostatic immediately after casting. However, as shown in Fig. 55, the decrease in pressure after casting was dependant on the forming material. The study illustrates the importance of using rigid, self-supporting column apparatus to monitoring lateral pressure variations, especially when pressure sensors are attached to the formwork material. If the column material is not rigid enough, as was the case of the plain sonotube that can imbibe water, the rate of lateral pressure drop would seem to be sharp given the swelling of the column

88

material and separation of the pressure sensor that was initially set flush with the plastic concrete.
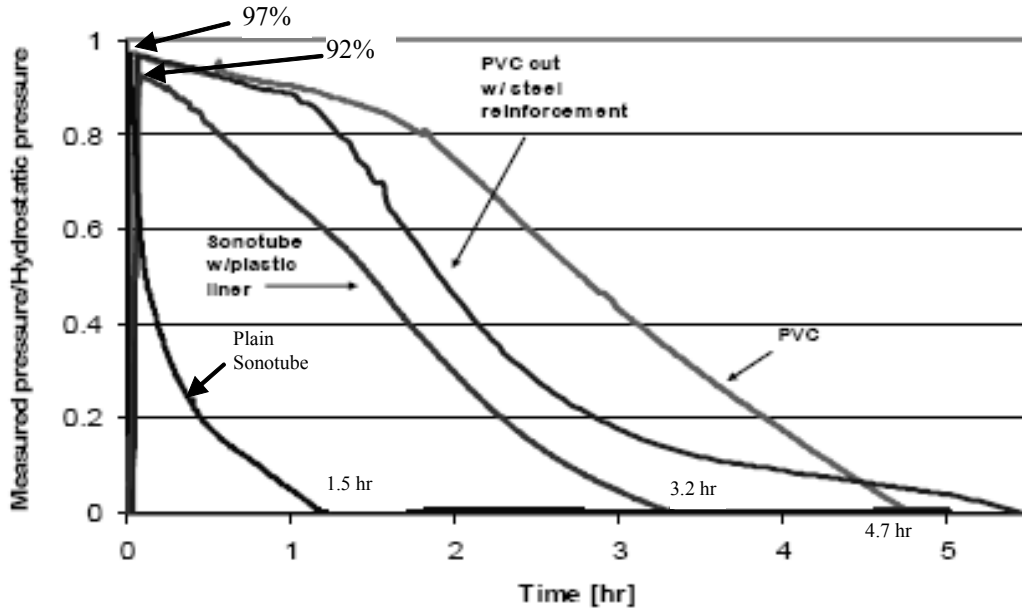
Fig. 55 - Evolution of measured pressure for SCC cast in different formwork materials [Tejeda-Dominguez and Lange, 2005]

4.4.4 Water drainage at inner formwork surfaces

In the study conducted by Arslan [2002], four types of geotextile materials (Table 4) were used as inner liners to investigate the effect of such liners on formwork pressure. The liner materials were applied on wall elements measuring 1 m in length; 2 m in height and 0.15 m in width. The walls were cast at a placement rate of 1 m/h using a conventional concrete made with Type I cement and no admixture and having a slump of 100 mm and approximate temperature of 25 °C. The maximum lateral pressure was shown to decrease when using drained and lined formwork compared to the reference forms and the limiting pressure value recommended by ACI 347. By enabling drainage to the formwork surface and covering the surface with Type IV geotextile, the lateral pressure of concrete was shown to decrease by 40%.

89

Table 4 - Different types of geotextile used by Arslan [2002]

Type of Geotextile	Condition	Unit weight, kg/m^2	Tensile strength, kN	Break-off stretch, %	Penetration resistance, kN
Geotextile I	Non-woven	0.500	1.260	56	0.915
Geotextile II	Non-woven	0.130	0.208	15	0.190
Geotextile III	Non-woven	0.200	0.286	29	0.225
Geotextile VI	Non-woven	0.200	0.260	30	0.220

4.4.5 Formwork surface roughness

Djelal and co-workers [Djelal, 2001; Djelal et al. 2004; Vanhove et al. 2000] demonstrated that the roughness of the forming material has significant influence on dynamic friction that can develop upon concrete placement. It follows that lateral stresses exerted by plastic concrete on a formwork system can decrease with the increase in dynamic friction when the freshly cast concrete slides against the forming material during concrete placement. Formwork roughness measurements were performed on site using a portable roughness meter where it was determined that the R_a and R_t were equal to 0.3 and 2.3 μ_m, respectively. As illustrated in Fig. 56, R_a is the mean arithmetic deviation of the roughness profile in comparison with a medium line, and R_t is the distance between the highest and the lowest peaks of the roughness profile.
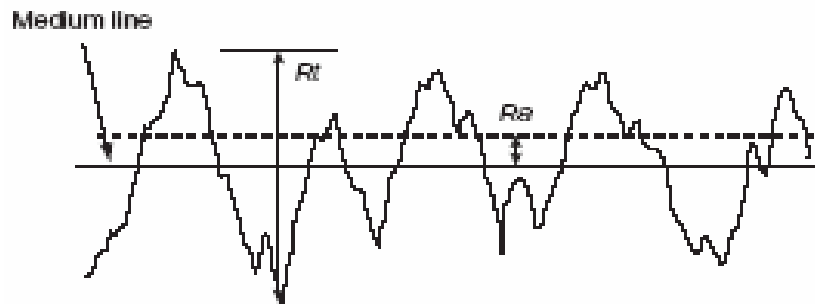
Fig. 56 - Roughness parameters [Vié et al., 2001]

Based on Djelal's study [2001], a plate was made of XC38 steel having the same characteristics as formwork wall materials. Another plate of greater roughness (R_a = 1.6 μ_m and R_t = 13.6 μ_m) was also included in the study to understand the friction mechanisms at the concrete/wall interface that can result at various concrete pressure values. Changes of friction coefficient with overhead contact pressure are plotted in Fig. 57 for a sliding velocity of 2.5 mm/s. No demolding agent was employed in these experiments. The friction coefficient between the formwork material and sliding fresh concrete is shown to depend on the roughness characteristics of the formwork material and sliding velocity of the plate against the concrete, which corresponds to different casting rates.
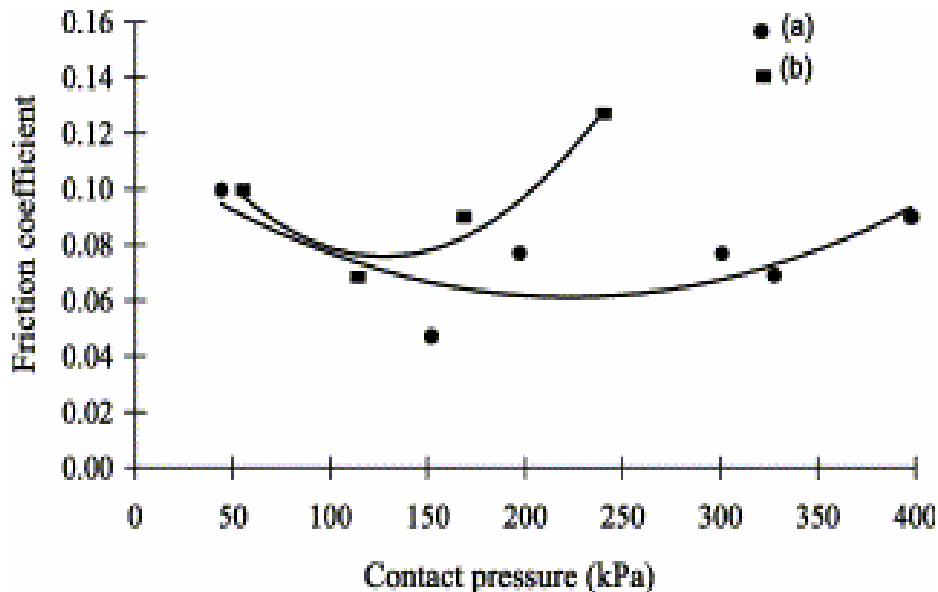
Fig. 57 - Evolution of friction coefficient according to contact pressure for sliding velocity of 2.5 mm/s: (a) R_a = 0.3 μm; (b) R_a = 1.6 μm [Djelal et al., 2004]

From the above results, there appears to be a minimum friction for both roughness configurations. The lateral pressure applied to the plastic concrete could be transmitted to the granular phase and cement paste causing part of the liquid phase and fines to migrate towards the interface between the concrete and the forming material. A lubricating surface (or boundary) layer made of water and fines can be formed at the interface of the formwork material, as noted in Fig. 58-a. A forming material of slight roughness (0.3 μ_m) has ridges that are not deep enough for the surface layer to seep out. The surface layer then remains at the concrete/plate interface under pressure capable of recapturing part of the normal stress.

When the normal pressure is higher than 140 kPa, it could be assumed that the liquid phase, which was at first confined to the boundary layer, begins to move into the sample under the effect of pressure, as illustrated in Fig. 58-b. The material in contact with the surface can adopt a granular behavior during shearing, which explains the increase in friction coefficient.
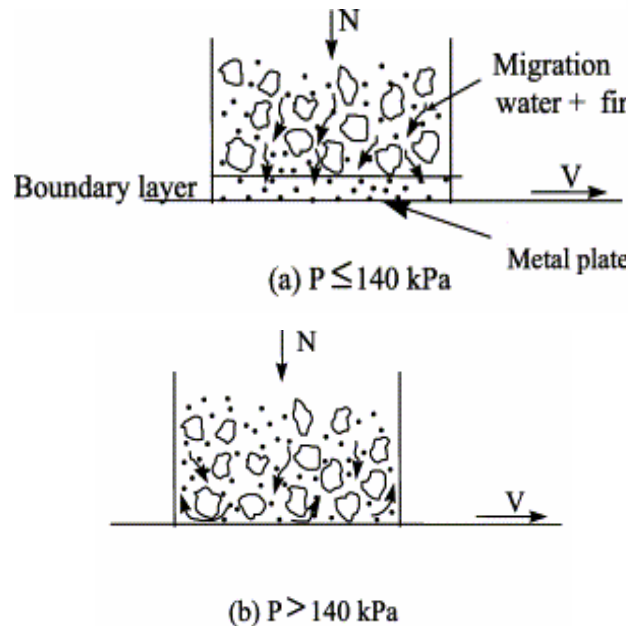
Fig. 58 - Schematic representation of a concrete/metal plate interface ($R_a = 0.3$ μm)

When the plate roughness increases to about 1.6 μm, the friction coefficient was more or less equal to that in the previous case. For normal pressures below 110 kPa, the roughness R_t was 13.6 μm which allowed some of the particles in the boundary layer to become lodged into the ridges. Shear can then occur mainly in this layer, as depicted in Fig. 59-a. In the case of normal pressure values above 110 kPa, part of the boundary layer can migrate towards areas under less stress, as illustrated in Fig. 59-b. The grains of sand or gravel had been directly in contact with the tips of the ridges, and the force exerted by these tips during plate displacement had caused them to rotate, thus producing considerable energy dissipation. As a result, there was a more rapid increase in friction coefficient.
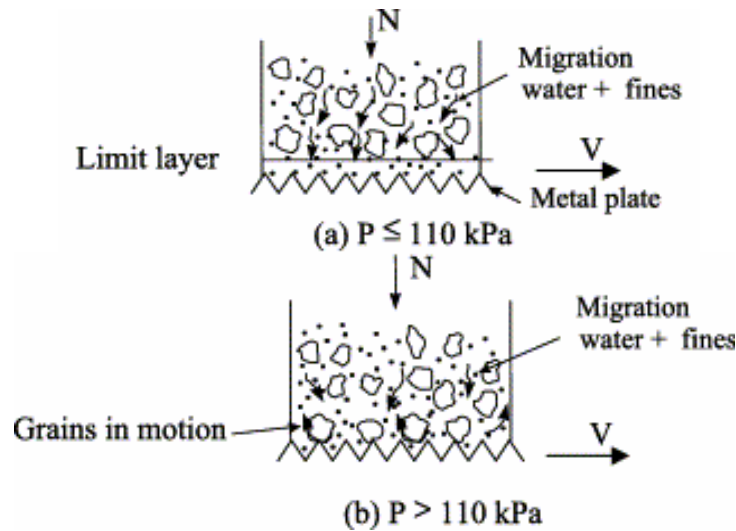
Fig. 59 - Schematic representation of a concrete/metal plate interface (R_a = 1.6 μm)

4.4.6   Demolding agents

In order to investigate the effect of form oil on the friction that can be developing between the forming material and the rising fresh concrete during casting, Djelal et al., [2002] carried out experiments to compare the friction that can be obtained when using demolding agents. Two vegetable-based demolding agents (Oil 31E and Oil 30S) were used. The Oil 31E oil is a water/oil emulsion with surface-active agents. This emulsion ensures a homogeneous oil layer. The Oil 30S is a mixture of oil and solvent that contains a surface-active agent.

Table 5 sums up the characteristics of the two oils. The results of the tribological experiments carried out with forming materials treated with each of the demolding agents and that without any treatment are plotted in Fig. 60. The changes in dynamic friction coefficient as a function of contact pressure indicate that there is a decrease in the frictional coefficient with increasing normal stresses for both oils tested. For a pressure less than 140 kPa, shearing takes place in the surface layer (water + fines + demolding agent). When the pressure exceeds this critical value, the change in friction stress depends on the characteristics of the interface agent in use.

Table 5 - Characteristics of the two demolding oils used by Djelal et al. [2004]

Characteristics	Oil 31E	Oil 30S
Type	Water + oil	Solvent + oil
Density at 20 ºC (kg/m^3)	1000	800
Viscosity at 25 ºC (mPa.s)	5	4.5
Contact angle (degree)	39.4	4
Tensio-activity (%)	2 to 2.2	2.5
Fatty acid	0	1
Active material (%)	15	35
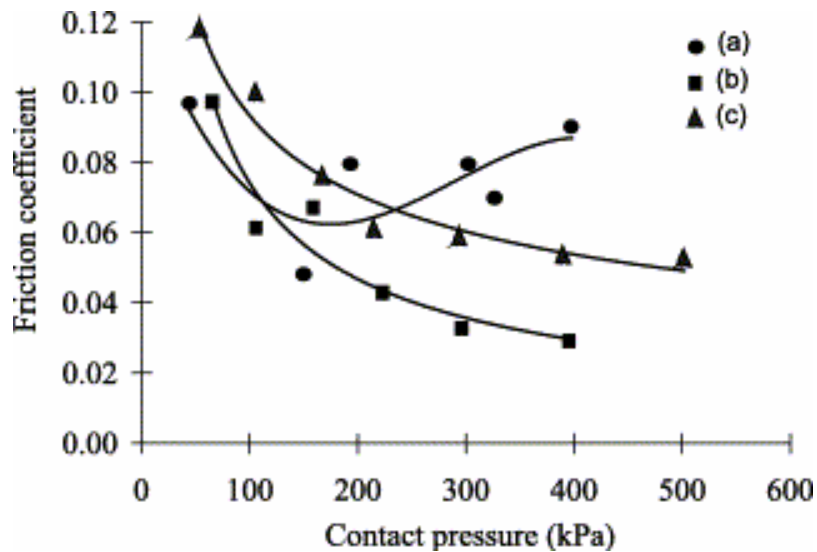
Fig. 60 - Evolution of the friction coefficient according to contact pressure for a sliding velocity of 2.5 mm/s: (a) no oil, (b) Oil 30 S, (c) Oil 31 E [Djelal et al., 2004]

From the above results, the authors [Djelal et al., 2004] deducted that two criteria can prove to be particularly influential with regard to friction stress:

− The quantity of active material deposited in the case of Oil 30S is sufficient for the esters, which are in contact with calcium hydroxide, to be converted into insoluble carboxylate (soaps) and form a hydrophobic film, thus preventing the concrete from adhering;

− The presence of surface-active agents in the Oil 31E and 30S is essential for the concrete to be hydrophobic. The water at the surface of the concrete is thus emulsified. In the case of the Oil 31E, all the esters are used in the emulsion, which is a less favorable situation

than that occurring with Oil 30S.

The percentage of active material content in Oil 30S (35%) is higher than that in Oil 31E (15%), which explains the fact that the increase in friction coefficient is lower than for the first oil. The wetting power of the demolding agents (e.g., the contact angle) seems to act directly on the friction coefficient. Indeed, Oil 30S has the lowest friction coefficient and highest wetting power, while the viscosities are similar. Thus, it was concluded that Oil 30S formulation would be more suitable to minimize friction stresses.

5. LATERAL PRESSURE MEASURING SYSTEMS

5.1 Instruments and devices to monitor lateral pressure

A number of methods have been adopted to measure lateral pressure exerted by plastic concrete on formwork. Roby [1935] measured the concrete pressure by deflection of a steel plate extending to the full width of the form and resting on movable edges 700 mm apart. The steel plate located near the bottom of the formwork measured 150 mm in width and 10 mm in thickness. By means of a pivoting bar connected to a lever to give a ratio of 10:1, the deflection at the center of the plate was determined on a scale graduated in increments of 0.4 mm. By using a magnifying glass, it was possible to read within 0.1 mm, which corresponds to a plate deflection of 0.01 mm. The thickness of the timber sheathing above and below the steel plate was designed to give the same deflection under load as the steel plate. For a maximum pressure of 7,000 kPa, the deflection at the center of the plate was 6 mm. Such deflection can be considered quite appreciable and might have the effect of relieving the steel plate of some pressure.

Macklin [1946] determined the pressure of concrete against the formwork by measuring the deflection of the wood sheathing. The deflection of the sheathing relative to the supporting studs was measured by means of a dial-type micrometer mounted on a bridge arrangement. Stanton [1937] used pressure sensors consisting of a metal disk. A sheet-rubber diaphragm was clamped to one side of the sensors in a manner similar to that of a drumhead. The shallow space between the rubber diaphragm and the disk was filled with liquid that would operate as ordinary pressure gage mounted on the back of the disk. The

pressure sensors, 150 or 300 mm in diameter, were inserted into the form wall such that the rubber diaphragm was flush with the inside surface of the wall. Special care was taken to extract all air from the pressure sensors. No indication was given as to the volume change undergone by the sensors when the concrete pressure was applied.

Gardner and Ho [1979] employed Cambridge-type load cells to determine the formwork pressure. The total load capacity of the cell was around 2500 N. The vertical and horizontal measuring strips were 65 mm in width and 8 mm in thickness. The two gages on each measuring strip were wired in series of eight pairs of two pairs per load cell.

Khayat and co-workers selected pressure sensors from Honeywell (Model AB MP) to monitor formwork pressure. The strain-gage based pressure sensors shown in Fig. 61 are known as flush diaphragm millivolt output type pressure transducers. Typically, the diameter of the sensor used by the authors for SCC was 20 mm, though greater diameters can be used when the concrete ha large nominal size aggregate. The sensors are calibrated against an analog pressure gage using an oil pump and are also calibrated using a given water head. During the experiments, the sensor is connected to a data acquisition system with a scanning voltage of 5 mV. The pressure sensors are set flush with the inner side of the formwork through drilled holes. A thin film of grease is applied to the sensors to protect them from the concrete.

Fig. 61 - Sensors used for measuring pressure of concrete [Assaad et al., 2003B]

Andreas and Cathleen [2003] used the sensor shown in Fig. 62 to measure the concrete pressure of SCC and conventional vibrated concrete. The sensors used were

manufactured by Baumer Electric AG and were built to record a maximum pressure of 1.6 bars. The area of the calibrated sensors exposed to pressure is 7.5 cm^2.

Fig. 62 - The sensor used by Andreas and Cathleen [2003]

Billberg [2003] measured lateral pressure through the determination of stresses exerted on formwork tie rods. This method requires that the base of the formwork can move freely on its foundation in order to prevent friction leading to unreliable results. Such base friction could be minimized using rollers [Brameshuber and Uebachs, 2003].

Andriamanantsilavo and Amziane [2004] measured the lateral pressure using a diaphragm pressure transducers mounted flush with the forming material. Under the pressure of the fluid or gas materials, the membrane deforms and produces a variation in both the sensor wire resistance and the output voltage. When a material is setting, the deformation of the transducer diaphragm due to flow of freshly mixed paste is not reversible, although no pressure is being applied by the transducer (Fig. 63-a). The transducer operating principle is based on the implementation of a controlled air backpressure, which is continuously balanced with the pressure exerted by the tested medium (Fig. 63-b). The device is composed of two interconnected measuring chambers (Fig. 63-c). The first chamber is equipped with an absolute pressure transducer connected to a compressed air control valve. The second chamber is equipped with an inductive standard displacement transducer attached to a thin elastometric latex membrane. The other side of the membrane is in direct contact with the material tested. During the test, the pressure in both chambers is controlled so that the membrane is kept in a vertical position. Indeed, this position is indicative of the pressure equilibrium on both sides of the membrane.

Consequently, the pressure exerted by the material on the formwork is equal to the pressure measured in the chambers.
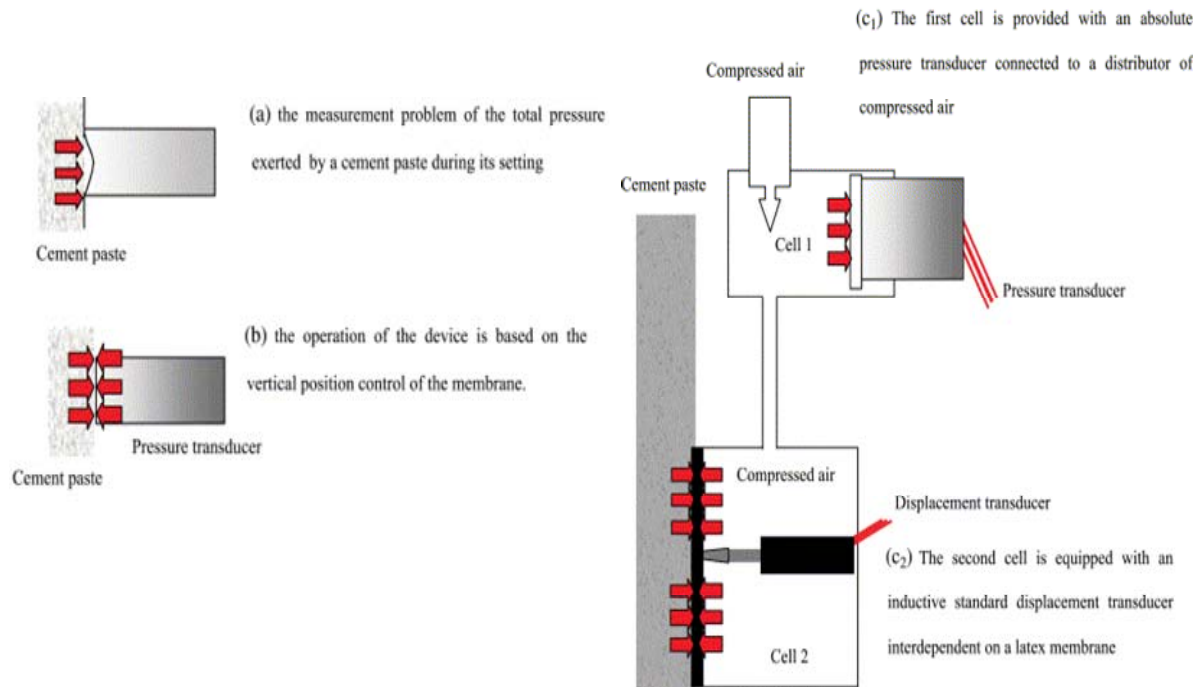
Fig. 63 - Design of the total lateral pressure measurement device
[Andriamanantsilavo and Amziane, 2004]

Arslan et al., [2005] measured the formwork lateral pressure exerted by fresh concrete using two strain gage plates (Fig. 64). Full bridge (Wheatstone bridge) with 10-mm long gages, −10% transverse sensitivity, and 120 ± 03 Ω resistance were set up on every strain gage plate, as seen in Fig. 64. Strain gage plates were calibrated by applying known forces. For each strain gage plate, a regression formula between the applied forces and corresponding strain values was developed. Strain gage plates were then mounted at each bottom side of formwork. The full bridge circuits are connected to a computer-based data logger via a switching box to monitor form pressure variations with time.
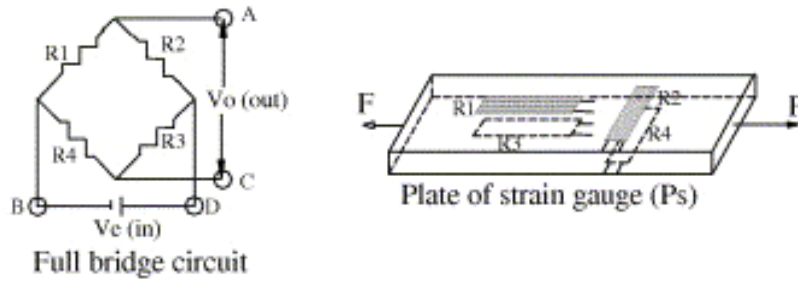
Fig. 64 - Strain gage plate and strain measurement system proposed by Arslan et al., [2005]

Andreas et al. [2005] used five sensors, (produced by Baumer Electric AG) located on the inner surface of the formwork to measure the pressure. The principle of the sensors is based on the change in electrical resistance of thin-film metal wire strain gages when they are deformed due to pressure.

5.2 Pore water pressure measurements to determine lateral pressure

Soil mechanics principles consider that lateral pressure exerted by soil-like material to be the sum of pore water pressure and pressure exerted by the submerged solid skeleton:

$$\sigma = \sigma' + [U \times (A - A_c) / A] \qquad \text{…............. (83)}$$

where σ is the total lateral pressure, σ' is the effective pressure resulting from the solid particles, U is the pore water pressure, and A_c and A denote the area of contact points on a given plane and the total area of the plane, respectively. The above equation, developed initially by Terzaghi and Peck [1967], assumes that the value of A_c can be neglected compared to that of A, thus leading to: $\sigma = \sigma' + U$. Furthermore, the lateral pressure exerted by a dry granular material on a frictional surface is proportional to the vertical pressure, as follows:

$$P_h = K \times P_v \qquad \text{…............. (84)}$$

where P_h is the lateral pressure and $P_v = \gamma \times g \times h$ is the vertical pressure (γ, g, and h being the unit weight, gravity, and head of granular material, respectively). The K value corresponds to the lateral earth pressure coefficient, which depends on internal friction of the material and on whether the lateral pressure is active (K_a), passive (K_b), or at-rest (K_o).

During tests carried out by Alexanridis and Gardner [1981], it was considered that the undrained cohesion and coefficient of internal friction values are both pore-water-pressure-dependent for concrete. This assumption was based on the fact that pore pressure developed under field conditions can differ significantly from those in the laboratory due to different drainage conditions. Therefore, it is difficult to appreciate the applicability of any results obtained without taking into account pore water pressure. The authors reported that at very early age and low vertical stress, the fresh concrete behaves as a fluid with vertical stresses transformed into lateral stresses, and the at-rest K_o coefficient for the solid phase approaches unity. However, as the fresh concrete starts to gain shear strength, K_o decreases rapidly and approaches that of Poisson's ratio for cured concrete. The authors noted that this result is in disagreement with conventional soil mechanics unless the pore fluid has a density close to that of fresh concrete. Nonetheless, the density of the fluid phase corresponds to that of concrete during vibration, and eventually decreases to that of the density of water.

Radocea [1994] studied the evolution of pore water pressure with time until the setting for cement paste (Fig. 65). The pore water pressure is shown to decrease from P1 to P2 due to settlement of the cement grains after placing [Radocea, 1994]. In the same period, bleeding can also occur at the surface. The initial pressure P1 depends on the density of the paste and the depth of the measurement. The surface is covered with bleeding water during the period from t1 to t2 and the pore water pressure will remain stable. At time t2, the surface starts to dry out because of free evaporation, and the pore water pressure will decrease. This is due to the formation of meniscus at the surface and the hydration of the cement. The effect of cement hydration can be seen at t3 where the pore pressure is decreasing in a sealed sample. If the specimens are water cured, the rate of pore water pressure decrease will be reduced because the water will be transported into the specimens due to suction caused be the lower pore water pressure [Radocea, 1994].
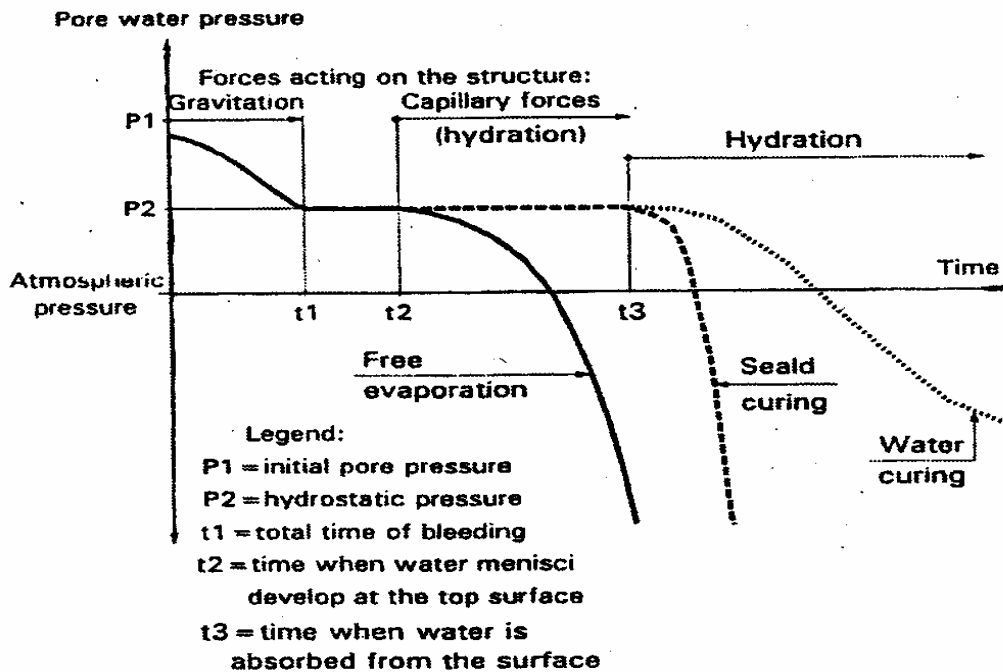
Fig. 65 - Variations of pore water pressure in cement paste with time [Radocea, 1994]

Amziane and Baudeau [2000] evaluated the drop in lateral and pore water pressures of four types of cement pastes made with 0.30 to 0.45 *w/c*. An experimental column measuring 1 m in height and 110 mm in diameter equipped with two pressure transducers was used. Lateral and pore water pressures were found to be strongly affected by the *w/c*, and the level of stress to which the cement paste is subjected. Initially, both pressures were found to be equal to the theoretical hydrostatic pressure exerted by the mixture, and their rates of drop were perfectly identical. After the cancellation of lateral pressure, depressions of tens of kPa were recorded for the pore water pressure before stabilization at zero (Fig. 66). The authors suggested that this could be generated by a rupture of the capillaries as a consequence of the formation of hydrates that could break their continuities.
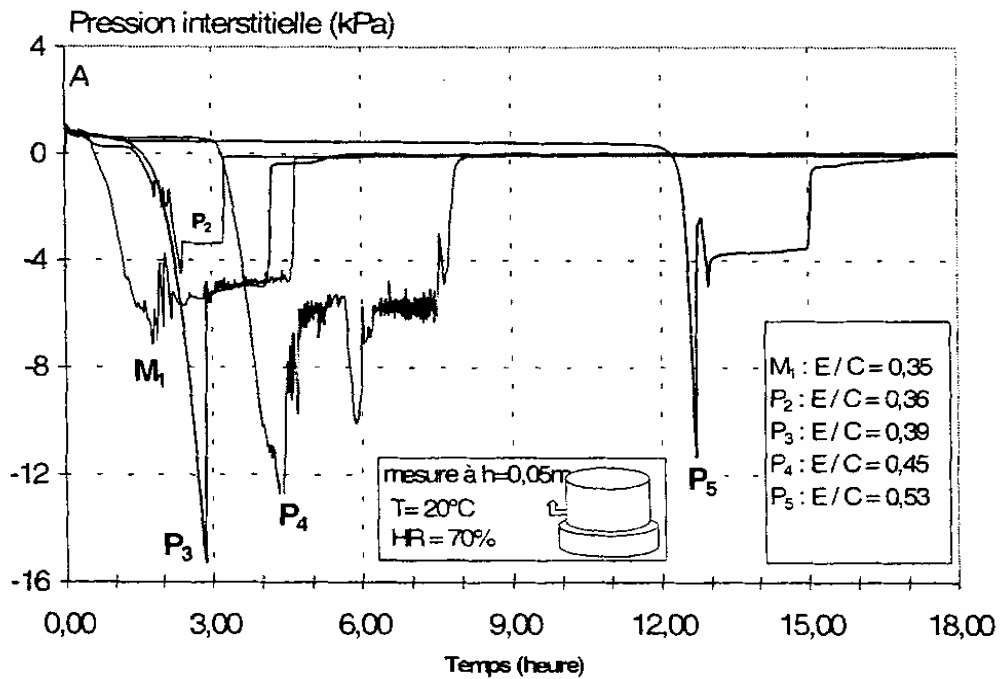
Fig. 66 - Variations of pore water pressure with time for cement paste made with 0.30 to 0.45 w/c [Amziane and Baudeau, 2000]

Assaad and Khayat [2004] compared the lateral pressure exerted by SCC to measurements of pore water pressure. The lateral and pore water pressures exerted by the concrete were determined using an experimental column measuring 1 m in height and 200 mm in internal diameter. The lateral pressure was measured using three pressure sensors mounted at 50, 150, and 350 mm from the base. At the same heights, pore water pressure sensors were used to determine the pressure resulting from the fluid phase. Variations of pore water and lateral pressures with time measured for the sensors located at 50 and 150 mm from the base are plotted in Fig. 67 for SCC made with o.46 sand-to-total aggregate ratio. Fig. 68 shows the variations of both pore water and lateral pressure at 50 mm from the base of the experimental column as well as the temperature variation measured at the center of the 200-mm diameter column for SCC made with 10 mm MSA and 0.50 sand-to-total aggregate ratio. As shown here, a depression of approximately -10 kPa was measured from the pore water pressure sensors; this corresponds to the limit of the pore water pressure sensor. Such sensors require continuously water saturation to function. As the hardening process takes place, concrete can cause some suction of the water in the sensor, hence interrupting any further measurements.

Fossa [2001] suggested that the mechanism of pore water pressure drop is governed by chemical shrinkage caused by cement hydration that starts as soon as the cement begins to react with water. However, it is after the end of the plastic stage that progressive formation of hydration products can cause the creation of a network of connections and development of empty capillary pores. The largest capillary pores will begin gradually to dry, and gel pores formed during the hydration will start to drain water from the coarsest capillary pores, as free water is held by forces that are inversely proportional to the apparent diameter of the capillary pore (self-desiccation process) [Aïtcin, 1999]. The consequence of such process is the formation of meniscus at the water/vapor interface, resulting in a decrease in relative humidity and drop in pore water pressure towards negative values [Fossa, 2001].
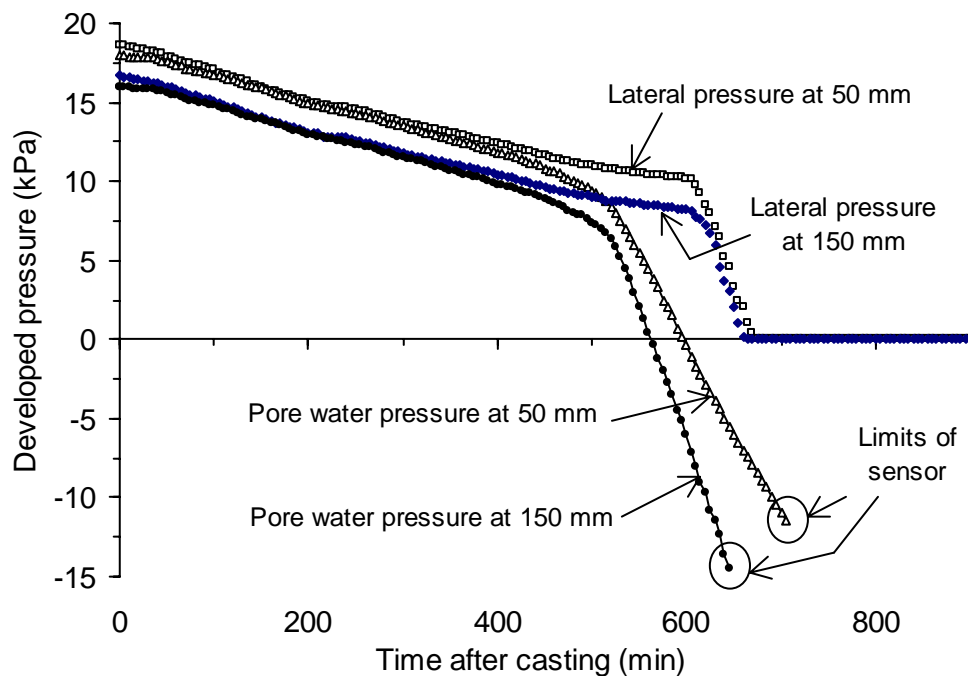
Fig. 67 - Variations of pore water and lateral pressures with respect to height for the 0.46-SCC mixture [Assaad and Khayat, 2004]
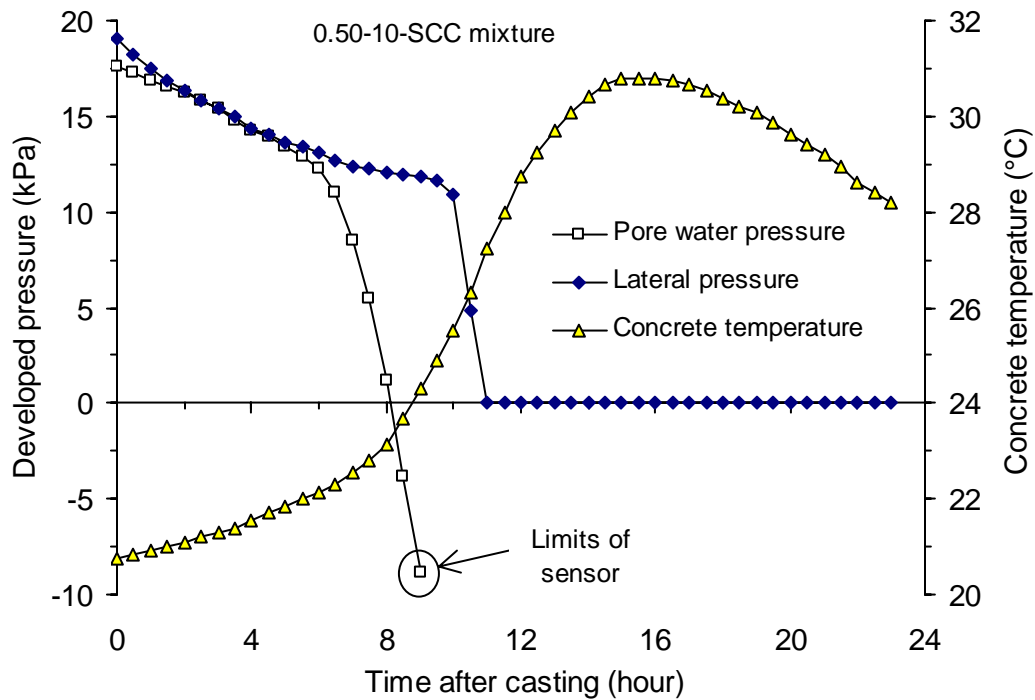
Fig. 68 - Variations of pore water and lateral pressures and concrete temperature for the 0.50-10-SCC mixture [Assaad and Khayat, 2004]

Andriamanansilav and Amziane [2004] tried also to relate the kinetics of variations in lateral pressure to that of pore water pressure and stiffening of cement paste. An experimental setup made of a tubular glass column measuring 1.1 m in height and 110 mm in diameter was used (Fig. 69). The column is connected to two pressure-measuring devices positioned at a height of 50 mm from the base. In order to simulate the equivalent hydrostatic pressure of fresh cement paste at heights of 5 and 10 m, an equivalent pressure is applied by an air actuator on the surface of the material inside the column. In addition to the total lateral pressure, pore water pressure, temperature, and setting of cement paste using the Vicat test were determined.
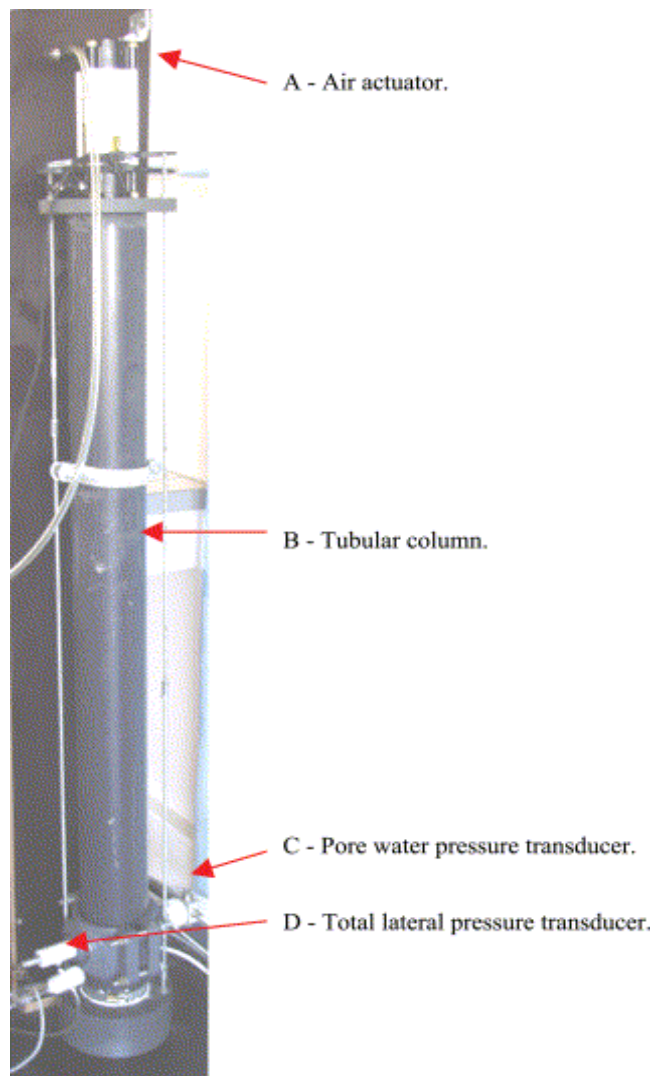
Fig. 69 - View of the set-up device [Andriamanansilav and Amziane, 2004]

Cement paste with *w/c* of 0.30, 0.36, and 0.45 was used. The paste was cast into the tubular column in two layers, each vibrated for 15 sec. The results presented in Fig. 70 describe the evolution of pore water pressure, total lateral pressure, temperature, autogenous shrinkage, and penetration of Vicat needle. The pore water pressure kinetics of the fresh cement paste with *w/c* equal to 0.30, 0.36, and 0.45 are shown in Fig. 70.
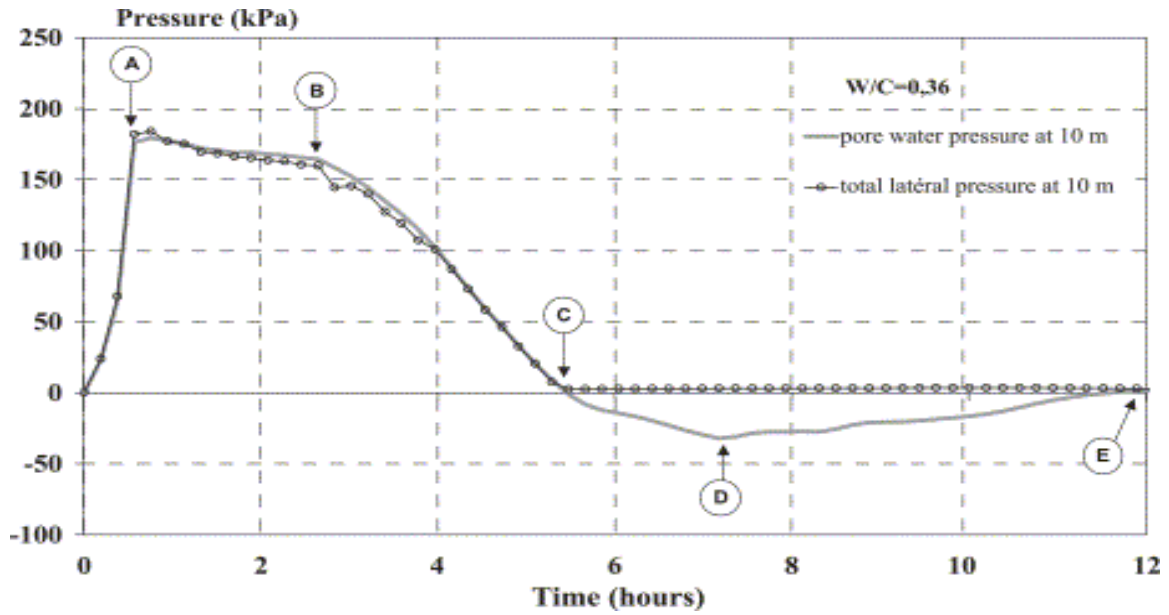
Fig. 70 - Diagram of the evolution of pore water pressure and total lateral pressure
[Andriamanansilav and Amziane, 2004]
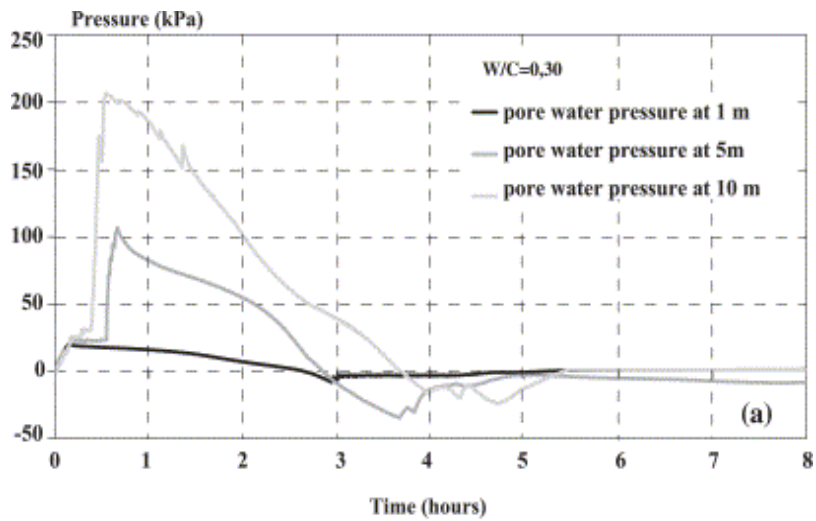
Fig. 71 - Kinetics of pore water pressure of fresh cement paste (a) *w/c* = 0.30, (b) *w/c* =
0.36, and (c) *w/c* = 0.45 [Andriamanansilav and Amziane, 2004]
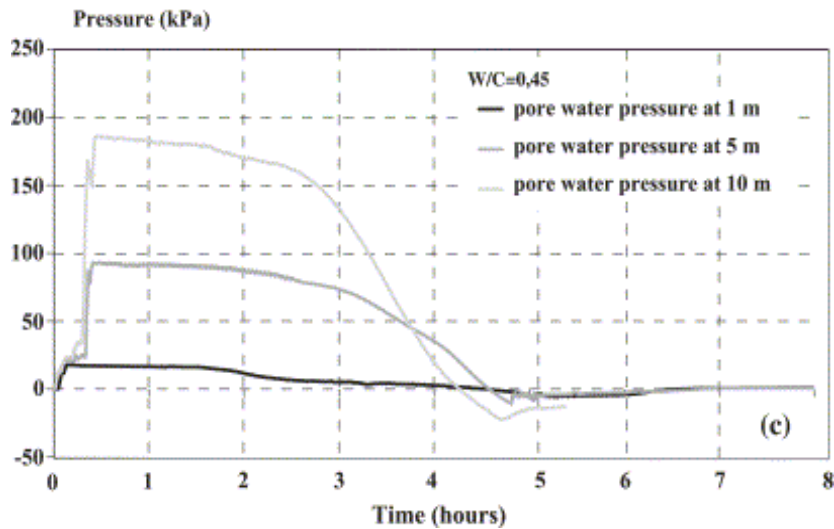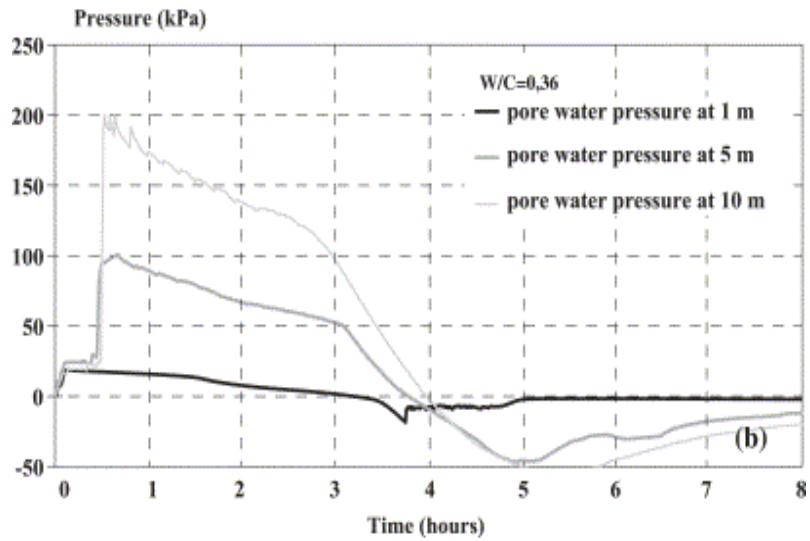
Fig. 71 (cont.) – Kinetics of pore water pressure of fresh cement paste (a) $w/c = 0.30$, (b) $w/c = 0.36$, and (c) $w/c = 0.45$ [Andriamanansilav and Amziane, 2004]

From the above results, the authors concluded that the time of lateral pressure cancellation was delayed with the increase in w/c. For cement paste, the profiles of the pore water and the total lateral pressures remained hydrostatic from the initial state until pressure cancellation. During this period, the kinetics of evolution of both pressure measurements was identical. Once the total lateral pressure was nil, the pore water pressure passes to a depression state. The w/c, depth of casting, and vibration frequency period were shown to have considerable impact on the kinetics of the lateral and pore water pressures.

5.3 Case studies for formwork pressure measurements exerted by SCC

The French research center on buildings and infrastructures (CEBTP) reported in 1999 on the results of an experimental study to determine lateral pressure exerted by SCC on high experimental wall measuring 12.5 m in height (Fig. 72-a). The pressure of the concrete was measured using seven sensors placed at various heights. The concrete contained 350 kg/m^3 of cement and 100 kg/m^3 of limestone filler, a water-to-powder ratio (*w/p*) of 0.46 and HRWRA. The slump flow consistency at the time of casting was 700 mm. The SCC was cast from the top using a bucket at a rate of 18 m/h. This rate was 25 m/h for the second wall where the concrete was pumped from the bottom. The resulting lateral pressure envelopes are shown in Fig. 72-b and indicate that the pressure distribution is not linear and is lower than hydrostatic. A net deviation from the theoretical hydrostatic pressure was observed beyond 2.5 m from the top of the wall. At the base of the formwork, the deviation from the hydrostatic distribution was 30% in the case of SCC pumped from the bottom and 35% for concrete cast using a bucket from the top. The difference between hydrostatic and measured pressures was attributed to the reduction in hydraulic head due to friction between the rising concrete during placement and the surface of the steel formwork [Vié et al., 2001].

Similar studies were carried in Sweden [Skarendahl, 1999] during the casting of bridge piers measuring 5 m in height. The pier was cast in successive layers of approximately 0.5 m in height with rest periods that were unspecified, resulting in low placement rate. For these conditions of placements, the lateral pressure exerted by the SCC at the base of the formwork was approximately half of that resulting from normal-consistency concrete consolidated by internal vibration.

In 2000, three industrials including the GTM Construction (France) and NCC AB (Sweden), and Sika Admixtures (Spain) conducted a large field-experimental program dealing with the surface quality and lateral pressure of SCC. The report was published in 2000 as part of the Brite-EuRam Project entitled "Rational Production and Improved Working Environment Through Using Self-Compacting Concrete" [Tejeda-Dominguez et al., 2005]. Special emphasis was placed on the effect of wall geometry and concrete casting rate on lateral pressure exerted by SCC.
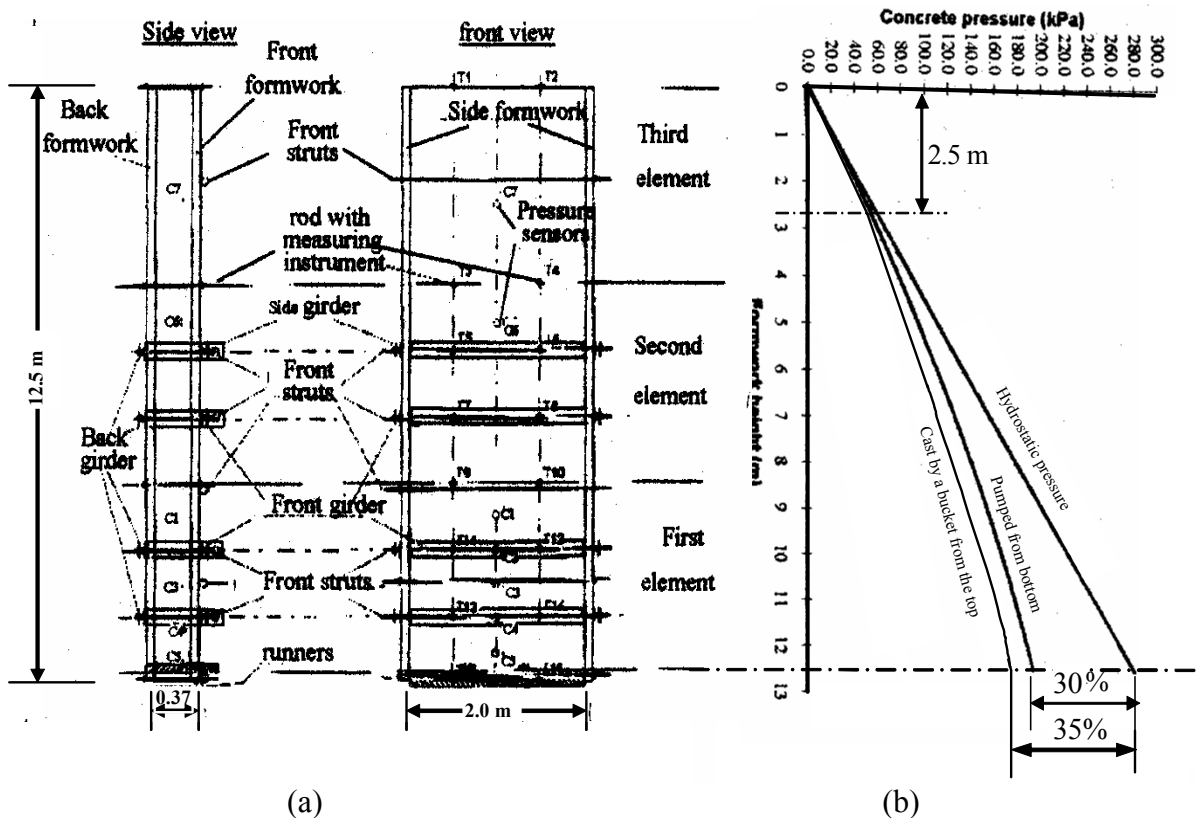
Fig. 72 - Pressure sensors and formwork (a) and pressure envelope (b) [CEBTP, 1999]

The GTM Construction tested two types of SCC prepared with and without VMA that are intended for cast-in place civil engineering construction. The cement (CPA CEM I 52.5 R) and filler (Limestone Picketty Type A) contents were fixed at 290 and 174 kg/m³, respectively. The sand-to-total aggregate ratio was 0.46, by mass. A fixed dosage of 9 kg/m³ of HRWRA (Sikament 10) was used. The water content was then adjusted to secure slump flow value between 700 to 880 mm. Different formwork dimensions were used: the length was set to 1.25 and 2.5 m, the height to 2.8 and 5.6 m, and the width to 0.25 and 0.40 m. A mesh of reinforcing bars was placed in the formwork corresponding to 50 or 80 kg/m³ for walls having a width of 0.40 or 0.25 m, respectively. A large range of concrete casting rates varying between 10 and 150 m/h was tested during the trials. Different concrete placement methods were studied, which included pumping the concrete from the bottom of the formwork and placement by pump or bucket from the top. Lateral pressure measurements were made using two different systems. The principle of the first system (GTM pressure equipment) consisted of casting water into a system made of stiff pipes and rubber bags and

109

measuring SCC pressure directly with the manometer. The second system consisted of electronic pressure sensors of 200 mm in diameter that enables instantaneous lateral pressure measurements. The experimental data indicated that both systems led to equivalent results. For most of the tested SCC mixtures, the measured lateral pressure was close to the hydrostatic pressure. This can be due to the very high casting rates and high deformability of the concrete. In general, it was reported that for a given slump flow and casting rate, mixtures containing VMA exhibited higher initial pressure and lower rate of pressure drop with time; this may well be because of the greater water content of these mixtures since the HRWRA dosage was held constant, and the water content was adjusted to secure the required slump flow consistency. Casting the concrete using bucket from the top was reported to reduce slightly the maximum pressure, despite the relatively high casting rate of 50 m/h. When pumping from the bottom was used, the lateral pressure was observed to significantly increase.

In the case of the NCC AB Company, 10 full-scale trial castings were conducted on wall elements in Billeberga, Sweden. Eight of the trials were carried out on a wall element measuring 2.65 m in height, 5.7 m in length, and 0.16 m in width. The last two trials were conducted on walls having higher heights of 5.3 and 8 m. A single SCC mixture was used to fill all walls. The cement and limestone filler (Ignaberg 500) contents were set at 330 and 125 kg/m³, respectively. The *w/c* was 0.55. The contents of sand (0-8 mm) and coarse aggregate (8-16 mm) were 1,047 and 702 kg/m³, respectively. A polycarboxylate-based HRWRA (Sika Viscocrete 2) was used at a dosage of 1.7%, by cement mass. The slump flow of the tested mixtures varied from 620 to 780 mm. The lateral pressure was measured using hydraulic jacks located at various elevations. Different techniques were used to place the concrete in the formworks. A pump was used to place the concrete in seven walls, while buckets were used to place the remaining three walls. All placements were from the top of the formwork. When the pump was used, a fireman's hose was added at the end of the pump line to limit the freefall of the concrete to approximately 750 mm. The casting rates varied from 6 to 120 m/h. Despite these high casting rates, NCC AB engineers reported that the developed pressure right after the end of casting was considerably lower than hydrostatic pressure. For example, for the wall measuring 8 m in height and cast at rate of

rise of 120 m/h, the pressure measured at 550 mm from the bottom was 29% of the hydrostatic value. In the case of the wall measuring 5.3 m in height, this pressure was 59% of the hydrostatic limit.

Proske and Graubner [2002] evaluated the influence of casting rate and slump flow value on formwork pressure developed by SCC. Eleven experimental tests were conducted on columns measuring 4 m in height and 0.3 m × 0.3 m in cross-sectional dimensions. Ten columns were reinforced. The casting rate and slump flow value varied from 12.5 to 160 m/h and 550 to 750 mm, respectively. The SCC mixture used for casting the columns had a *w/c* of 0.43 and a sand-to-coarse aggregate ratio of 0.48. The author reported that the SCC mixtures of 750 mm slump flow placed at casting rates of 25, 40, 80, and 160 m/h., developed almost hydrostatic pressure. For the casting rate of 12.5 m/h, the SCC was shown to exhibit a pressure reduction of 23% from the hydrostatic limit. On the other hand, for a fixed casting rate of 25 m/h, the decrease in slump flow from 750 to 550 mm was reported to reduce the maximum pressure by approximately 40% of the hydrostatic pressure.

Andreas and Cathleen [2003] compared lateral pressure characteristics of SCC of varying workability levels to that of conventional vibrated concrete. Experimental wall elements measuring 2.7 m in height, 0.75 m in length, and 0.20 m in width were used (Fig. 73). The walls were reinforced with 10-mm diameter bars employed at a density of 50 kg/m^3. Five pressure sensors were used to determine the lateral pressure distribution. The walls were cast at approximate rate of 8 m/h. The walls were filled with two batches, each taking 1.5 min to cast with 20-min break between the lifts. SCC cast from the top displayed between 87% and 90% of the hydrostatic pressure. The conventional concrete developed about 55% of the hydrostatic pressure. Within the first 20 min, the pressure decay at the lowest sensor ranged between 7% and 20%. Within two hours, the concrete pressure reached about 50% of the maximum initial pressure. Andreas and Cathleen [2003] also reported that the slump flow of SCC had no great influence on the maximum pressure when the casting rate was about 8 m/h. This was, however, not the case a slower casting rate of 4 m/h was tried. The incorporation of VMA was shown to lead to lower lateral pressure.

In the case of SCC pumped into the formwork from its base, the pressure was shown to rise locally above hydrostatic values, and that the maximum pressure might be dependent on the pump pressure.
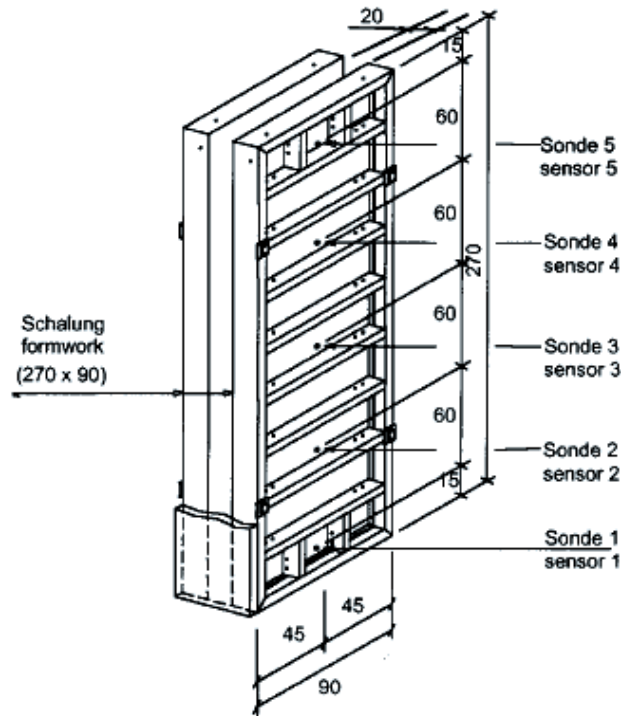
Fig. 73 - Test set-up for pressure measurements in laboratory (wall 2.70 × 0.75 × 0.20 m)
[Andreas and Cathleen, 2003]

Khayat and co-workers [2005B] evaluated formwork pressure characteristics exerted by SCC used for the repair of an underpass retaining wall in Montreal, Canada that was carried out in 2003. The repair consisted in removing the outer layer of concrete to a depth of 0.15 to 0.20 m and the first layer of steel, and replacing it with high-performance SCC. New vertical and horizontal reinforcing bars were provided. The SCC was cast through a pump line from the top of the wall panels measuring 6.7 m in width. In the work reported here, the lateral pressure was monitored along 5.5-m high repair sections. Seven pressure sensors were mounted at various heights along the plywood formwork to monitor the pressure. The mixture compositions and fresh characteristics of the tested mixtures are given in Table 6.

Table 6 - Mixture proportion and workability of SCC used in repair [Khayat et al., 2005B]

Identification	BIN-0.50-Nap	TER-0.50-Nap	TER-0.44-Nap	TER-0.54-Nap-Fib	TER-0.54-Poly-Fib
Cement T10, kg/m³	237	-	-	-	-
Binary cement T10E-SF, kg/m³	238	-	-	-	-
Ternary cement T10EF-SF, kg/m³	-	475	475	475	475
Tuf-Strand synthetic fibers, kg/m³	-	-	-	2.3	2.3
w/cm	0.40	0.40	0.40	0.40	0.40
Sand, kg/m³	780	770	670	850	850
Coarse aggregate (2.5-10 mm), kg/m³	790	775	880	675	650
PNS HRWRA, L/m³	7.3	6.8	8.6	8.2	-
PC HRWRA, L/m³	-	-	-	-	4.3
Water reducer, mL/100 kg of binder	200	200	200	200	-
VMA, mL/100 L of water	1100	1100	1100	1000	260
AEA mL/100 kg of binder	80	85	110	100	50
Casting rate (m/hour)	6.0	6.5	7.5	9.5	8.0
Initial temperature of fresh concrete (°C)	8.0	20.4	17.0	22.8	14.0
after 60 minutes *	7.0	18.7	14.0	21.0	13.0
Initial slump flow after pumping (mm)	665	740	590	640	600
after 60 minutes (mm) *	565	650	505	540	660
Initial slump flow through J-Ring (mm)	650	810	470	540	585
after 60 minutes (mm) *	580	640	390	460	500
Initial L-box blocking ratio (h2/h1)	0.63	0.97	0.58	0.47	0.52
after 60 minutes *	0.49	0.58	0.26	0.33	-
Initial filling capacity (%)	87.5	93.2	76.0	63.6	67.9
after 60 minutes (%) *	70.2	88.4	51.9	35.7	79.3
Initial air volume (%)	7.1	7.9	5.1	7.1	5.7
after 60 minutes (%) *	5.8	5.9	4.9	5.8	4.8
Unit weight (kg/m³)	2,160	2,250	2,225	2,200	2,230
Maximum surface settlement (%)	0.49 – 0.54				

* hand-mixed concrete before the 60-minute measurements

Figure 74 compares the variations in time of normalized lateral pressures developed by the five SCC mixtures, as determined from the first sensor placed 0.3 m from the bottom where the maximum pressure was measured. The SCC TER-0.44-Nap mixture made using a

higher concentration of coarse aggregate (S/A of 0.44) developed the lowest maximum pressure; this mixture also had the highest thixotropy value. The maximum initial pressure was limited to 40% of the hydrostatic limit. This was due to the lower initial slump flow and greater internal friction caused by the higher coarse aggregate concentration of this concrete. The TER-0.44-Nap mixture exhibited relatively long time before pressure cancellation. This is believed to be due to the retarding effect of the naphthalene-based HRWRA that was incorporated at relatively high dosage.

The TER-0.50-Nap and BIN-0.50-Nap mixtures developed the highest lateral pressure of approximately 60% of hydrostatic pressure. Contrary to the BIN-0.50-Nap SCC, the former SCC exhibited sharp pressure decay. This was related to the differences in concrete temperature (8 ºC vs. 20 ºC) of the fresh concrete as well as the ambient temperatures during the early stages of hardening, which were higher in the case of the TER-0.50-Nap SCC.
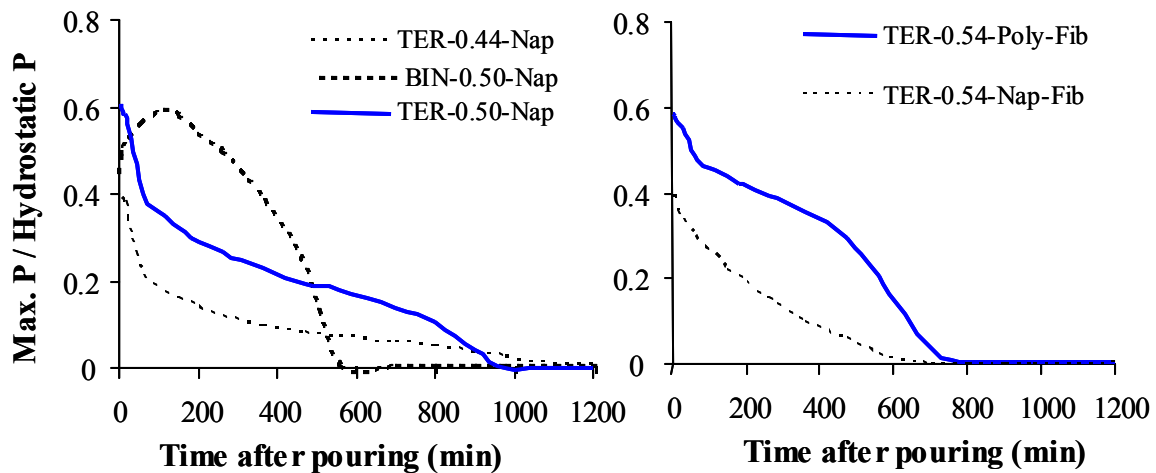
Fig. 74 - Variations in relative lateral pressure at 0.3 m from the bottom of 5.5-m high repair wall sections determined for different repair SCC mixtures [Khayat et al., 2005B]

Billberg [2003] used two SCC mixtures (SCC1 and SCC2 with 0.40 and 0.45 *w/c*, respectively) and one conventional concrete to cast eight experimental wall elements measuring 3 m in height, 3.5 m in length, and 0.3 m in width. The slump flow at the time of casting was 730 ± 50, 700 ± 50 for the SCC1 and SCC2, respectively. The formwork surface material was timber on one side and plywood on the other. A form-releasing agent was applied on half of each form-side. The concrete was dropped from a height of 1 ± 0.5 m

above the concrete surface. Relatively low casting rates were used in casting the wall elements, as indicated in Table 7. The pressure envelopes for the eight tested mixtures are shown in Fig. 75. The lateral pressure for the vibrated concrete (NC) was slightly lower than that of SCC placed at the same casting rate. The increase in the rate of casting led to greater pressure. A linear relationship was established between the maximum initial lateral pressure and the casting rate; this relationship was presented earlier in the report in Fig. 44.

Table 7 - Variation of mixture designs and casting rates [Billberg, 2003]

Casting no.	Mix type	Casting rate
1	1	1.4
2	2	1.3
3	2	1.0
4	1	0.8
5	1	1.5
6	2	2.2
7	1	2.3
8	NC	1.5
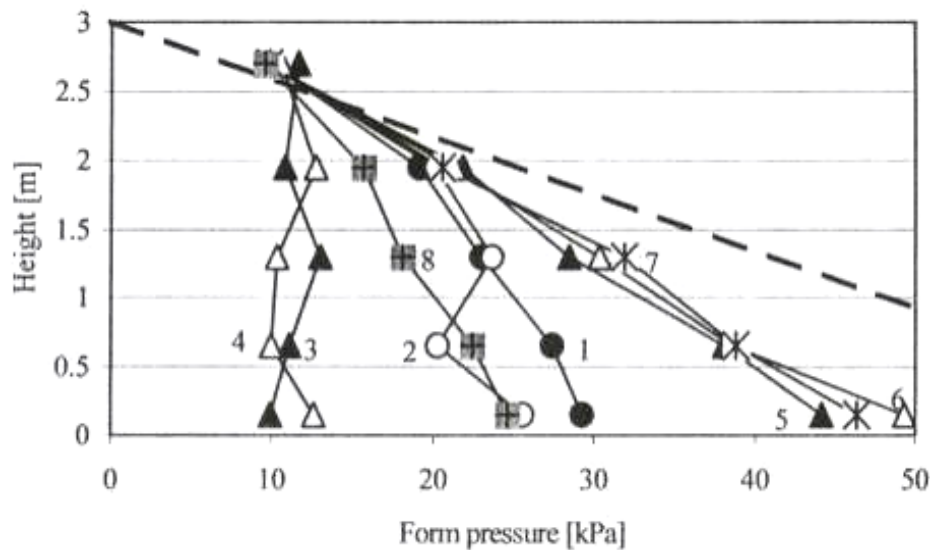
Fig. 75 - Final form pressure envelopes for fully cast walls using SCC (casting no. 1-7) and conventionally vibrated concrete (casting no. 8) [Billberg, 2003]

Tejeda-Dominguez et al. [2005] carried evaluated the lateral pressure exerted by SCC during the casting of a massive reaction wall at the Civil Engineering lab facility at the University of Illinois at Urbana-Champaign. The wall was heavy reinforced and measured 24.4 m in length, 1.5 m in width, and 8.5 m in height (Fig. 76). The concrete was cast

continuously from the top using a pump at a mean casting rate of 1.22 m/h; the rate of rise of the SCC in the formwork fluctuated between 0.61 to 1.68 m/h. The targeted slump flow was 710 mm with occasional variations from 600 mm to 735 mm. The concrete temperature at the time of casting was 16 $^{\circ}$C on the average and peaked at 60 $^{\circ}$C by the second day after placement. The initial and final setting times, determined by penetration resistance (ASTM 403), were 5.9 and 7.8 hours, respectively.

The distribution of the lateral pressure was determined using seven sensors placed along the wall. As shown in Fig. 77, hydrostatic pressure was not achieved throughout the entire height of the wall. The maximum pressure recorded was only 23% of the maximum hydrostatic pressure. The highest pressures were not measured at the bottom of the wall, where the head of concrete was larger, but corresponded to the periods in time where the casting rates were faster. The maximum pressure reached in the third wall was only 32% of the maximum hydrostatic pressure.

Fig. 76 - Formwork of 8.5-m high strong reaction wall [Tejeda-Dominguez et al., 2005]

Fig. 77 - Envelope of maximum pressure exerted by the SCC in the reaction wall
[Tejeda-Dominguez et al., 2005]

6. REFERENCES

ACI Committee 622, "Pressures on Formwork," *ACI Journal Proceedings*, V. 55, No. 2, August 1958, pp. 173-190.

ACI Committee 347, "Guide to Formwork for Concrete," American Concrete Institute, Farmington Hills, Michigan, 2001, 32 pp.

ACI Committee 347R-03, "Guide to Formwork for Concrete," American Concrete Institute, Farmington Hills, Michigan, 2004, 32 pp.

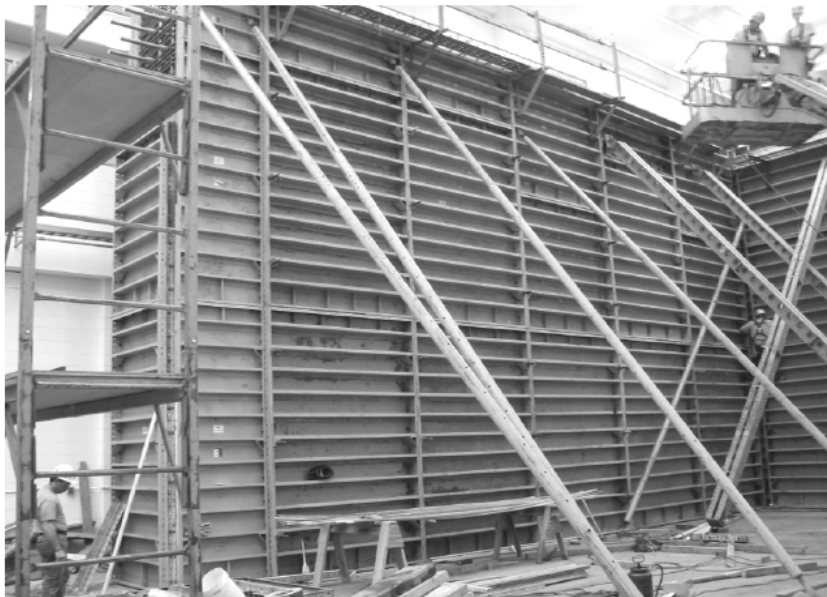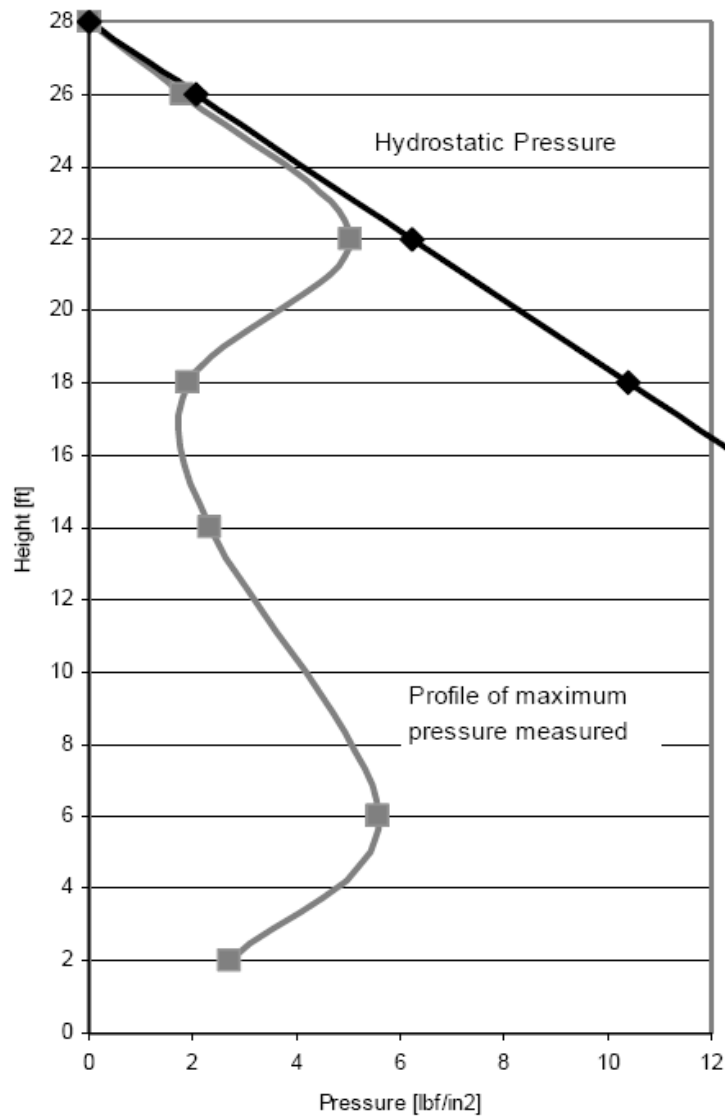Adam, M.; Bennasr, M.; and Santos Delgado, H., "Formwork Pressure of Fresh Concrete," (in French), Annales de l'Institut Technique du Bâtiment et des Travaux Publics, Série Béton, March-April 1963, No. 207-208, pp. 403-423.

Aïtcin, P.-C., "Autogenous Shrinkage Measurement," Proceedings*, International Workshop on Autogenous Shrinkage of Concrete*, Hiroshima, Japan, Ed. Tazawa, E., 1999, pp. 257-268.

Alexandridis, A., and Gardner, N. J., "Mechanical Behavior of Fresh Concrete," *Cement and Concrete Research*, V. 11, 1981, pp. 323-339.

Amziane, S., and Baudeau, P., "Effects of Aggregate Concentration and Size in Fresh Concrete Pressure on Formwork Walls," (in French), *Materials and Structure*, V. 33, No. 225, 2000, pp. 50-58.

Andreas, L., and Cathleen, H., "Pressure of Self-Compacting Concrete on the Formwork," *Proceedings of the 3rd International RILEM Symposium on Self-Compacting Concrete*, Eds. Wallevik, O., and Nielsson, I., Reykjavik, Iceland, August 2003, pp. 288-295.

Andreas, L.; Cathleen, H.; and Frank W., "Influence of the Mixture Design on the Formwork Pressure of Self-Compacting Concrete," *Proceedings of the 2nd North American Conference on the Design and Use of Self-Consolidating Concrete (SCC)* and *the 4th International RILEM Symposium on Self-Compacting Concrete*, Eds. Shah, S.P., Chicago, 2005, pp. 635-640.

Andriamanantsilavo, N. R., and Amziane S., "Maturation of Fresh Cement Paste Within 1- to 10-m-large Formworks," *Cement and Concrete Research*, Vol. 34, No. 11, November 2004, pp. 2141-2152.

Arslan, M.; Osman, S.; and Serkan, S., "Effects of Formwork Surface Materials on Concrete Lateral Pressure," *Construction and Building Materials*, V. 19, No. 4, May 2005, pp. 319-325.

Arslan, M., "Effects of Drainer Formworks on Concrete Lateral Pressure," *Construction and Building Materials*, V. 16, No. 5, July 2002, pp. 253-259.

Assaad, J., "Formwork Pressure of Self-Consolidating Concrete – Influence of Thixotropy," Ph.D. Thesis, Department of Civil Engineering, Université de Sherbrooke, 2004, 453 pp.

Assaad, J., and Khayat, K. H., "Effect of Viscosity-Enhancing Admixtures on Formwork Pressure and Thixotropy of Self-Consolidating Concrete," *ACI Materials Journal*, V. 103, No. 4, 2006, pp. 280-287.

Assaad, J., and Khayat, K. H., "Formwork Pressure of Self-Consolidating Concrete Made with Various Binder Types and Contents," *ACI Materials Journal*, V. 102, No. 4, 2005A, pp. 215-223.

Assaad, J., and Khayat, K. H., "Kinetics of Formwork Pressure Drop of SCC Containing Various Types and Contents of Binder," *Cement and Concrete Research*, V. 35, 2005B, pp. 1522-1530.

Assaad, J., and Khayat, K. H., "Effect of Coarse Aggregate Characteristics on Lateral Pressure Exerted by Self-Consolidating Concrete," *ACI Materials Journal*, V. 102, No. 3, 2005C, pp. 145-153.

Assaad, J., and Khayat, K. H., "Variations of Lateral and Pore Water Pressure of Self-Consolidating Concrete at Early Age," *ACI Materials Journal*, V. 101, No. 4, 2004, pp. 310-317.

Assaad, J.; Khayat, K. H.; and Mesbah, H., "Assessment of Thixotropy of Flowable and Self-Consolidating Concrete," *ACI Materials Journal*, V. 100, No. 2, 2003A, pp. 111-120.

Assaad, J.; Khayat, K. H.; and Mesbah, H., "Influence of Thixotropy on Variations of Formwork Pressure of Flowable and Self-Consolidating Concrete – Laboratory Tests," *ACI Materials Journal*, V. 100, No. 1, 2003B, pp. 29-37.

Banfill, P. F. G., and Saunders, D. C., "On the Viscometric Examination of Cement Pastes," *Cement and Concrete Research*, V. 11, No. N-3, 1981, pp. 363-370.

Barnes, H. A., "Thixotropy – A Review," *Journal of Non-Newtonian Fluid Mechanics*, V. 70, Issues 1-2, May 1997, pp. 1-33.

Barnes, H. A.; Hutton, J. F.; and Walters, K., "An Introduction to Rheology," Elsevier, Amsterdam, 1989, 199 pp.

Beitzel, M.; Muller; and Harald, S., "Modeling Fresh Concrete Pressure on Vertical Formwork," CD ROM, *Proceedings of the 5th International Symposium in Civil Engineering*, Taylor & Francis Group, London, 2004, pp 1-6.

Billberg, P., "Form Pressure Generated by Self-Compacting Concrete – Influence of Thixotropy and Structural Behaviour at Rest," Ph.D. Thesis, School of Architecture and the Built Environment, Division of Concrete Structures, Royal Institute of Technology, Stockholm, Sweden, 2006, 91 pp.

Billberg, P., "Form Pressure Generated by Self-Compacting Concrete," *Proceedings of the 3rd International RILEM Symposium on Self-Compacting Concrete*, Eds. Wallevik, O., and Nielsson, I., Reykjavik, Iceland, August 2003, pp. 271-280.

Billberg, P.; Silfwerbrand, J.; and Holmgren, J. "SCC Structural Behaviour at Rest and its Influence on Form Pressure," Submitted to *RILEM Materials and Structures Journal*, 2006.

Bonen, D., and Shah, S. P., "Fresh and Hardened Properties of Self-Consolidating Concrete," Progress in *Structural Engineering Materials Journal*, V. 7, No. 1, 2005, pp. 14-26.

Bonen, D., and Shah, S. P., "The Effects of Formulation on the Properties of Self-Consolidating Concrete," *Concrete Science and Engineering, A Tribute to A. Bentur*, *International RILEM Symposium*, Eds. Kovler, K.; Marchand, J.; Mindess, S.; and Weiss, J., RILEM Publications S.A.R.L. Evanston, IL, March 2004, pp. 43-56.

Brameshuber, W., and Uebachs, S., "Investigations of the Formwork Pressure Using Self-Compacting Concrete," *Proceedings of the 3rd International RILEM Symposium on Self-Compacting Concrete*, Eds. Wallevik, O., and Nielsson, I., Reykjavik, Iceland, August 2003, pp. 281-287.

CEBTP, "Performance of SCC in High Wall Sections," (in French), Internal Report, 1999, 12 pp.

Civil Industries Research and Information Association (CIRIA), "The Pressure of Concrete on Formwork," *Research Report No. 1*, London, 1965.

Civil Industries Research and Information Association (CIRIA), "Concrete Pressure on Formwork," *Research Report No. 108*, London, 1985.

Dally, W. J.; Riley, W. F.; and Kenneth, G. M., "Instrumentation for Engineering Measurements", Wiley, New York, 1984, 576 pp.

DIN 18218, "Frishbeton auf lautrechte" (Pressure of Fresh Concrete on Vertical Formwork), (only available in German), Berlin, 1980.

Djelal, C., "Designing and Perfecting a Tribometer for the Study of Friction of a Concentrated Clay-Water Mixture against a Metallic Surface," *Materials and Structures*, V. 34, No. 1, 2001, pp. 51-58.

Djelal, C.; Vanhove, Y.; and Magnin, A., "Tribological Behaviour of Self-Compacting Concrete," *Cement and Concrete Research*, V. 34, No. 5, May 2004, pp. 821-828.

Djelal, C.; Vanhove, Y.; Decaro, P.; and Magnin, A., "Role of Demoulding Agents during Self-Compacting Concrete Casting in Formwork" *Materials and Structures*, V. 35, No. 252, September. 2002, pp. 470-476.

Douglas, R.; Sun, Z.; Bonen, D.; and Shah, S.P., "The Effect of Ingredients and Shear History on the Thixotropic Rate of the Rebuilding of SCC," *Proceedings of the 2nd North American Conference on the Design and Use of Self-Consolidating Concrete (SCC 2005)* and *the 4th International RILEM Symposium on Self-Compacting Concrete*, Evanston, IL, Ed. Shah, S. P., 2005, pp. 591-596.

Dzuy, N. Q., and Boger, D. V., "Direct Yield Stress Measurement with the Vane Method," *Journal of Rheology*, V. 29, No. 3, 1985, pp. 335-347.

European Federation of Producers and Contractors of Specialist Products for Structures, (EFNARC), 2002, 32 pp, http://www.efnarc.org/pdf/SandGforSCC.PDF

European Federation of Producers and Contractors of Specialist Products for Structures (EFNARC), *Specification and Guidelines for Self-Compacting Concrete*, 2002, 32 pp., (http://www.efnard.org).

Fedroff, D.; Frosch; and Robert, J., "Formwork for Self-Consolidating Concrete," *Concrete International*, V. 26, No. 10, 2004, pp. 32-37.

Ferron, R.; Gregori, A.; Sun, Z.; and Shah, S. P., "Rheological Method to Evaluate the Thixotropy of Cement Pastes for SCC," *ACI Materials Journal*, 2006, (in press).

Fossa, K. T., "Slipforming of Vertical Concrete Structures," Ph.D. Thesis, Norwegian University of Science and Technology, 2001, 285 pp.

Gardner, N. J., "Formwork Pressures and Cement Replacement by Fly Ash," *Concrete International*, October 1984, pp. 50-55.

Gardner, N. J., "The Effect of Superplasticizers and Fly Ash on Formwork Pressures," *Forming Economical Concrete Buildings*, Portland Cement Association, Skokie, IL, 1982, pp. 21.1-21.12.

Gardner, N. J., "Pressure of Concrete Against Formwork", *ACI Journal*, Technical Paper, Title No. 77-31, 1980, pp. 279-286.

Gardner, N. J., and Ho, P. T.-J., "Lateral Pressure of Fresh Concrete," *ACI Journal*, Technical Paper, Title No. 76-35, July 1979, pp. 809-820.

Ghezal, A.; Khayat, K. H.; and Beaupré, D., "Effect of High-Range Water-Reducer – Viscosity-Modifying Admixture Combination on Rheological Properties of Concrete Equivalent Mortar," *Proceedings of the 1st North American Conference on the Design and Use of Self-Consolidating Concrete*, Eds. Shah, S. P.; Daczko, J. A.; and Lingscheit, J. N., Chicago, November 2002, pp. 159-165.

Graubner, C.-A., and Proske, T., "Formwork Pressure: A New Concept for the Calculation," *Proceedings of the 2nd North American conference on the Design and Use of Self-Consolidating Concrete (SCC 2005)* and *the 4th International RILEM Symposium on Self-Compacting Concrete*, Eds. Shah, S. P., Chicago, 2005A, pp. 605-613.

Graubner, C.-A., and Proske, T., "Formwork Pressure: A New Concept for the Calculation," personal communication to Khayat, K. H., 2005B.

Harrison, T. A., "Pressure on Vertical Formwork when Concrete is Placed in Wide Sections," *Cement and Concrete Association*, *Research Report 22*, 1983, 30 pp.

Hobbs D. W., "Influence of Aggregate Volume Concentration upon the Workability of Concrete and some Predictions from the Viscosity-Elasticity Analogy," *Magazine of Concrete Research*, V. 28, No. 97, 1976, pp. 191-202.

Hurd, M. K., "Putting the Pressure on Formwork," *Concrete International*, October 2002, pp. 49-55.

Ish-Shalom, M., and Greenberg, S. A., "The Rheology of Fresh Portland Cement Paste," *Proceedings of the 4th International Symposium on Chemistry on Cement*, Washington, 1962, pp. 731-748.

Janssen H., "Versuche uber Getreidedruck in Silozellen," *VDI Zeitschrift*, V. 39, 1885, pp. 1045-1049.

Jiang, W., and Roy, D. M., "Rheology in Hydration and Setting," *Proceedings of the International RILEM Workshop on Hydration and Setting of Cements*, Dijon, France, 1991, pp. 333-340.

Khayat, K. H., "Workability Testing and Performance of Self-Consolidating Concrete," *ACI Materials Journal*, V. 96, No. 3, 1999, pp. 346-353.

Khayat, K. H., and Assaad, J., "Effect of *w/cm* and High-Range Water-Reducing Admixture on Formwork Pressure and Thixotropy of Self-Consolidating Concrete," *ACI Materials Journal,* V. 103, No. 3, 2006, pp. 186-193.

Khayat, K. H., and Assaad, J., "Use of Rheological Properties of SCC to Predict Formwork Pressure," *Proceedings of the 2nd North American Conference on the Design and Use of Self-Consolidating Concrete (SCC 2005)*, and *the 4th International RILEM Symposium on Self-Compacting Concrete*, Evanston, IL, 2005A, Ed. Shah, S. P., pp. 671-677.

Khayat, K. H., and Assaad, J., "Influence of Internal Friction and Cohesion on Formwork Pressure of Self-consolidating Concrete," *Proceedings of the 1st International Symposium on Design, Performance and Use of Self-Consolidating Concrete (SCC 2005)*, Changsha, Hunan, China, May 26-28, 2005B, Ed. Yu, Z.; Shi, C.; Khayat, K. H.; and Xie, Y., pp. 607-615.

Khayat K. H.; Assaad, J.; Mesbah, H., and Lessard, M., "Effect of Section Width and Casting Rate on Variations of Formwork Pressure of Self-Consolidating Concrete," *Materials and Structures*, V. 38, 2005A, pp. 73-78.

Khayat, K. H.; Petrov, N.; Assaad, J.; Morin, R.; and Thibeault, M., "Performance of Self-Consolidating Concrete in Repair of Concrete Wall Elements" *Proceedings of the 2nd North American Conference on the Design and Use of Self-Consolidating Concrete (SCC 2005),* and *the 4th International RILEM Symposium on Self-Compacting Concrete*, Eds. Shah, S. P., Chicago, 2005B, pp. 1003-1012.

Khayat, K. H; Saric-Coric, M.; and Liotta, F., "Assessment of Thixotropy and Impact on Stability of Cementitious Grout and Concrete," *ACI Materials Journal*, V. 99, No. 3, 2002A, pp. 234-241.

Khayat, K. H.; Assaad, J.; and Mesbah, H., "Variations of Formwork Pressure of Self-Consolidating Concrete-Effect of Section Width and Casting Rate," *Proceedings of the 1st North American Conference on the Design and Use of Self-Consolidating Concrete*, Eds. Shah, S. P.; Daczko, J. A.; and Lingscheit, J. N., Chicago, November 2002B, pp. 295-302.

Khayat, K. H.; Paultre, P.; and Tremblay, S., "Structural Performance and In Situ Properties of Self-Consolidating Concrete Used for Casting Highly Reinforced Columns," *ACI Materials Journal*, V. 98, No. 5, 2001, pp. 371-378.

Khayat, K. H.; Hu, C.; and Monty, H.; "Stability of SCC, Advantages and Potential Applications," *RILEM International Conference on Self-Compacting Concrete*, Stockholm, September 1999, pp. 143-152.

Lapasin, R.; Papo, A.; and Rajgelj, S., "Flow Behavior of Fresh Cement Pastes. A Comparison of Different Rheological Instruments and Techniques," *Cement and Concrete Research*, V. 13, 1983, pp. 349-356.

Leemann, A., and Hoffmann, C., "Pressure of Self-Compacting Concrete on the Formwork," *Betonwerk und Fertigteil-Technik / Concrete Plant and Precast Technology*, V. 69, No. 11, November 2003, pp. 48-55.

Legrand, C., "Contribution to Study of the Rheology of Fresh Concrete" (in French), Ph.D. Thesis, Université Paul Sabatier, Toulouse, France, 1971, 150 pp.

Macklin, C., "Pressure of Plastic Concrete in Forms," USA, *Proceedings of the Society for Experimental Stress Analysis*, V. 4, No. 1, 1946, pp. 112-122.

Martin, D. J., "Economic Impact of SCC in Precast Applications," *Proceedings of the 1st North American Conference on the Design and Use of Self-Consolidating Concrete*, Eds. Shah, S. P.; Daczko, J. A.; and Lingscheit, J. N., Chicago, November 2002, pp. 147-152.

Mewis, J., "Thixotropy - a General Review," *Journal of Non-Newtonian Fluid Mechanics*, V. 6, No. 1, 1979, pp. 1-20.

Mullarky, J. I., and Vaniker, S., "Opportunities and Challenges for SCC in Highway Structures," *Proceedings of the 1st North American Conference On the Design and Use of Self-Consolidating Concrete*, Eds. Shah, S. P.; Daczko, J. A.; and Lingscheit, J. N., Chicago, November 2002, pp. 177-180.

Murdock, L. J., and Blackledge, G. F., *Concrete Materials and Practice*, Edward Arnold Publishers, London, Chapter 16, 1968, pp. 226-251.

NF P93-350, French Standard, "Banches industrialisées pour ouvrages en béton, (Industrial Formwork for Concrete Structures)," June 1995.

Okamura, H., and Ouchi, M., "Applications of Self-Compacting Concrete in Japan," *Proceedings of the 3rd International RILEM Symposium on Self-Compacting Concrete*, Eds. Wallevik, O., and Nielsson, I., Reykjavik, Iceland, August 2003, pp. 3-5.

Olsen, R. H., "Lateral Pressure of Concrete on Formwork," P.hD. Thesis, Oklahoma State University, 1968, 122 pp.

Ore, E. L., and Straughan, J. J., "Effect of Cement Hydration on Concrete Form Pressure," *ACI Journal*, Title No. 65-9, 1968, pp. 111-120.

Ovarlez, G.; Fond, C.; and Clément, E., "Overshoot Effect in the Janssen Granular Column: A Crucial Test for Granular Mechanics," *Physics Review*, V. 67, No. 6, June 2003, pp. 060302-1 to 060302-4.

Ozawa, K.; Maekawa, K.; Kunishima, M.; and Okamura, H., "Development of High Performance Concrete Based on the Durability Design of Concrete Structures," *Proceedings of the 2nd East-Asia and Pacific Conference on Structural Engineering and Construction* (EASEC-2), Chiang Mai, Thailand, V. 1, January 1989, pp. 445-450.

Proske, T., and Graubner, C.-A., "Self-Compacting Concrete - Pressure on Formwork and Abiliy to Deaerate," *Concrete Structures,* V. 17, Darmastadt, 2002, (http://www.darmstadt-concrete.de/2002/dearate.html).

Radocea, A., "A Model of Plastic Shrinkage," *Magazine of Concrete Research*, V. 46, No. 167, 1994, pp. 125-132.

Ritchie, A. G. B., "The Triaxial Testing of Fresh Concrete," *Magazine of Concrete Research*, V. 14, No. 40, 1962A, pp. 1027-1030.

Ritchie, A. G. B., "The Pressures Developed by Concrete on Formwork," *Civil Engineering and Public Works Review*, Part 1, V. 57, No. 672; Part 2, V. 57, No. 673, 1962B, 10 pp.

Roby, H. G., "Pressure of Concrete on Forms," *Civil Engineering*, V. 5, March, 1935, 162 pp.

Rodin, S., "Pressure of Concrete on Formwork," Proceedings, *Institute of Civil Engineers* (London), V. 1, Part 1, No. 6, November 1952, pp. 709-746.

Roussel N., and Ovarlez G., "A Physical Model for the Prediction of Pressure Profiles in a Formwork," *Proceedings of the 2nd North American conference on the Design and Use of Self-Consolidating Concrete (SCC 2005)* and *the 4th International RILEM Symposium on Self-Compacting Concrete*, Eds. Shah, S. P., Chicago 2005, pp. 647-654.

Saak, A., "Characterization and Modeling of Rheology of Cement Paste: with Applications toward Self-Flowing Materials," *Material Science and Engineering*, Northwestern University: Evanston, 2000, 249 pp.

Saak, A. W.; Jennings, H. M.; and Shah, S. P., "New Methodology for Designing Self-Compacting Concrete," *ACI Materials Journal*, V. 98, No. 6, 2001, pp. 429-439.

Schlagbaum, T., "Economic Impact of Self-Consolidating Concrete (SCC) in Ready Mixed Concrete," *Proceedings of the 1st North American Conference On the Design and Use of Self-Consolidating Concrete*, Eds. Shah, S. P.; Daczko, J. A.; and Lingscheit, J. N., Chicago, November 2002, pp. 135-140.

Schojdt R., "Calculations of Pressure of Concrete on Forms," *Proceedings of the American Society of Civil Engineers*, V. 81, May 1955, pp. 1-16.

Shaughnessy, R., and Clark, P. E., "The Rheological Behavior of Fresh Cement Pastes," *Cement and Concrete Research*, V. 18, 1988, pp. 327-341.

Skarendahl, A., "Self-Compacting Concrete for Improved Productivity, Working Environment and Performance," *IREX-Meeting*, Paris, February 1999, 12 pp.

Stanton, T. E., "Measured Pressure on Forms from Fresh Concrete," *Concrete*, V. 45, 1937, pp. 11-16.

Struble, L. J., "The Rheology of Fresh Cement Paste," Proceedings, *Conference of the American Ceramic Society*, Boston, 1991, pp. 7-29.

Szecsy, R.; Kaufman, S.; Henson, D.; and Abbott, T., "A Modeling Approach for the Economical, Practical Production, and Placement of SCC for Residential and Commercial Application," *Proceedings of the 1st North American Conference On the Design and Use of*

Self-Consolidating Concrete, Eds. Shah, S. P.; Daczko, J. A.; and Lingscheit, J. N., Chicago, November 2002, pp. 197-202.

Tah, J. H. M., and Price, A. D. F., "Computer-Based Modeling of Concrete Pressures on Complex Shaped Wall Formwork," *Building and Environment*, V. 26, Issue 2, 1991, pp. 223-229.

Tattersall, G. H., and Banfill, P. F. G., "The Rheology of Fresh Concrete," Pitman Advanced Publishing Program, London, First Edition, 1983, 356 pp.

Tattersall G. H., and Bloomer S. J., "Further Development of the Two-Point Test for Workability and Extension of its Range," *Magazine of Concrete Research*, V. 31, No. 109, 1979, pp. 202-210.

Taylor, W.H., "Concrete Technology and Practice," Third Edition, American Elsevier Publishing Company, New York, Chapter 8, 1965, pp. 157-161.

Tejeda-Dominguez, F., and Lange, D. A., "Effect of Formwork Material on Laboratory Measurements of SCC Formwork Pressure," *Proceedings of the 2ⁿᵈ North American conference on the Design and Use of Self-Consolidating Concrete (SCC 2005)* and *the 4ᵗʰ International RILEM Symposium on Self-Compacting Concrete*, Evanston, IL, Ed. Shah, S. P., 2005, pp. 525-532.

Tejeda-Dominguez, F.; Lange, D. A.; and D'Ambrosia, M. D., "Formwork Pressure of Self-Consolidating Concrete (SCC) in Tall Wall Field Applications," *84ᵗʰ Annual Meeting Transportation Research Board*, Compendium of Papers CD-ROM, Washington, DC, January 2005.

Terzaghi, K., and Peck, R. B., "Soil Mechanics in Engineering Practice," John Wiley & Sons, Inc., New York, 1967,729 pp.

Vanhove, Y.; Djelal, C.; and Magnin, A., "A Device for Studying Fresh Concrete Friction," *Cement Concrete and Aggregates*, V. 26, No. 2, December 2004A, pp. 35-41.

Vanhove, Y.; Djelal, C.; and Magnin, A., "Prediction of the Lateral Pressure Exerted by Self-Compacting Concrete on Formwork," *Magazine of Concrete Research*, V. 56, No. 1, February 2004B, pp. 55-62.

Vanhove Y.; Djelal C.; and Magnin, A., "A Prediction of the Pressure on Formwork by Tribometry," *Pressure Vessel and Piping Conference, Emerging Technologies for Fluids, Structures and Fluid-Structure Interactions – 2001, The American Society of Mechanical Engineers,* Atlanta, July 2001, V. 431, pp. 103-110.

Vanhove, Y.; Djelal, C.; and Magnin, A., "Friction Behaviour of a Fluid Concrete Against a Metallic Surface", *International Conference on Advances in Mechanical Behaviour, Plasticity and Damage*, Elsevier Science LTD, Euromat 2000, Tours, Novembre 2000, V. 1, pp. 679-684.

Vié, D.; Djelal, C.; Vanhove, Y.; and Magnin, A., "Pressure of Self-Compacting Concretes," (in French), Annales du Bâtiment et des Travaux Publics, No. 6, December 2001, pp. 5-13.

Wallevik, J., "Rheology of Particle Suspensions," Ph.D. Thesis, Department of Structural Engineering, Norwegian University of Science and Technology: Trondheim, Norway, 2003, 397 pp.

Wallevik, O. H., "Rheology - a Scientific Approach to Develop Self-Compacting Concrete," *3rd International RILEM Symposium on Self-Compacting Concrete*, Eds. Wallevik, O., and Nielsson, I., Reykjavik, Iceland, August 2003, pp. 23-31.

Walraven, J., "Self-Compacting Concrete in the Netherlands," *Proceedings of the 1st North American Conference On the Design and Use of Self-Consolidating Concrete*, Chicago, Eds. Shah, S. P.; Daczko, J. A.; and Lingscheit, J. N., November 2002, pp. 399-404.

Wolfgang B., and Stephan U., "Investigation on the Formwork Pressure Using Self-Compacting Concrete," *Proceedings of the 3rd International RILEM Symposium on Self-Compacting Concrete*, Eds. Wallevik, O., and Nielsson, I., Reykjavik, Iceland, August 2003, pp. 281-287.